Characterization of PF Resol/Isocyanate Hybrid Adhesives

Darren A. Riedlinger

Thesis submitted to the faculty of the
Virginia Polytechnic Institute and State University
in partial fulfillment of the requirements for the degree of

Master of Science
in
Macromolecular Science and Engineering

Dr. Charles E. Frazier
Dr. Judy S. Riffle
Dr. Maren Roman

February 1, 2008
Blacksburg, VA

Keywords: phenol-formaldehyde, isocyanate, adhesives, morphology, rheology, ^{13}C NMR, DSC, fracture testing, wood adhesion

Characterization of PF Resol/Isocyanate Hybrid Adhesives

by

Darren A. Riedlinger

Charles E. Frazier, Chairman

Macromolecular Science and Engineering

ABSTRACT

Water-based resol phenol formaldehyde, PF, and organic polymeric methylenebis(phenylisocyanate), pMDI, are the two primary choices for the manufacture of exterior grade wood-based composites. This work addresses simple physical blends of pMDI dispersed in PF as a possible hybrid wood adhesive. Part one of this study examined the morphology of hybrid blends prepared using commercially available PF and pMDI. It was found that the blend components rapidly reacted such that the dispersed pMDI droplets became encased in a polymeric membrane. The phase separation created during liquid/liquid blending appeared to have been preserved in the cured, solid-state. However, substantial interdiffusion and copolymerization between blend components also appeared to have occurred according to measured cure rates, dynamic mechanical analysis, and atomic force microscopy. In the second part of this study a series of PF resins was synthesized employing the so-called "split-cook" method, and by using a range of formaldehyde/phenol and NaOH/phenol mole ratios. These neat PF resins were subjected to the following analyses: 1) steady-state flow viscometry, 2) free formaldehyde titration, 3) non-volatile solids determination, 4) size exclusion chromatography, 5) quantitative solution-state ^{13}C nuclear magnetic resonance, NMR, 6) differential scanning calorimetry, 7) parallel-plate oscillatory cure rheology, and 8) dielectric spectroscopy. The neat PF analytical results were unremarkable with one exception; NMR revealed that the formaldehyde/phenol mole ratio in one resin substantially differed from the target mole ratio. The neat PF resins were subsequently used to prepare of series of PF/pMDI blends in a ratio of 75 parts PF solids to 25 parts pMDI solids. The resulting PF/pMDI blends were subjected to the following analyses: 1) differential scanning calorimetry, 2) parallel-plate oscillatory cure rheology, and 3) dielectric spectroscopy. Similar to what was inferred in part one of this study, both

differential scanning calorimetry (DSC) and oscillation cure rheology demonstrated that cure of the PF continuous phase was substantially altered and accelerated by pMDI. However within actual wood bondlines, dielectric analysis detected little variation in cure speed between any of the formulations, both hybrid and neat PF. Furthermore, the modulated DSC curing experiments detected some latent reactivity in the hybrid system, both during initial isothermal curing and subsequent thermal scanning. The latent reactivity may suggest that a significant diffusion barrier existed between blend components, preventing complete reaction of hybrid blends even after thermal scanning up to 200 °C. Part three of this work examined the bonded wood mode-I fracture performance of hybrid resins as a function of the resol formaldehyde/phenol ratio and also the alkali content. A moderate increase in unweathered fracture toughness was observed for hybrid formulations relative to neat PF. Following accelerated weathering, the durability of the hybrid blends was promising: weathered hybrid toughness was equivalent to that of weathered neat PF. While the resol F/P ratio and alkali content both influenced hybrid fracture toughness, statistical modeling revealed interaction between these variables that complicated result interpretation: the influence of hybrid alkali content depended heavily on each formulation's specific F/P ratio, and vice versa.

This work is dedicated to my mother and father,
for their unending sacrifice, support and love.

ACKNOWLEDGEMENTS

First and foremost I must express the deepest possible gratitude to my major professor and mentor, Dr. Charles Frazier. His patience, guidance and encouragement have expanded the limits of my own potential and his raw enthusiasm has been an awesome source of inspiration. While Dr. Frazier's contributions to my scientific development are unquestionable, I feel even more indebted for the profound way he has affected me personally. I doubt that I will ever again have the opportunity of working under such a remarkably unselfish teacher, role-model and friend; I will always strive to live up to the unequalled standard that he embodies.

I also wish to acknowledge my committee members, Dr. Judy Riffle and Dr. Maren Roman. Their comments and insights have greatly improved the quality of this research effort. Meanwhile, their respective contributions to the polymer science and wood science programs here Virginia Tech will continue to add value to this degree long after my graduation.

Throughout my graduate study I have been extremely lucky to have had the friendship, support and dialogue afforded to me by fellow members of the Virginia Tech Wood Adhesion Group. Sudip Chowhardy, Sudipto Das, Francisco López-Suevos, Dakai Ren, Scott Rennecker and Jun Zheng deserve special mention; each has contributed in their own way towards making the last few years an enriching and enjoyable experience. Several members of the university staff also deserve special recognition; Linda Caudill, Rick Caudill, Debbie Garnand, Tom Glass and David Jones have each gone out of their way to create a supportive and friendly environment for myself and fellow graduate students.

Lastly, none of this would have been possible without the love, encouragement, support, and sacrifice of my family—especially my parents, Karen and Donald Riedlinger. This work is dedicated to them.

ATTRIBUTION

Several colleagues and coworkers aided in the research behind several of the chapters of this dissertation. A brief description of their background and their contributions are included here.

Prof. Charles E. Long- Ph.D. (Department of Wood Science, Virginia Tech) is the primary Advisor and Committee Chair. Prof. Frazier provided oversight and guidance throughout this research and writing effort.

Chapter 3: Fracture Performance of PF/pMDI Hybrid Adhesives.

Hongzhang Zheng- Ph.D. candidate (Department of Statistics, Virginia Tech) assisted in statistical modeling of PF/pMDI fracture toughness.

Appendix A.2: Tg as an index of conversion in pMDI impregnated wood.

Dr. Nanjian Sun- Postdoctoral research associate (Department of Wood Science, Virginia Tech) currently at DuPont China, was a member of the author's research group. Dr. Sun conducted approximately 40% of the experimentation behind Appendix A.2.

TABLE OF CONTENTS

LIST OF FIGURES

LIST OF TABLES

CHAPTER 1. INTRODUCTION

Alkaline phenol-formaldehyde has been an important wood adhesive since early in the 20th century. Only in the last 35 years has polymeric methylenebis(phenylisocyanate) emerged as an alternative for the manufacture of certain wood-based composites. By North American standards, these two resins (respectively PF and pMDI) remain the only choice for the mass production of exterior grade structural wood composites. No other adhesive has become a significant option.

This work speaks to a possible alternative that involves a physical blend of aqueous PF with liquid pMDI. At first glance, such a system may hardly seem novel. However, upon blending these immiscible resins interesting possibilities arise from both the structure of the resulting emulsion and from the corresponding solid-state multiphase morphology. Previous results from our laboratory demonstrated that the properties of these blends were dominated by emulsion effects and that co-reaction between resins provided an added layer of complexity [1]. Therefore, commercial implementation of this system will likely require extensive research on the interactions between emulsion effects and PF resin chemistry. Compelling justification for such development was first provided by Pizzi et al [2]. PF/pMDI blends were reported to provide excellent performance for industrial plywood manufacture using difficult-to-bond woods and remarkable resistance to six-hour boiling water treatment was also claimed. Since this 1993 report, no significant industrial use of the PF/pMDI blend has occurred in North America. However, there has been recent industrial interest as revealed in the United States patent literature. One invention includes the blending of pMDI with powdered PF [3]. Another involves the preparation of protected phenolics that deprotect during hot-pressing and subsequently react with pMDI [4]. A third patent discusses the simplest method, which is to mix aqueous PF with liquid pMDI just prior to adhesive application [5].

Our research focuses on this latter system, a simple physical blend of aqueous PF and liquid pMDI. Both classes of adhesives are commercially available and hence, could provide a cost effective approach toward improved adhesive development. Fracture

cleavage of bonded-wood double cantilever beams revealed that hybrids containing a PF continuous phase were substantially toughened. This toughening was attributed to a putative polyurea/biuret/urethane dispersed phase arising from pMDI [1]. Hybrids containing a dispersed PF phase, however, did not substantially toughen the isocyanate-borne continuous phase [1].

The first part of this investigation examines the multiphase morphology of the hybrid system. Using commercial resol and isocyanate formulations the liquid and solid state morphology is studied using a variety of microscopy techniques. The phase separated structure is further characterized using dynamic mechanical analysis and the residual reactivity is examined using Fourier Transform infrared spectroscopy.

In the second part of this investigation, factors affecting the curing of the hybrid resins are probed using a series of PF resols synthesized with differing formaldehyde to phenol (F/P) ratios and differing alkali contents. The PF resols are thoroughly characterized using steady state flow rheology, solids content analysis, free formaldehyde determination, ^{13}C NMR spectroscopy and gel permeation chromatography (GPC). The cure kinetics of hybrid resins prepared from these synthesized PF resins are then studied using differential scanning calorimetry and parallel plate cure rheology. Finally, the bulk resin curing results are compared to the actual in-situ curing of hybrid resins using micro-dielectric analysis of hot-pressed wood composites.

In the final part of this study, the actual performance and durability of hybrid resins formulated using the previously synthesized resols is investigated using double cantilever beam fracture analysis of bonded wood composites. Statistical modeling is used to relate these results to the derivative resol chemistries.

References:

1. Zheng, J., S.C. Fox and C.E. Frazier, Forest Prod. J. 54(10):74-81 (2004).
2. Pizzi, A., J. Valenzuela and C. Westermeyer, Holzforschung. 47:68-71 (1993).
3. Rosthauser, J.W. and W.D. Detlefsen, US Patent 6,214,265 (2001).
4. Miller, T. R., L.D. Creel and W.D. Detlefsen, US Patent 6,478,998 (2002).
5. Hsu; Wu-Hsiung Ernest, US Patent 6,297,313 (2001).

CHAPTER 2. LITERATURE REVIEW

2.1. Phenol-Formaldehyde (PF)

2.1.1. Overview

As early as 1872 a unique resinous product was observed in reactions between phenol and formaldehyde [1, 2]. However, despite intensive research [1-10], the novel product remained little more than a laboratory curiosity for several decades. In 1899 the first patent specifically covering phenol-formaldehyde (PF) resins was granted (as substitutes for hard rubber) [1, 11] and by 1903 continued study of acid catalyzed reactions led to the commercial scale production of the first wholly synthetic polymer, sold under the trade name 'Laccain' [8, 12]. Still, despite this significant achievement, Laccian's rudimentary manufacturing process and limited number of applications generally made production economically unfeasible. In 1907, assisted by significant advancement in the understanding of alkali catalyzed PF reactions [13-16], Leo Baekeland applied for his revolutionary "heat and pressure" patent covering the processing of PF resins [1, 17, 18]. Commercial production using Baekeland's method was a success. While Baekland's production process made commercialization feasible, his accurate knowledge of these versatile resins and his broad entrepreneurial vision facilitated their eventual introduction in diverse applications spanning the molding compounds, paper impregnates, adhesive and coating industries—ultimately making the polymer he coined 'Bakelite' a household name.

Owing to their versatility and low cost, phenolic resins still account for a significant percentage of all plastics currently produced worldwide [1]. By varying the catalyst type and formaldehyde to phenol (F/P) molar ratio, two distinct classes of PF resins are created: resols and novolaks. These classes significantly differ in both structure and function. Resols are formulated with excess formaldehyde ($F/P > 1$), are catalyzed by alkali and crosslink under the influence of heat alone. Novolaks are formulated with excess phenol ($F/P < 1$), are acid catalyzed and require addition of a separate crosslinker (typically hexamethylenetetramine, HMTA) to cure the otherwise

linear oligomers. This additional crosslinking step typically results in slower cure of novolaks compared to resols [19].

The possibility of using PF resins for laminating wood veneer was mentioned in Baekeland's original 1907 patent but it was not until the 1930's that these resins were actually used commercially as binders for particleboard and plywood [2,4]. Their introduction boosted wood composites to commodity status. PF resins have since remained one of the most important adhesives for wood composite manufacture, especially for exterior applications. As of 2002, PF resins accounted for 27.1 percent of the total 2.01 million metric tons of resin solids consumed by the North American wood composites industry [5]. For wood composite manufacture, PF resols are used almost exclusively over novolaks. Resol properties are well suited to exterior structural wood composite manufacture, possessing high rigidity, durability, chemical resistance and dimensional stability [4]. They find widespread use as binders for plywood, particleboard and oriented strandboard (OSB). Compared to polymeric methylenebis(phenylisocyanate), the only other binder currently used in North American OSB manufacture, PF resols have the advantage of low cost and high thermal stability while still maintaining reasonably fast cure rates.

2.1.2. Resol Chemistry

Resols result from the step growth polycondensation of phenol with excess formaldehyde in alkaline conditions. Unsubstituted phenol is tri-functional as a condensation monomer; formaldehyde is di-functional. Consequently, condensation at F/P levels greater than 1.0 permit formation of a crosslinked network. Under alkaline conditions an initial addition reaction between phenol and formaldehyde forms substituted hydroxymethylphenol (HMP). Subsequent HMP condensation reactions are relatively slow unless the HMPs are highly substituted. Thus, hydroxymethylation occurs as a distinct stage prior to condensation. The latter condensation stage can be further divided into the chain-growth/prepolymer-formation occurring during synthesis (at temperatures < 100 ^{0}C) and the crosslinking/curing of the synthesized prepolymer at the time of application (under desiccating conditions > 100 ^{0}C).

2.1.2.1. Hydroxymethylphenol Formation by Addition

PF resols are synthesized in an aqueous alkali environment. In this environment formaldehyde is present almost exclusively in its hydrated form as methylene glycol. The alkaline environment also deprotonates phenol into the significantly more reactive phenoxide ion. Resonance stabilization of the phenoxide ion results in increased electron density at both the ortho and para positions, promoting electrophihlic aromatic substitution of methylene glycol at these sites (Figure 2.1).

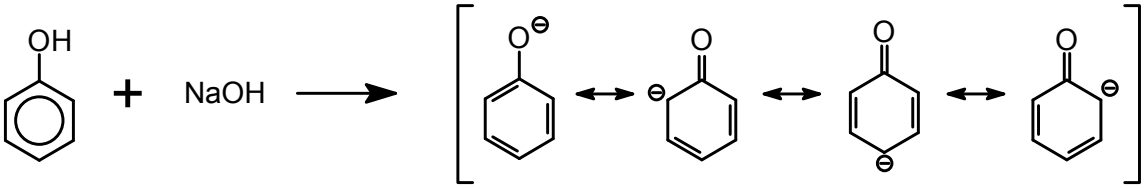

Figure 2.1. Resonance structures of phenol in an alkaline environment show ortho and para reactivity

Alkylation occurs almost exclusively at these electron-rich ortho and para positions, with HMP formation proceeding through a quinone methylol transition state [20]. Continued reaction may still occur at the remaining ortho and para sites, resulting in di- and tri-substituted HMPs (Figure 2.2).

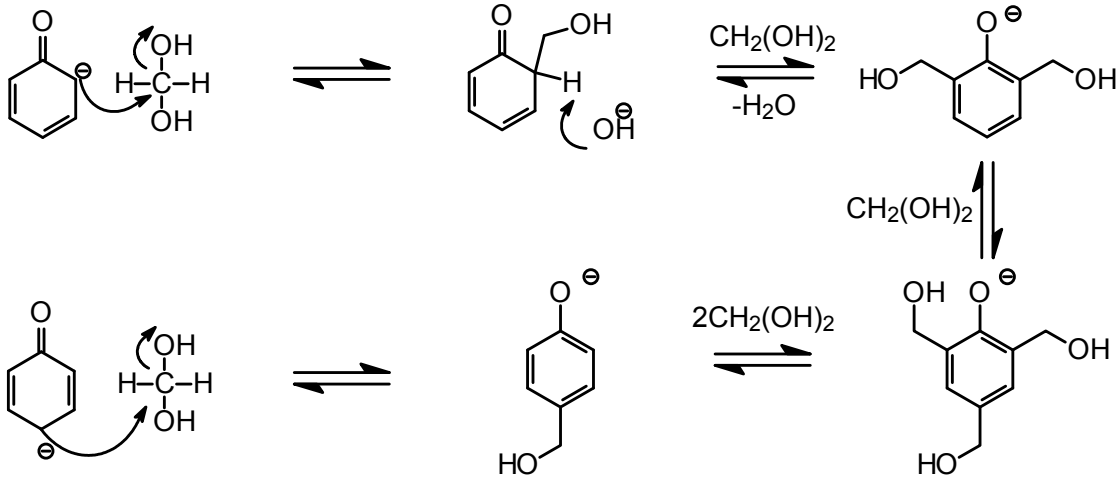

Figure 2.2. Methylene glycol addition forms mono-, di- and tri-substituted HMPs

The phenoxide para position is believed to have a slightly greater affinity for methylene glycol than the ortho position. However, the ortho position is twice as abundant as the para position and this greater abundance results in a greater relative amount of ortho HMP substitution [21-24]. Since the methylol group is slightly electron withdrawing, hence ring deactivating [25, 26], methylol substitution at the para position results in decreased reactivity toward additional formaldehyde. However, the expected deactivating effect is not observed for ortho-substituted HMPs; both the mono- and di-substituted derivatives are significantly more reactive than either the unsubstituted phenoxide or the para-HMP. It is presumed that in the ortho-substituents deactivating effect is counteracted by intramolecular hydrogen bonds which add stability to the carbanion resonance forms and therefore promote the formation of polysubstituted HMPs (Figure 2.3) [23, 27].

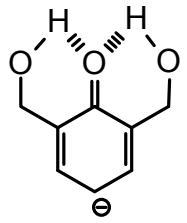

Figure 2.3. Ortho substituents form intramolecular hydrogen bonds which are para activating

The alkali metal hydroxides commonly used as resol catalysts also significantly affect the ortho/para substitution ratio. It is believed that metal cations form chelates which are ortho directing (Figure 2.4). The greater the electron delocalizing potential of the cation the greater is its chelating strength. Thus ortho substitution increases along the series K<Na<Li<Ba<Sr<Ca<Mg when these metal hydroxides are used as catalysts [23, 28-30].

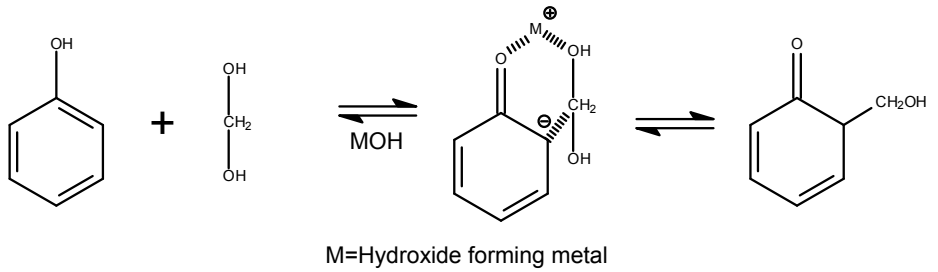

Figure 2.4. Metal hydroxide (MOH) chelates catalyze ortho HMP formation

To summarize, chelate formation and intramolecular hydrogen bonding not only favor ortho substitution but also increase the aromatic reactivity of the system as substitution proceeds. Therefore, resol resins contain a high degree of di- and tri-functional HMPs prior to condensation [1, 21]. While polysubstitution favors increased crosslink density, it also means that resols contain a relatively high percentage of unreacted phenol. This consequence is observed even when high F/P ratios are employed [20, 27] and is disadvantageous for both processing and environmental reasons [1].

2.1.2.2. Resol Prepolymer Formation by Condensation

PF resol reactions are typically divided into three stages: the initial resol (A stage), the resitol (B stage) and the resite (C stage). The resol stage refers to the resin as an early mixture of HMP monomers and dimers while the resite stage refers to the fully cured insoluble network. Commercial resols for use in wood composites are typically advanced to the intermediate resitol stage with precise molecular weight distributions tailored to specific composite products. Advancement to a fully cured resite subsequently occurs during hot pressing of the bonded wood composite.

Industrially, resol self-condensation between mono-, di- and tri-substituted HMPs is preformed between 60 and 100 ^{0}C; below 60^{0}C this reaction is negligible [31]. The condensation reaction is widely believed to proceed via a quinone methide intermediate [23, 32, 33]. Quinone methide is a strong electrophile and readily substitutes onto the electron rich ortho- and para- sites of other phenoxides to form methylene bridges, as illustrated in Figure 2.5. The reaction between two HMPs is substantially faster than the reaction between HMP and unsubstituted phenol [34]. As a result, methylol groups have a strong activating effect on the condensation reaction, again favoring the formation of a

highly crosslinked network at the cost of allowing a portion of unreacted phenol to remain in the finished resin. Furthermore, condensation at the para position is substantially more common than at the ortho position, possibly related to greater steric hindrance at the ortho position. As a result, para-para and ortho-para methylene linkages dominate, while ortho-ortho linkages rarely occur [24, 35]. In contrast to novolaks, the formation of methylene ether linkages is rare under typical resol synthetic conditions. Those which do form are thermally unstable and usually revert to simple methylene bridges upon heating through the loss of formaldehyde [24, 35-38].

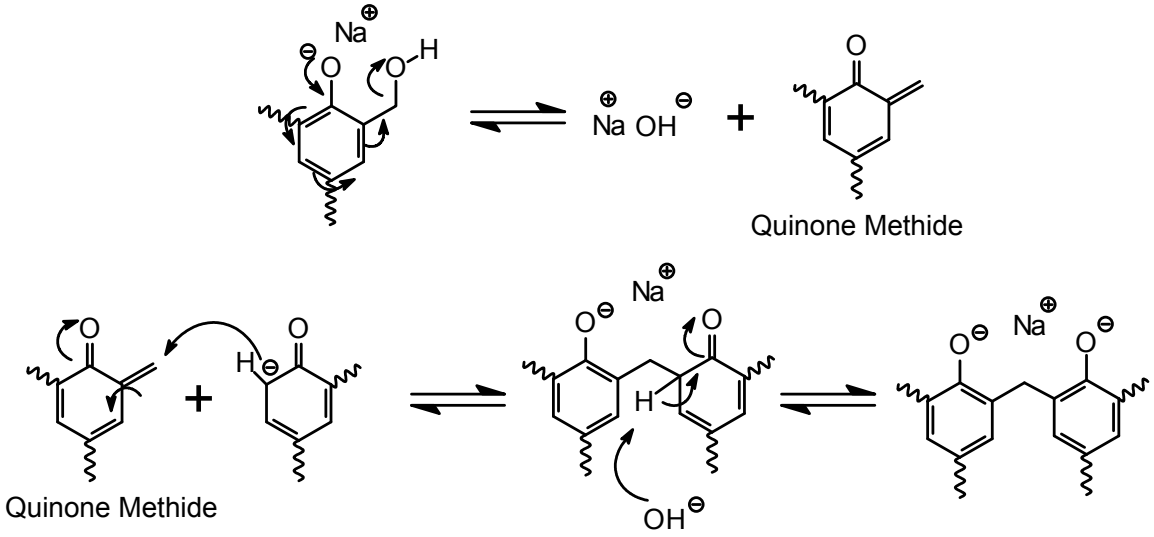

Figure 2.5. Condensation through a quinone methide intermediate

Generally, commercial resol synthesis is stopped at the oligomeric (resitol) stage. The exact endpoint is determined by periodically monitoring resin viscosity and depends on the intended application. For instance, commercial oriented strand board (OSB) resins typically have a viscosity of 100 to 500 mPa.s corresponding to a number average molecular weight between 200 and 500 g/mol. On the other hand, plywood resols are more advanced with viscosities up to 2000 mPa.s and number average molecular weights between 1000 and 2000 g/mol [39]. To achieve accurate endpoints the final stages of resol synthesis are conducted at a reduced temperature, between 40 and 60 ^{0}C [37].

2.1.3. Nature of PF-Wood Adhesion

Resol curing occurs within bonded wood composites following the addition of heat and pressure. The curing reactions are generally simple extensions of the same quinone methide mediated HMP condensation that occurred during resitol synthesis [32, 40]. Ether bridges are again both unfavorable and unstable [37, 41]. However, conditions within the wood composite mat are quite different from what is typical during synthesis. For instance, the maximum temperature within a particle board core reaches between 100 and 105 ^{0}C over a pressing time of 7 to 15 s per millimeter of thickness. Although this maximum temperature is maintained for only 20 to 60s [37], the high temperature promotes some unusual crosslinking mechanisms not observed during synthetic conditions. Resulting products include ether bridges between phenoxides and HMPs (Figure 2.6a), free formaldehyde crosslinks between methylene bridges (Figure 2.6b) and condensation between methylene carbons and hydroxymethyl groups (Figure 2.6c) [31, 42].

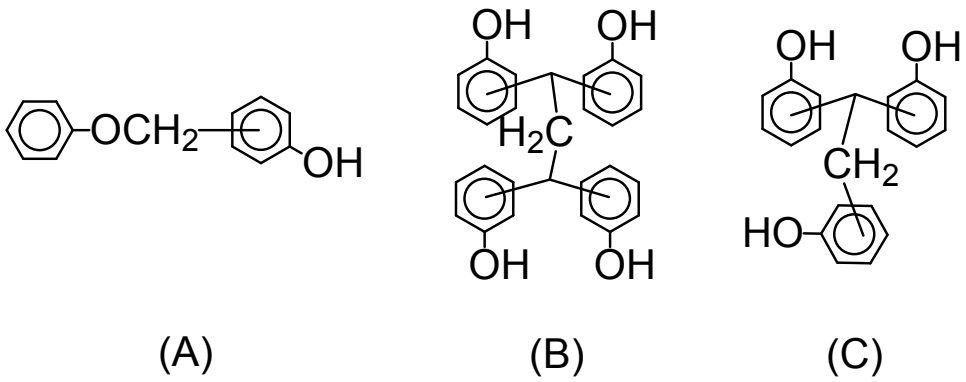

Figure 2.6. Unusual crosslinks believed to occur in PF resols

Regarding the nature of adhesion, it is generally accepted that under hot pressing conditions PF does not covalently bond with wood; covalent bonding requires significantly higher temperatures and longer cure times [37, 43]. Instead, the strong adhesion is the net result of many hydrogen bonds and other intermolecular associations between PF and wood [37, 44-46]. Although covalent bonding is not observed, it is well established that wood does substantially alter PF cure kinetics and strength development [47]. The altered kinetics have been attributed to the catalytic activating effect that

secondary interactions have on the various PF monomers and oligomers [48-51]. As such, characterization of a particular neat adhesive may not necessarily reflect the same adhesive's properties within a bonded wood composite.

2.1.4. Relation Between Resol Synthetic Variable and Physical Properties

Resol synthetic mole ratios and formulation variables are precisely tailored for individual production needs. Among the most significant variables are the type and quantity of catalyst, the F/P mole ratio, the order of reactant additions (the cooking procedure) and the addition of additives/fillers. These variables have been extensively studied and affect both the chemical structure and solid-state performance of the resols [22, 39, 52, 53].

2.1.4.1. Influence of Catalyst Type and Quantity

As previously mentioned, metal hydroxide catalysts with high chelating potential preferentially promote ortho over para hydroxymethylation [1, 28-30]. This trend is even more distinct for the transition metals, with zinc and then magnesium oxide being the most ortho directing catalysts. Non-metalic alkali catalysts such as ammonia can also be used, with the resulting polymer exhibiting significantly less branching than metal hydride catalyzed reactions [1].

In addition to directly catalyzing the reaction and reducing cure times, resol catalysts also play an important role in maintaining the solubility and flow properties of the resol. For example, the sodium hydroxide content of plywood adhesives is typically increased to ensure adequate flow properties and good wood penetration ability in these highly advanced resins [39]. However, high alkali contents do pose a distinct disadvantage—at least for alkali hydroxide catalyzed wood composite adhesives in which the catalyst is seldom separated from the resin. In these resins the hygroscopic nature of the residual catalyst may lead to high water absorption and poor dimensional stability [1].

2.1.4.2. Influence of F/P Molar Ratio

Theoretically, a fully reacted resol network will form with an F/P ratio equal to 1.5. In practice the resin F/P ratio is generally increased to between 1.8 and 3 for wood adhesives [1]. This increased ratio has several distinct advantages. As can be inferred from the reaction mechanism, a high relative formaldehyde content promotes a highly substituted, branched network structure with low free phenol content [1, 38, 53]. Conversely, low F/P ratios result in more linear molecules with a greater proportion of unreacted phenol. Due to the lower quantities of free ortho- and para- HMP positions, high F/P resins also exhibit more methylene ether crosslinks. Regarding the impact of F/P ratio on isomeric structure, the literature is not in agreement. While So et al. [54] report that F/P ratio has no significant influence on isomeric structure, Pakkenen [53] found high F/P ratios correlate with high ortho substitution, high para-para' methylene linkages and high hemiformal content. The latter researchers also found high F/P ratios increase the degree of polymerization while decreasing polydispersity. Their study further demonstrated that DSC of high F/P neat resins exhibits a bimodal separation between the addition and condensation exotherms, suggesting that in these resins the addition reactions occur as a distinct step prior to condensation.

2.1.4.3. Influence of Formulation Procedure

Intense competition mandates that PF resols often be tailored to their specific end use. This necessitates a flexible manufacturing procedure which is generally not amenable to continuous processing [1]. Early resols were produced through a single caustic cook in which all reactants were charged simultaneously. The bulk of the reaction occurred at 90 ^{0}C, though the resins were finished closer to 70 ^{0}C to facilitate better endpoint control. This basic procedure has since been modified by modern producers to allow greater control over the properties of the adhesive system. One common modification is to charge the caustic in multiple additions. This double caustic or split cook procedure creates a broader molecular weight distribution in the adhesive. As a result, the flow properties are well suited to the specific needs of plywood adhesives. The second caustic addition may also convert unreacted phenols, thereby

lowering the toxicity of the resin [39]. Another common modification from the single caustic cook involves continuous addition of formaldehyde over a set period of time. Typically the maximum reaction batch size is limited to control the heat of exotherm during formaldehyde addition [1]. Incremental formaldehyde addition partially alleviates this effect, but also impacts the structure of the adhesive—reducing unreacted phenol monomer and altering the resin's isomeric structure [39]. Finally, the temperature regime employed during synthesis is commonly modified to limit exotherm and bring about the desired resin properties [1].

2.1.4.4. Influence of Additives

A wide variety of additives are employed industrially to modify resol structure, stability and performance. For instance, urea is commonly added following resin synthesis to scavenge free formaldehyde monomer. Urea additionally improves tack, shortens pressing times and enhances resin functionality [52]. Provided the quantity is low, urea's effect on bond durability is negligible. Other common additives include preservatives, defoamers, cellulosic filler, surfactant and plasticizers [52].

2.2. Polymeric methylenebis(phenylisocyanate)

2.2.1. Overview

Polymeric methylenebis(phenylisocyanate), or pMDI, was first introduced as a wood binder in the mid 1960's and has since become an important adhesive for the manufacture of oriented strand board (OSB) [52, 55]. As of 2001 pMDI represented 21% of the total resin solids used in the manufacture of OSB [56]. Compared to commodity PF resins, the increased cost of pMDI is at least partially offset by its improved dimensional stability, lower curing temperature, faster cure speed, lower required resin loadings, absence of formaldehyde emissions and higher moisture tolerance [57]. The moisture tolerance of pMDI is of particular industrial importance; pMDI actually requires the wood moisture content to be greater than 10% and moisture contents up to 18% will not negatively impact performance [58-60]. Since wood chips do not need to be dried as

thoroughly, pMDI also reduces the energy costs and VOC emissions associated with wood drying. However, pMDI adhesives have the disadvantages of high acute toxicity and poor tack. Furthermore, special anhydrous storage conditions are required to prevent premature curing. Additionally, pMDI will adhere to press platens and this necessitates the application of release agents unless its use is exclusively restricted to the composite core [57].

Commercial OSB pMDI is composed of roughly half MDI monomer and half higher oligomers. Of this monomer fraction, nearly 90% is 4, 4'-MDI and 10% is 2,4'-MDI; only trace amounts of 2, 2'-MDI are present. The resin has an average functionality of approximately 2.8 indicating an isocyanate content of ~32% [61, 62]. The generalized structure of pMDI is given in Figure 2.7; Figure 2.8 is of the constituent monomers.

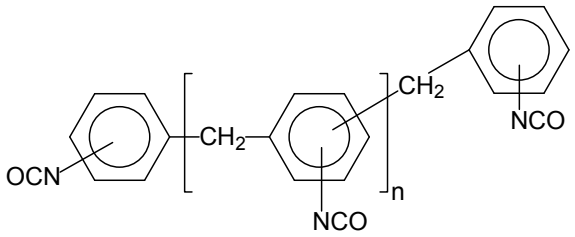

Figure 2.7. Generalized structure of pMDI

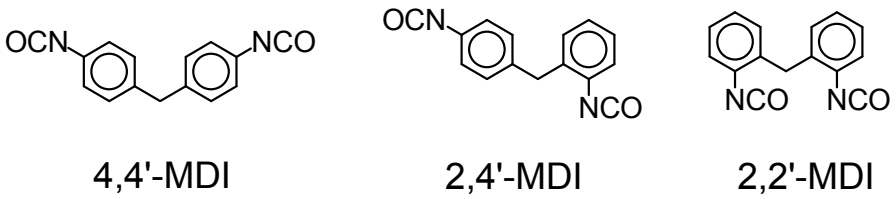

Figure 2.8. 4,-4', 2,-4' and 2,2' MDI monomers

2.2.2. pMDI Synthesis

The only commercially important route for pMDI synthesis is direct polyamine phosgenation. Detailed mechanisms of this reaction are reviewed by *Twitchett* [62] and Ranney [63] has compiled a thorough review of technical manufacturing processes from the patent literature. Manufacture is completed in two steps: polyamine synthesis and polyamine phosgenation.

2.2.2.1. Polyamine Synthesis

The starting material in the polyamine synthesis is aniline, which reacts with formaldehyde to form a mixture of diaminodiphenylmethane isomers. Two processes are of commercial importance. In the less common process, formaldehyde is reacted with a large excess of aniline under heat and pressure in the presence of a catalyst, typically an acid, salt or acidic-clay. In the more common process, aniline is treated with a measured quantity of formaldehyde in a stirred reactor at low temperatures. The reaction mixture is then heated to 100 ^{0}C to isomerize the secondary amines into primary amines. The latter process generally yields higher relative amounts of the desirable 4, 4' MDI isomer. The reaction is highly exothermic, however, and a complex series of reactions in each process may potentially generate large amounts of impurity.

Mechanistically, when formaldehyde is added to aniline in acidic conditions a strongly electrophilic imminium ion is formed with the elimination of water (Figure 2.9).

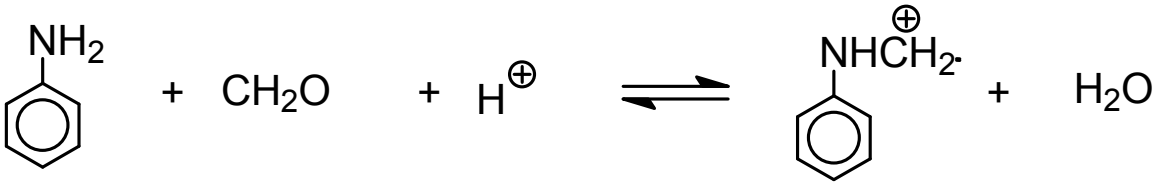

Figure 2.9. Imminium ion formation

The imminium ion reacts with an aromatic nucleus to yield *p*-aminobenzylaniline (Figure 2.10a). Subsequent reaction may in turn generate higher poly(aminobenzylaniline) oligomers of this species (Figure 2.10b).

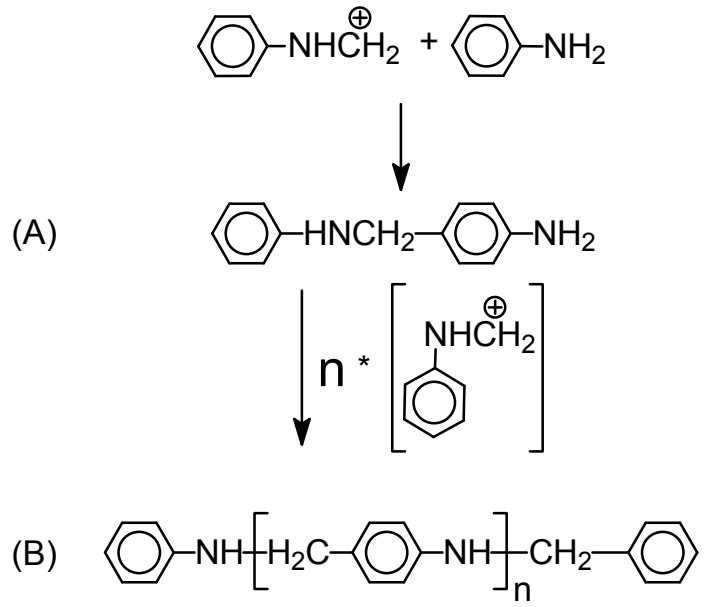

Figure 2.10. Formation of *p*-aminobenzylaniline and poly(benzylaniline)

The second stage of polyamine synthesis is the "isomerization" of the secondary aminobenzylanilines into primary amines. The isomerization is a bimolecular reaction between non-protonated aniline and a protonated secondary polyamine. Because the reaction requires that only the polyamine be protonated, the reaction is highly pH dependent. It is usually accelerated by heating to 95-100 ^{0}C. Aniline may undergo substitution at either the ortho or para positions, resulting in the respective 4,4'- or 2,4'-diamines (Figure 2.11). The reaction mixture must be thoroughly heated until the isomerization reaction is virtually complete. Following completion, the polyamine is separated and washed to remove acid and water.

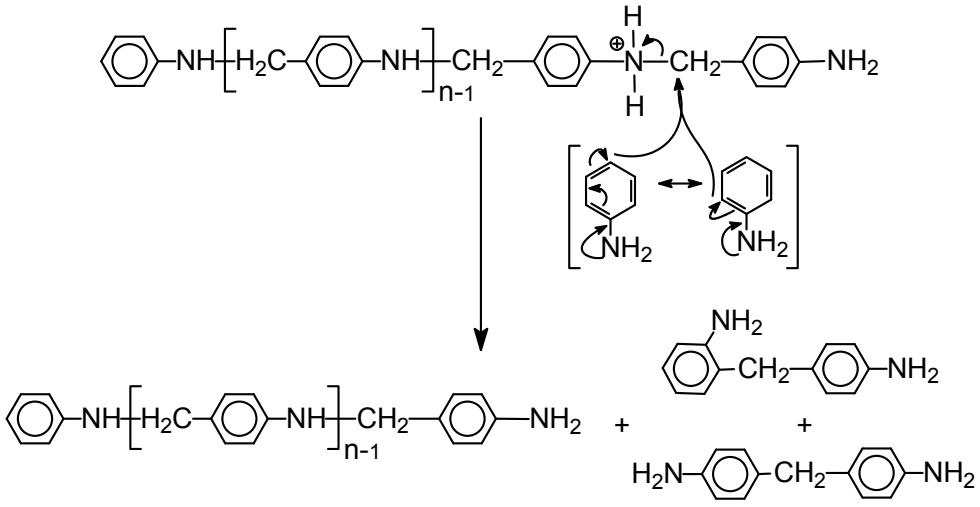

Figure 2.11. Isomerization to 4,4'- and 2,4'- diamine

Precise control of pH, temperature, formaldehyde addition rate and dilution is essential to suppress formation of the many undesirable pMDI isomers, oligomers and side products. For instance, triamine impurities are produced when polyamine replaces aniline in the above isomerization reaction. Figure 2.12 illustrates such triamine generation from the 4,4'-diamine isomer. Other relatively common impurities are 3-methyldiphenylmethane-4,4'-diamine (Figure 2.13a), unreacted secondary amine and 3-phenyl-3,4-dihydroquinazoline (Figure 2.13b). The latter two are especially deleterious as they give rise to acid chloride containing impurities during phosgenation. While the 4,4'-diamine can be fractionally distilled from the impurities prior to phosgenation, this is generally not preformed industrially.

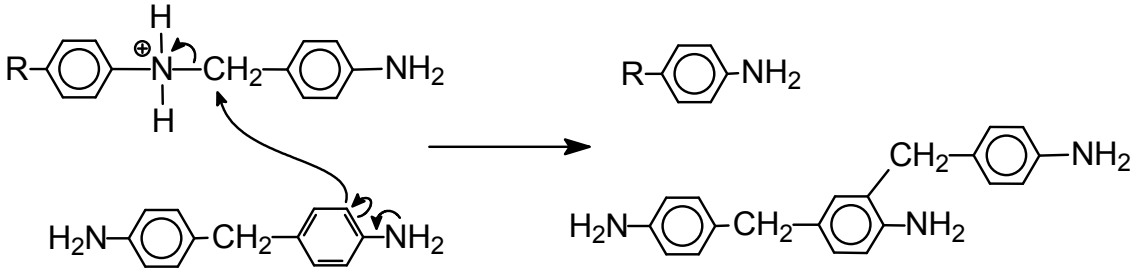

Figure 2.12. Generation of triamine impurity

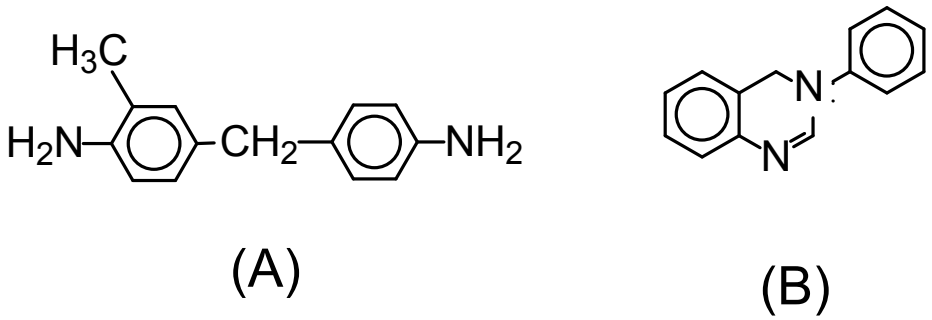

Figure 2.13. Notable impurities: (a) 3-methyldiphenylmethane-4,4'-diamine; and (b) 3-phenyl-3,4-dihyroxyquinazoline

2.2.2.2. Polyamine Phosgenation

Industrially, the anhydrous polyamine mixture (including impurities) from the previous step is prepared as a dilute (5-25%) solution in a high boiling solvent such as chloro- or dichloro-benzene. Gaseous phosgene is introduced in a 20 – 50% stoichiometric excess [64]. On a laboratory scale, trisphosgene may be substituted to partially alleviate the safety risks associated with phosgene. The reaction between phosgene and polyamine is complex, but the main reaction forms equimolar proportions of carbamoyl chloride and polyamine hydrochloride (Figure 2.14a). The carbamoyl chloride converts to isocyanate when heated near 50 ^{0}C (Figure 2.14b). The amine hydrochloride is converted to isocyanate upon reaction with additional phosgene, but requires temperatures in excess of 100 ^{0}C(Figure 2.14c).

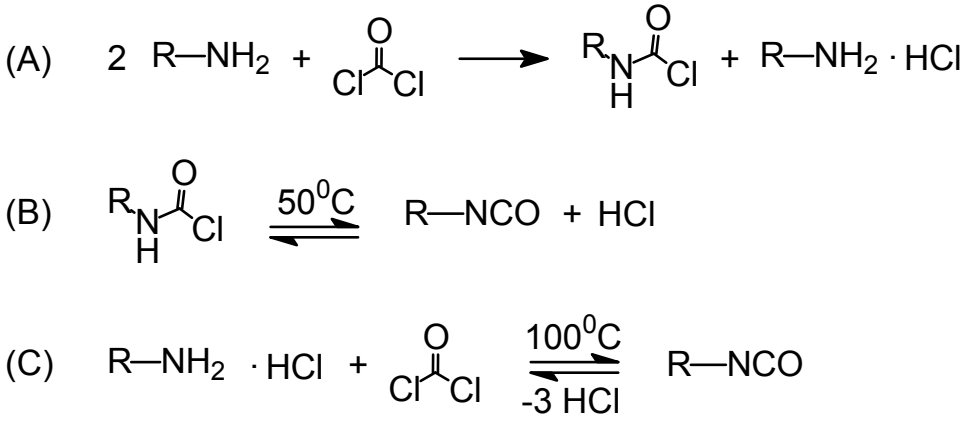

Figure 2.14. Amine phosgenation reactions

Since pMDI is rarely distilled from the reaction mixture, control of undesirable phosgenation side reactions is of critical importance. One such detrimental side reaction results in the formation of urea, biuret, triuret and polyurets (Figure 2.15). Subsequent reaction with phosgene generates isocyanide dichlorides (Figure 2.16). Another chlorine containing impurity results from phosgenation of aminobenzylanilines which were not converted during isomerization (Figure 2.17). While the latter impurity can be prevented with long polyamine reaction times that ensure complete isomerization, both impurities may be partially remedied by high temperature treatments of the pMDI solution under specialized conditions. During this treatment it is believed that carbonyl chlorides decompose to carbodi-imides with release of phosgene and HCl. The carbodi-imide may subsequently react with isocyanate to form uretonimines (Figure 2.18). The uretonimines will increase viscosity and reducing processibility, but are less detrimental than the original chlorinated compounds.

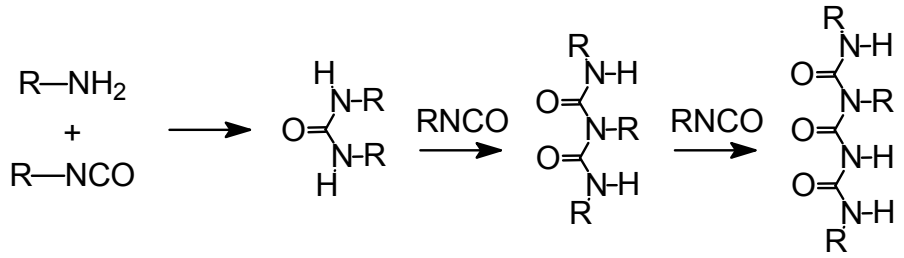

Figure 2.15. Urea and polyuret formation

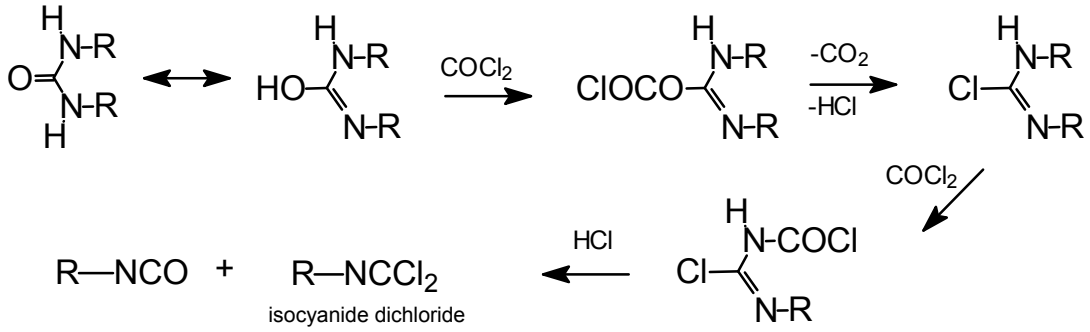

Figure 2.16. Isocyanide dichloride formation

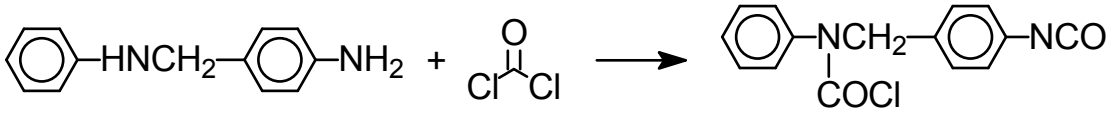

Figure 2.17. Formation of secondary carbamoyl chloride

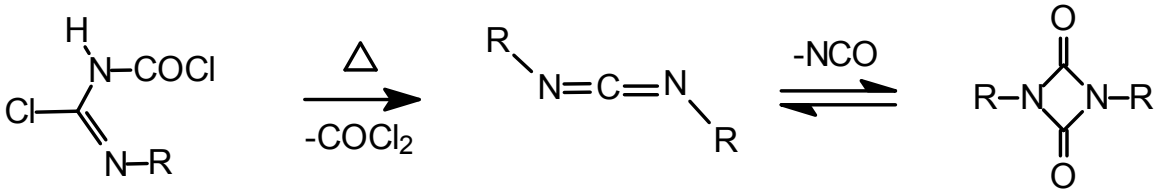

Figure 2.18. Conversion of chloroformamidine-N-carbonyl chloride to uretonimine

2.2.3. Important Reactions of pMDI

Isocyanates belong to a class of molecules known as heterocumulenes: heteroatomic compounds containing a system of cumulative double bonds [65]. Like most heterocumulenes, isocyanates exhibit high reactivity in a variety of reaction classes. This high reactivity mainly arises from the resonance hybrids of the –NCO group, with pronounced electrophilic character at the carbon atom and nucleophilicity at both the nitrogen and oxygen atoms (Figure 2.19). Aromatic isocyanates are generally more reactive than aliphatic isocyanates, due both to conjugation and the greater inherent electronegativity of sp^2 hybridized carbons relative to sp^3 carbons [64, 66].

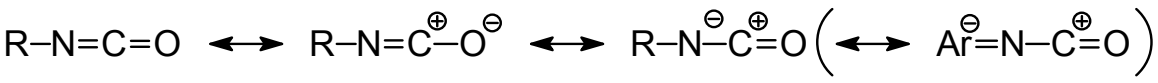

Figure 2.19. Isocyanate resonance structures

Although the diversity of potential isocyanate reactions is immense [67], the major reactions will be outlined in three classes: self-polymerization reactions, reactions with protic nucleophiles and miscellaneous reactions not involving protic nucleophiles.

2.2.3.1. pMDI Self Polymerization Reactions

Nucleophilic catalysts readily substitute with isocyanates to form a reactive complex which may subsequently undergo reversible dimerization with a second pMDI molecule to form a uretidine dione ring (Figure 2.20)[68]. Highly reactive isocyanates such as pMDI exhibit some dimerization even at room-temperature and in the absence of catalyst; this is accompanied by a concomitant increase in resin viscosity [66]. This dimerization is generally unwanted as it reduces resin processibility. The uretidione structure is commonly eliminated by heating the resin to 200 ^{0}C followed by rapid quenching [69]. Subsequent trimerization of pMDI generally requires heating and/or catalysis, but the resulting isocyanurate ring is stable and the reaction irreversible (Figure 2.21).

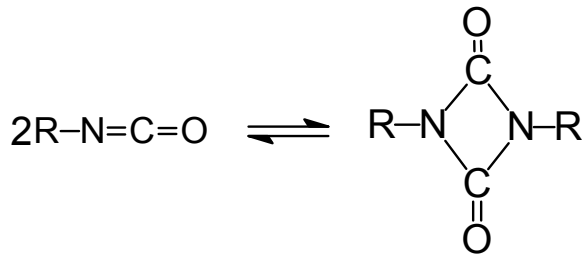

Figure 2.20. Isocyanates undergo reversible dimerization

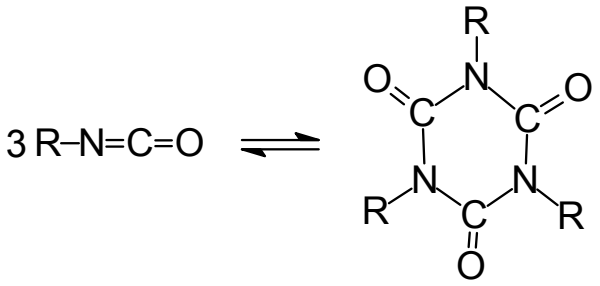

Figure 2.21. Isocyanates undergo irreversible trimerization

2.2.3.2. pMDI Reactions With Protic Nucleophiles

The isocyanate group readily adds to nearly all compounds containing active hydrogen atoms H-X. In each case the mechanism is similar: the active hydrogen adds to the isocyanate nitrogen while the substituent adds to the carbon (Figure 2.22).

Generally the reaction proceeds at room temperature or with only mild heating, although the exact rate of reaction depends on the species, the presence of substituents, steric hindrance, the reaction medium, the temperature and the catalyst [68, 69].

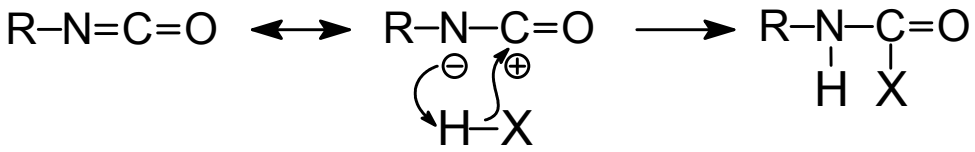

Figure 2.22. Generalized reaction between isocyanates and active proton donors H-X

A brief and partial summary of important reactions between isocyanates and protic nucleophiles follow:

Water: Initially a carbamic acid derivative is formed, which decomposes to a primary amine with the evolution of carbon dioxide. Excess isocyanate may then react with the primary amine to yield ureas (Figure 2.23) [68]. However, in alkaline environments the primary amine is the principal product with urea formation decreased considerably [70].

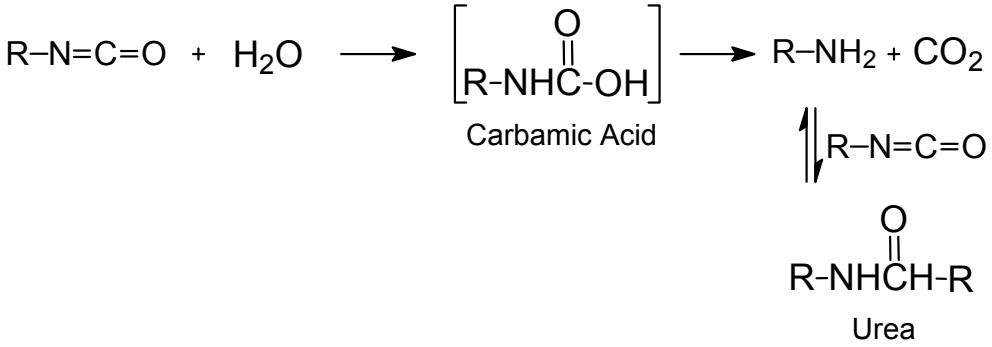

Figure 2.23. Isocyanates react with water to form urea

Alcohols: Isocyanates readily react with alcohol to form urethanes and other carbamates (Figure 2.24). Primary alcohols react the fastest, followed by secondary and then tertiary alcohols [69]. Subsequent reaction with the urethane will yield allophonates (Figure 2.25).

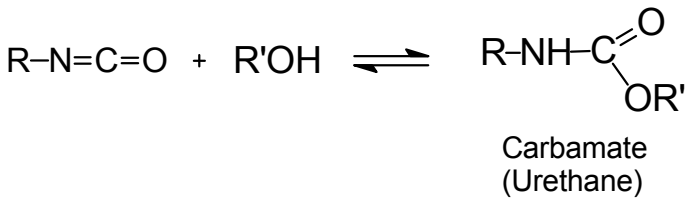

Figure 2.24. Reaction with alcohols results in urethane formation

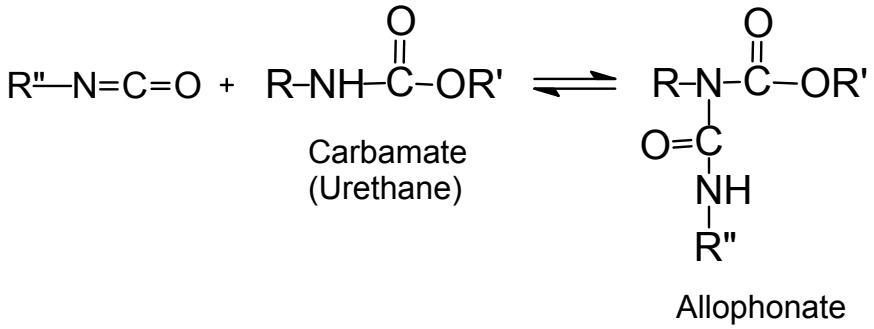

Figure 2.25. Reaction with urethanes yields allophonates

Nitrogenous Compounds: Practically all compounds containing an active hydrogen attached to a nitrogen atom react with isocyanate. Amines give rise to substituted ureas and polyureas (Figure 2.26). This reaction is the fastest of all active hydrogen reactions and is often used for isocyanate titration [71]. Other nitrogenous compounds follow the same general reaction mechanism [69].

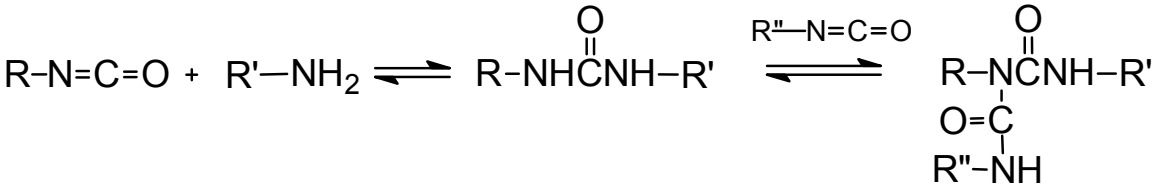

Figure 2.26. Reaction with amines yields urea and polyureas

Carboxylic Acids: Reaction with carboxylic groups generally proceed slowly [67]. Mixed anhydrides are formed, which may subsequently decompose to amides with CO_2 evolution (Figure 2.27). Carboxylic anhydrides and ureas may also be formed through dehydration (Figure 2.28).

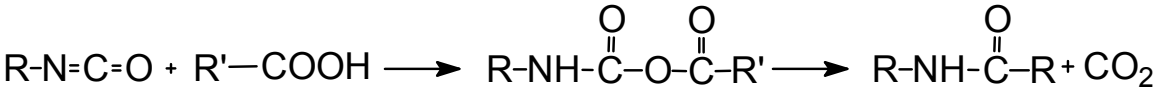

Figure 2.27. Reaction with carboxylic acid yields an amide

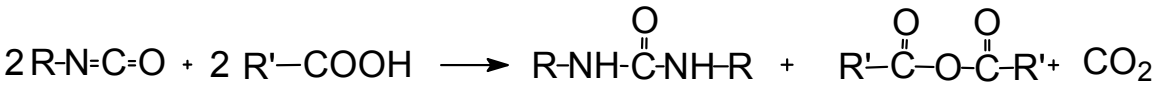

Figure 2.28. Reaction with carboxylic acids may also generate urea and an anhydride

2.2.3.3. pMDI Reactions Other Than With Protic Nucleophiles

Reactions not involving active hydrogen compounds or polymerization are few [68]. A brief sampling of this class includes catalyzed reactions with aromatic hydrocarbons (Figure 2.29a), reactions with chlorine (Figure 2.29b) and reactions with dimethylformamide (Figure 2.29c).

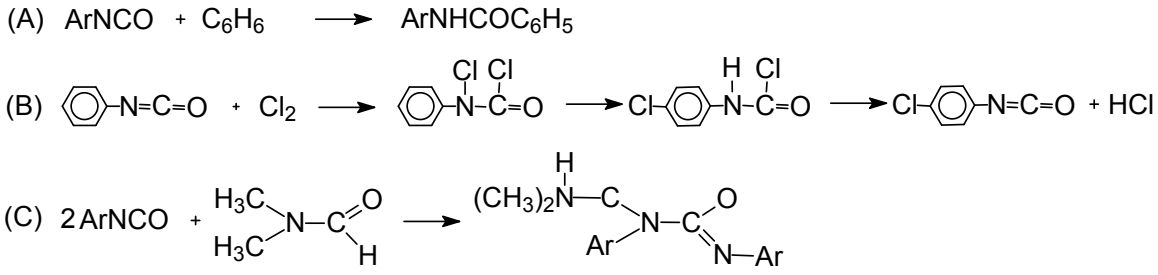

Figure 2.29. Reactions not with protic nucleophiles

2.2.4. Nature of pMDI—Wood Adhesion

As demonstrated previously, pMDI participates in a large variety of reactions. This reactivity has somewhat hindered a complete understanding of the wood-pMDI bondline, despite pMDI's acceptance as an excellent wood adhesive. Wood does contain numerous alcohols and phenols with which pMDI is at least capable of reacting. In fact, many studies have demonstrated that crosslinking will occur [58, 72-75], but these studies were either performed in anhydrous environments, with excess amounts of pMDI, or with the addition of catalyst—each at temperatures and durations that may not adequately represent typical wood bonding conditions. Other studies have instead

inferred the presence of chemical bonding from the strength of the dry-wood adhesive bond [55, 76, 77]. However, such claims based on the performance of unweathered specimens in simple strength based tests are dubious; mechanical interlock and secondary interactions alone can result in strong adhesion with a high degrees of wood failure. More information would be provided by tests such as mode-I fracture cleavage of weathered specimens, which more directly probes the durability of the adhesive bond. Other solid state NMR studies by *Frazier et al* using ^{13}C and ^{15}N NMR have indirectly shown that while covalent urethane linkages are present, they seem to occur to a minor extent and are not likely the dominant mode of adhesion [78-81].

While the extent of wood-pMDI covalent bonding is unclear, both wood and the sorbed water of wood have a catalytic effect of pMDI's condensation into polyureas [82]. Furthermore, low molecular weight pMDI is capable of plasticizing wood [83]; this suggests the possibility that pMDI forms a durable interpenetrating network within the wood polymers.

2.3. Hybrid Resol/Isocyanate Thermosetting Adhesives

PF and pMDI are currently the only adhesive options economically suitable for the mass production of exterior grade wood composites. Despite intense industrial competition, no other adhesive has become a significant option. Given the widespread use of the individual systems, a potentially synergistic adhesive combining both PF and pMDI may hardly seem novel. In fact, vague patent interest in combining these two systems for improved wood bonding actually predates pMDI's commercial introduction as a stand-alone wood adhesive [84]. More specific and rigorous academic investigation began in the early 1970's, shortly after pMDI's commercial implementation as a wood binder [55]. Although these systems have shown some promise, technological obstacles coupled with incomplete understanding of the complexities of these multi-phase systems have prevented any significant commercial implementations within the wood industry. PF/pMDI systems have seen commercial use in the foundry and the polyurethane foam industries since the 1950's [85-87], but all such implementations utilize solvents, catalysts and processing methods that limit technology transfer to the wood composites industry [88, 89]. Despite the aforementioned obstacles, a survey of the research and

patent literature reveals continued interest in hybrid PF/pMDI systems suitable for wood bonding. Particular embodiments include blends containing powdered resol [88], blends containing PF novolak [90], blends containing protected isocyanate groups which deprotect upon hot pressing [91], blends containing emulsifiable pMDI [92], direct physical blends of liquid PF with liquid pMDI [93] and processes for sequential application of PF and pMDI [94].

In regards to possible synergistic performance, one study reports that direct blending of neat PF and pMDI imparts excellent performance to marine and exterior grade plywood [92]. The authors note the adhesive's ability to bond high moisture content veneers of difficult-to-bond species. Furthermore, the increased emulsion viscosity and reduced pot-life did not inhibit successful industrial trials. The same authors found emulsifiable pMDI unsuitable for incorporation in hybrid PF systems; it was proposed that residual emulsifier significantly weakened the bondline. A separate study also reported good mechanical properties when PF and pMDI were sequentially applied to particleboard furnish [94]. In a patent for powdered PF blended with pMDI, better stability was reported in comparison to neat PF resols [88]. The patent also claims improved performance of the blended system relative to sequentially applied powdered resol and pMDI. Within our own research group, a previous study by *Zheng and Frazier* investigated the rheology, chemistry and performance of commercial liquid PF/commercial pMDI physical blends [89]. The blend's viscosity was non-Newtonian and elevated relative to either neat adhesive. Interestingly, the viscosity was found to depend not only on blend ratio, but also on the rate of mixing during blend preparation—indicating the importance of emulsion effects. The unweathered fracture energy of bonded wood specimens was significantly higher for most hybrid adhesives than for either neat adhesive, with maximum toughness observed in a 75:25 weight percent PF:pMDI blend. Sequential application of PF and pMDI did not result in improved fracture performance relative to neat PF. In contrast to other studies, however, accelerated weathering was found to drastically reduce the hybrid adhesive's performance [89]. Base catalyzed hydrolysis of the copolymeric network was suggested.

The chemical composition of cured PF/pMDI hybrids has also been studied by several research groups. Isocyanates are capable of reacting with several functionalities

present in aqueous PF. Potential reaction possibilities include polymerization with PF phenols, polymerization with PF benzylic methylols and self-polymerization with water. Urea is commonly added to PF resins as a formaldehyde scavenger and provides a further reactive site. Uncatalyzed solution rate constants for the reaction of pMDI with various primary hydrogen donors are reported in Table 2.1. By itself this data indicates that pMDI preferentially reacts with PF methylols, while the reaction with water is slightly less favorable and the reaction with PF phenolic hydroxyls appear to be rather unfavorable. However, Table 2.1 is for uncatalyzed reactions in toluene. The highly alkaline environment typical of resols is known to deprotonate the phenolic hydroxyl, increasing its electron density and therefore its reactivity [95]. Although the exact magnitude of this rate increase in the presence of sodium hydroxide catalyst has not been studied, the reactivity of isocyanate and phenols with N,N-dimethylcyclohexylamine catalyst has been studied. Dimethycyclohexylamine functions similarly to sodium hydroxide in that both deprotonate the phenolic hydroxyl group, thereby increasing its reactivity. In this analogous case a rate increase in excess of three orders of magnitude was observed for the reaction between isocyanate and phenolic hydroxyls [96].

Table 2.1. Phenyl isocyanate reactivity in toluene. [71]

	Rate Constant ‡		Activation Energy
Compound	25 ^{0}C	80 ^{0}C	(Kcal/Mol)
Aromatic Amine	10-20	--	--
Primary -OH	2-4	30	8-9
Secondary -OH	1	15	10
Tertiary -OH	0.01	--	--
Water	0.4	6	11
Phenol	.01	--	--
Urea	--		--

‡ Kx10^4, mole^{-1} sec. @ 99% stoichiom

Haider et al.[95] conducted additional kinetic studies under conditions more closely approximating the pH, concentration and solvent conditions that exist in pMDI/resol reactions. The model phenolics were phenol, benzyl alcohol and *p*-hydroxybenzyl alcohol. For all three compounds significant amounts of urethane were detected, indicating co-reaction (Figure 2.30). For phenol and benzyl alcohol the

urethane formation was more prevalent than diphenylurea (DPU) formation. Interestingly, for the less reactive *p*-hydroxybenzyl alcohol case, DPU formation was dominant and no phenolic alcohol reactions were observed. *Zhuang and Steiner* [97] also confirm the greater reactivity of benzylic hydroxyls over phenolic alcohols using DSC kinetic studies. Similarly, *Pizzi and Walton* [98] report preferential urethane relative to urea formation along with significant co-reaction even at room temperature. Their study postulates that resols with a high methylol content and low molecular weight (i.e. resins synthesized with a high F/P ratio for short reaction times) will allow for maximum pMDI co-reaction and maximum performance. In addition, a novel crosslinking reaction mechanism for the formation of methylene bridges between pMDI and PF is suggested (Figure 2.31). The above studies primarily relied on solution FTIR to determine the presence of urethane linkages. These studies therefore do not address the possibility that wood exerts a catalytic effect to significantly alter the reaction pathway. In the study by *Zheng and Frazier* [89] solid state ^{13}C and ^{15}N NMR was used to characterize the adhesive composition of resin impregnated wood cured under conditions closely approximating industrial hot-pressing. Urethane linkages were found to be present in only slightly lower concentrations than the predominant urea linkages. Nuclear relaxation experiments suggested nano-scale phase separation between the two domains. The exact concentration was dependent on the ratio of PF:pMDI used in blend preparation. Surprisingly, blends with the highest fracture toughness were not the same as blends with the highest urethane content, indicating that co-reaction may not be the determining factor in blend performance.

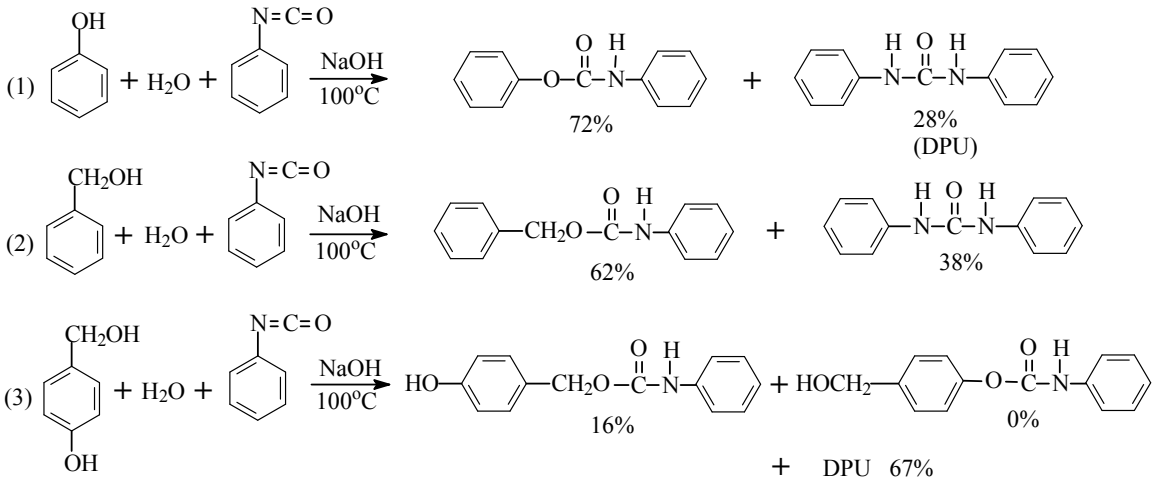

Figure 2.30. Model reactions conducted under conditions approximating those of PF/pMDI hybrid adhesive cure [95]

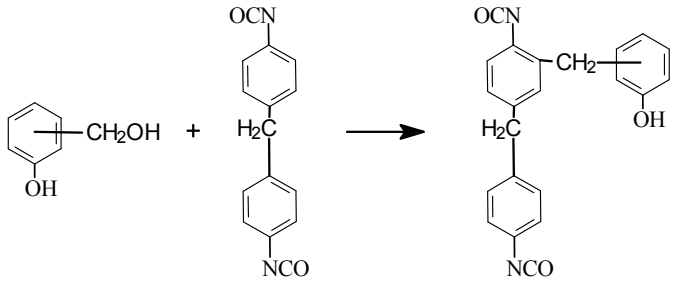

Figure 2.31. PF/pMDI methylene bridge formation as proposed by Pizzi and Walton [98]

Consideration must also be given to how the thermal and hydrolytic stability of urethane linkages will affect bond durability. General upper thermal stability temperatures for the two types of urethane linkages expected to be present in PF/pMDI blends are shown in Figure 2.32. However, urethane degradation is a complex process and depends on both the supramolecular structure of the polymer as well as the chemical conditions to which it is exposed. It is known that water and alkali play catalytic roles in the degradation [99]. In addition, press temperatures during OSB manufacture can reach as high as 220 ^{0}C. *Zheng and Frazier* [89] indeed confirm urethane reductions in certain PF/pMDI blends occurring both after thermal treatment and after accelerated weathering.

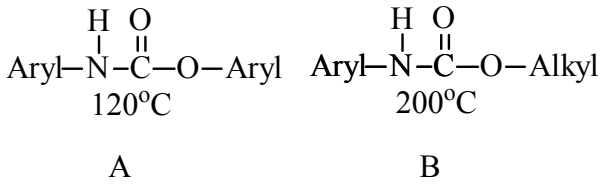

Figure 2.32. Upper thermal stability temperatures of the two urethane structures present in PF/pMDI blends

2.4. Thermoset Characterization

As implied by their name, thermosetting polymers become infusible and insoluble due to chemical reactions accompanying thermal cure. The resulting polymer, if properly processed, is a crosslinked three-dimensional network characterized by infinite molecular weight [100]. Polymerization proceeds from the crosslinking of branched oligomers and the molecular weight rises exponentially. As the reaction continues, eventually a network is formed of infinite molecular weight. This irreversible and abrupt transition is the gel-point. At gelation the polymer loses its liquid-like ability to flow and begins to exhibit properties characteristic of solids.

A separate transition which may occur at any point during cure is vitrification. Vitrification is a reversible and frequency dependent event occurring when the glass transition of the polymer chain segments reaches the cure temperature. It arises from the reduced mobility of constituent polymer chain segments due to continued reaction. Mechanically, vitrification marks the transition from a liquid or rubber to a brittle glass. Chemically, vitrification marks a sharp decrease in the reaction rate as cure shifts from kinetic to diffusion control. Subsequent heating of a polymer above the vitrification temperature results in devitrification and the resumption of kinetic rate control. Isothermal time-temperature-transformation diagrams (Figure 2.33), developed by Gillham, present an elegant summary of this principal [101]. Three critical temperatures are indicated on the temperature axis: T_{g0}, the glass transition of the unreacted material; ${}_{gel}T_g$, the temperature at which gelation and vitrification coincide; and $T_{g\infty}$, the glass transition of the completely reacted network. Time to gelation and vitrification are plotted as a function of the isothermal cure temperature. For instance, just below the

glass transition of the unreacted resin (T_{g0}) the resin is in a glassy state and reaction is very slow to occur. However, between T_{g0} and ${}_{gel}T_g$ the resin reacts without gelation until its rising glass transition equals the cure temperature.

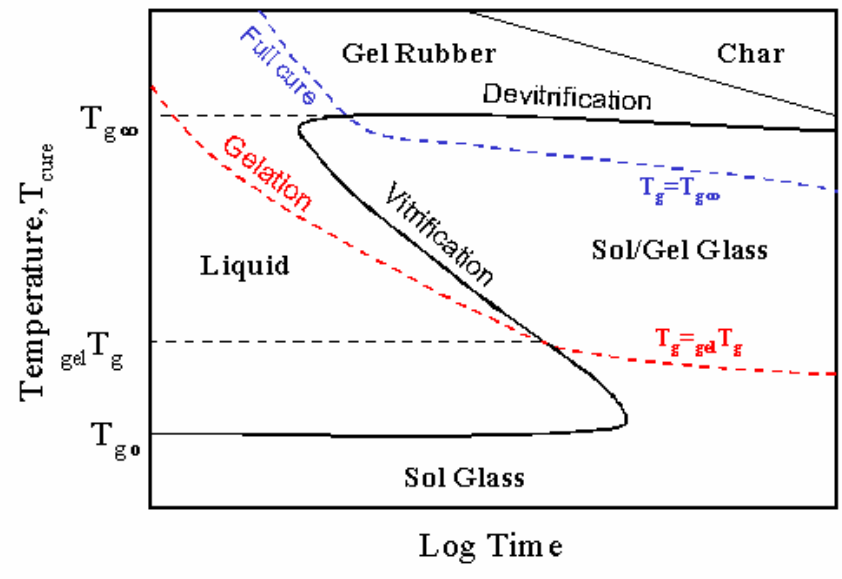

Figure 2.33. Generalized time temperature transition cure diagram [101]

Such diagrams highlight the broad range of polymer properties encountered during thermoset cure. Initially the polymer behaves as a viscous fluid, transitioning to a viscoelastic fluid, a rubber and finally a glass. The modulus of such a polymer may change over 10 orders of magnitude during cure, often necessitating multiple analytical techniques to fully characterize the polymer throughout this range. In the liquid state the polymer viscosity is of large importance, as is the molecular weight's influence on viscosity. Respectively, steady-state flow rheology and gel permeation chromatography are ideally suited to these analyses. The change in mechanical response during cure must be measured separately, generally using dynamic mechanical analysis and small amplitude oscillatory rheology. Polymer curing also results in electrochemical changes that may be studied using dielectric analysis. Finally, thermodynamic and kinetic processes are often studied using differential scanning calorimetry.

2.4.1. Molecular Weight by Gel permeation Chromatography

One of the most important characteristics of a polymeric material is its molecular weight (M) and the associated molecular weight distribution [102]. While all fully cured thermoset materials are characterized by an infinite molecular weight, the properties of different thermosets are still unique as they are derived from the molecular weight and architecture of the specific oligomers during polymerization. In the liquid state molecular weight not only influences the viscosity, but also the reaction kinetics as it relates to the individual polymer mobility. In the solid state the molecular weight of individual chain segments between crosslinks has a profound effect on the mechanical properties of a thermoset.

Gel permeation chromatography (GPC) has developed into one of the most useful methods for routine determination of molecular weights and molecular weight distributions of polymers [102]. GPC is based on the size exclusion principle in which molecules are separated based on their size, or more precisely, their hydrodynamic radii. A solution is passed through a column packed with a porous substrate and the time to elution is recorded. Ideally, interaction between the polymer and the stationary phase is negligent. As such, polymer separation is based solely on entropic effects driving the polymers to diffuse over the largest total free volume possible. Small molecules necessarily have access to a larger portion of the column interstitial area and therefore follow a longer flow path while eluting. Larger molecules elute first while small molecules elute last, allowing for separation.

Early GPC measurements relied on conventional calibration. In this method, samples of known molecular weight were chromatographed to empirically determine the relationship between molecular weight and elution time. Detection was performed using only a concentration detector, typically a differential refractometer. Samples were subsequently analyzed and their elution time was compared to that of the known calibration standards. As polymers are separated based upon molecular size and not molecular weight, calibration standards must be available with a chemical makeup very similar to the polymer of interest. The development by *Benoit et. al.* [103] relating polymer size to the product of molecular weight and intrinsic viscosity, [η], alleviated

this restriction. A differential viscometer added to the detector array allows calibration curves of log([η]*M) versus elution volume to be constructed that are identical for all polymers. Although this method allows for accurate (non-relative) molecular weight information, it still relies on a separate empirical calibration of the instrument's elution profile. As such, the method is susceptible to errors induced by both flow rate variations and non-ideal separation mechanisms. A further refinement was introduced by *Wyatt et. al.* [104] in the form of an inline laser light scattering detector. The light scattering detector provides an absolute means for measuring molecular weight, obviating the need for a calibration curve and accommodating small deviations from ideal SEC mechanisms. However, light scattering detectors are not sensitive to low molecular weight polymer fractions with low dn/dc values and may consequently overestimate the true molecular weight distribution.

GPC of PF resol poses practical difficulties owing to the low solubility of PF in most organic phases. Although reasonably accurate molecular weight distribution calculations have been achieved in GPC systems with an aqueous alkali mobile phase [105, 106], such systems are rather specialized and are not suitable for most routine polymer analyses. Furthermore, switching mobile phase alters the swelling of high performance GPC columns, causing them to prematurely degrade. As such, considerable efforts have been made to find a suitable method of solubilizing PF resins for standard organic phase GPC. Various methods of acetylating PF resins have been attempted; however, each seems to only partially solubilize the resol, resulting in aggregation of the high molecular weight fraction and artificially inflated molecular weight distributions [106-109]. Preparative methods involving precipitating, freeze- or spray-drying resols also appear to artificially alter the molecular weight distribution [107]. In a study by *Calve et. al.* [110], chromatograms were compared for systems using DMF, DMF + 0.1*M* LiCl and THF + 0.4% trichloroacetic acid (TCAA) mobile phases. The polydispersity measured in non-additized DMF was much broader than that measured in either DMF+LiCl or THF+TCAA, indicating aggregation in the non-additized solvent. However, the effectiveness of the additized solvents in entirely preventing aggregation could not be confirmed. More so, it should be noted that the flow paths of most GPC instruments is made of stainless steel, which is not entirely resistant to TCAA [111] and

could therefore discourage continuous use of such an additized mobile phase. A separate study [112] neutralized resol resins in a 2% acetic acid/DMF solution prior to analysis with a non-additized DMF mobile phase. Although not commented on in this paper, the more advanced resins showed a distinct peak eluting before the remainder of the sample, which is characteristic of aggregation [113]. Other studies utilizing TCAA to neutralize resins prior to analyses in a THF mobile phase have demonstrated good results for low molecular weight resols [114] and claimed good results for higher molecular weight samples [115]. However, the accuracy of these results need to be confirmed using alternative methods. In another study, *Nikpour et. al.* [108] treated resols with an ion exchange resin prior to analysis. For the low molecular weight resin studied, their method appears effective and was demonstrated to be an improvement over acetylation, although its suitability for higher molecular weight resols has not been demonstrated.

Despite the aforementioned limitations, organic mobile phase GPC does allow for qualitative comparisons between resins run on the same instrument and continues to be a valuable tool for resol characterization.

2.4.2. Steady State Rheology Flow Characterization

Steady state rheological studies allow for characterization of thermoset viscosity prior to gelation. Measurements are typically made using small angle cone and plate measuring geometries which provide a uniform shear rate across the entire cone surface [116]. The viscosity (η) is related to the shear rate (ẏ) and shear stress (τ) by: $\eta \equiv \frac{\tau}{\dot{\gamma}}$

Many simple non-polymer fluids such as gases, water and toluene exhibit Newtonian flow, where the viscosity is independent of shear rate. Polymer fluids and melts typically exhibit pseudoplastic (shear-thinning) or, less commonly, dilatant (shear-thickening) viscosity profiles. Illustrations of such flow curves are given in Figure 2.34. When the flow properties of pseudoplastic polymer melts and solutions are measured over a wide enough range of shearing, the flow curves generally appear as in Figure 2.35. At low shear rates there is not enough energy to overcome the associations between polymer chains. As a result the zero-shear viscosity is highest. As the shear rate increases the polymer molecules begin to align with the shear field and pseudoplastic behavior is

observed. At the highest shear rates, the molecules are fully aligned and an upper Newtonian plateau is observed.

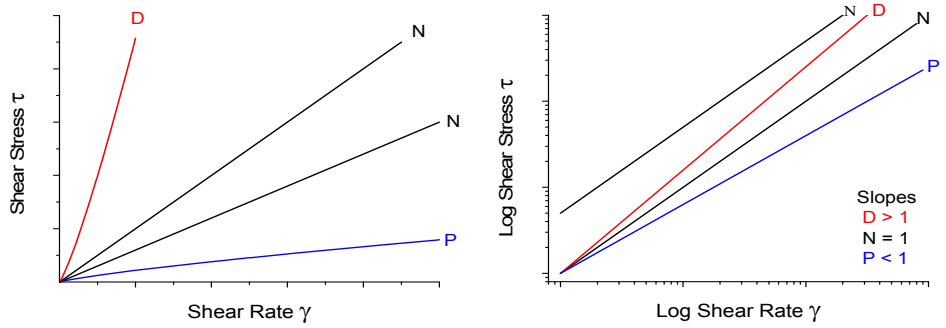

Figure 2.34. Illustration of dilatant (D), Newtonian (N) and pseudoplastic (P) flow behavior

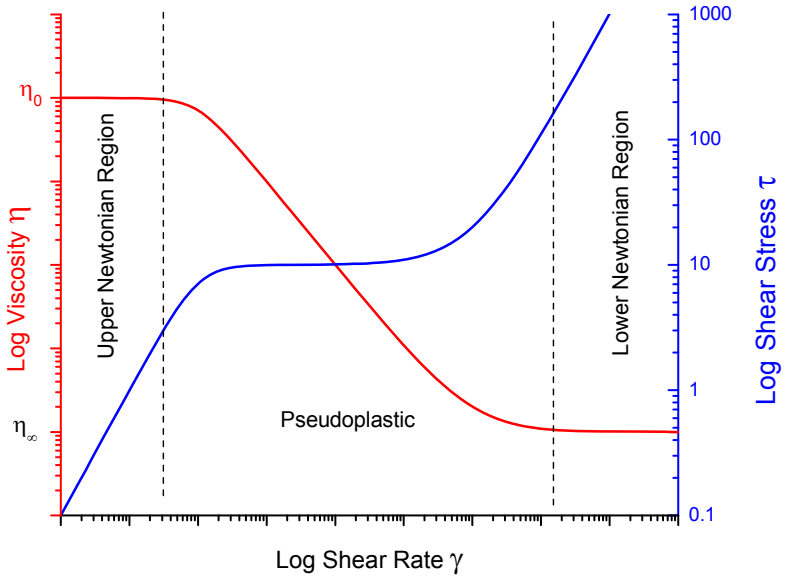

Figure 2.35. Typical broad range polymer flow behavior

Typical formulations of both neat PF resol and neat pMDI exhibit Newtonian behavior over the experimentally accessible range of shear rates. However, hybrid PF/pMDI adhesives are markedly pseudoplastic with a significantly increased zero-shear

viscosity relative to either neat adhesive [89]. Such behavior is typical for emulsion systems, although adhesive advancement through co-reaction may also contribute.

Adhesive viscosity plays a critical role in adhesive penetration into wood and can at least theoretically be related by the Washburn equation [117]:

$$L = \sqrt{\frac{\gamma_L (Cos\sigma) rt}{2\eta}}$$

where L is the depth of penetration, γ_L is the adhesive surface energy, σ is the contact angle between the wood capillary and the resin, r is the capillary radius and t is the time. However, for waterborne adhesives such as PF, this equation typically overestimates the penetration depth as it neglects the increase in viscosity occurring as water is preferentially drawn from the resin bulk into the wood cell wall [118].

2.4.3. Dynamic Rheological Cure Characterization

Dynamic rheological methods are well suited to thermoset cure characterization; the small oscillatory strain that is imposed does not disrupt molecular structure development [119]. However, during cure a thermoset's modulus may span well over three orders of magnitude, making it difficult to measure the entire range of material properties in a single experiment [120]. Typically, dynamic mechanical analysis (DMA) is used to measure the post-gelation, solid state properties of the system, whereas parallel plate small amplitude oscillation rheology is commonly used to monitor the properties surrounding the critical gel transition. However, many novel variations exist to overcome the above instrumental limitations. For instance, both fiberglass and wood substrates have been impregnated with adhesive to allow measurement of gelation and vitrification in a single DMA or parallel plate rheology experiment [48, 49, 51, 89, 121-126]. For wood substrates the method has the advantage of studying the thermosetting reactions in-situ, accounting for the catalytic activation wood can have on resin cure. Data interpretation, however, may be complicated by the presence of overlapping wood relaxations in the temperature region of interest. Furthermore, in the liquid state the mechanical properties of both impregnated systems are dominated by the substrate, overshadowing the early viscous response.

Thermoset gelation is defined unambiguously as the instant the weight average molecular weight diverges to infinity [119]. Knowledge of the gel point is important as it defines the processing window of an adhesive; all shaping and flow of the polymer must occur before gelation. Early rheological determinations of gelation were extrapolated from steady state experiments: either the divergence of zero shear viscosity or the onset of an equilibrium modulus (Figure 2.36). However, such methods relied on extrapolation and required long experiments at low shear rates to avoid disrupting the fragile critical gel formation [119]. More recently, using dynamic methods the crossover of the storage modulus G' and the loss modulus G" has, perhaps erroneously, been widely used to define gelation. As extensively shown by *Winter* [119, 127], such a definition is only valid for stoichometrically balanced thermoset chemistries far away from their glass transition. A more rigorous definition of the gel point is the point at which the loss tangent (tan δ) becomes independent of the frequency of dynamic oscillation. Experimentally, the frequency independence of tan δ can be measured using a multiwave experiment [128, 129]. In such an experiment, multiple oscillation frequencies are superimposed and the resulting individual stress strain data for each frequency is deconvoluted using a Fourier Transformation.

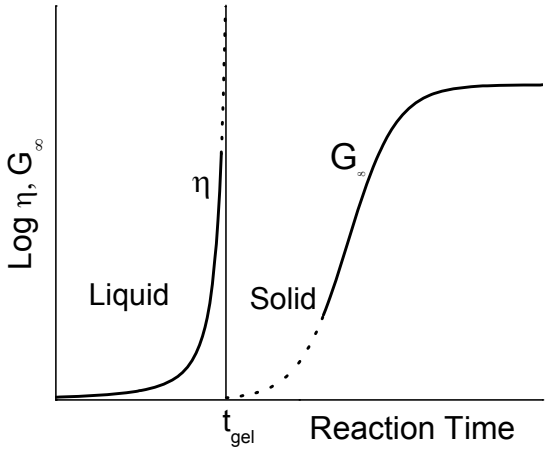

Figure 2.36. Extrapolation of the gel point from steady shear viscosity and equilibrium modulus values

Unlike gelation, there is not a generally accepted criterion for defining vitrification. Various definitions include the onset of G' frequency dependence, the peak

in tan δ at 1Hz, the peak in G" at 1Hz and the end of frequency dependence in G' [130]. Furthermore, for resol adhesives characterization is hindered by sample drying, boiling and foaming, resulting in non-uniform sample geometries.

2.4.4. Dielectric Cure Characterization

The principal advantage of dielectric analysis (DEA) in studying wood adhesive cure is its ability to monitor cure processes in-situ, at precise locations within a composite mat under actual pressing conditions. By measuring the mobility of ions and the rotational mobility of dipoles, DEA can provide information on chemical events such as gelation and vitrification. *Rials et. al. [131-134]* have used DEA extensively to study the cure kinetics of pMDI within composite mats. They found DEA more sensitive to the latter stages of network formation and vitrification than differential scanning calorimetry. Furthermore, kinetic models based on DEA analysis were found to fairly accurately represent in-situ pMDI curing reactions. For PF resols, *Garcia and Wang* [135] were able to monitor in-situ cure using DEA. However, the ionic mobility of moisture throughout the sample was found to be problematic.

2.4.5. Cure Kinetics and Thermodynamics Using DSC

Differential scanning calorimetry (DSC) is one of the most widely used thermal analysis techniques for characterizing thermosetting materials. In a DSC experiment, heat flow changes are measured under a controlled temperature profile. Such experiments are capable of measuring the extent and rate of chemical conversion, the glass transition temperature, the onset of vitrification, melting, crystallization, physical ageing and degradation [100]. In conventional DSC the sample is subjected to either a linearly ramped heating profile or a constant isothermal temperature. Modulated DSC (MDSC) is a more sophisticated extension of this general technique. In MDSC a sinusoidal perturbation is superimposed on top of the underlying linear heating rate (Figure 2.37), such that: $T = T_0 + \beta t + A_T \sin(2\pi ft)$, where T is the temperature, T_0 is the initial temperature, β is the underlying heating rate, A_T is the temperature modulation amplitude, f is the modulation frequency and t is the time. MDSC has an added

advantage over conventional DSC as it allows the heatflow to be de-convoluted into both the reversible and irreversible components. Thus, MDSC allows separation of overlapping events such as glass transitions, enthalpic relaxations, crystallization, curing, ect. MDSC also offers improved sensitivity towards heat capacity (C_P) measurements [136, 137]. Furthermore, quasi-isothermal MDSC experiments allow accurate detection of vitrification from the resultant step-wise decrease in C_p.

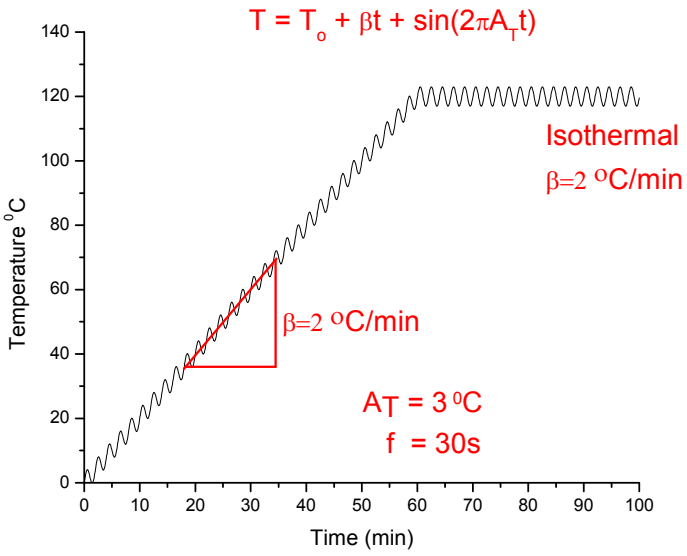

Figure 2.37. Illustration of MDSC temperature ramp and isothermal experiments

DSC studies of PF resols have typically been limited to conventional DSC [53, 138-143]. For both liquid and powdered resols, hermetic or high-pressure DSC pans are necessary to suppress endothermic volatilization events that overlap with exothermic cure. Two exotherm peaks are typically observed during resol cure. The first has generally been attributed to hydroxymethylation while the second exotherm has been attributed to condensation. This is supported by studies investigating exotherm behavior as a function of F/P ratio [143]. However, some disagreement surrounds the precise chemical significance of the exotherms [53, 144], highlighting the fact that DSC can not directly provide insight into chemical structure.

DSC studies of pMDI are more limited. *Galbraith and Newman* [58] used DSC to infer urethane bonding between pMDI and wood. However, the low sensitivity of

DSC required unrealistically large pMDI resin loadings, likely altering the product formation ratios. More recently, *Frazier and Das* [145] studied the wood species dependence of pMDI cure. Although higher activation energies were observed for pine relative to yellow-poplar specimen, catalytic activation was also higher in pine allowing for faster cure completion.

Regarding hybrid PF/pMDI adhesives, DSC investigations have only been performed by Zheng and Frazier [89]. Using MDSC a residual softening was observed between 70 and 90 °C in fully cured hybrid samples. The nature of the softening could not be determined, although it was suggested as a possible indication of micro-phase separation.

2.5. References

1. Knop, A. and W. Scheib, *Chemistry and Application of Phenolic Resin*. 1979, New York: Springer-Verlag.
2. Chen, D.T. and K.J. Laidler, Trans. Faraday. Soc., 1962. **58**: p. 480.
3. Bocker, E., Phenole and Alkylphenole, in Ullmanns Encyclopadie d. Techn. Chem. 1962, Urban und Schwarzenberg: Munchen.
4. Marra, A.A. 1992. Technology of Wood Bonding: Principles In Practice. New York: Van Nostrand Reinhold.
5. Sellers, T. 2004. Panel World 45 (1):34-36
6. Ko, H.C., et al., J. Chem. Eng. Data, 1964. **9**: p. 122.
7. Kortum, G., W. Vogel, and K. Andrusson, *Dissociation Constants of Organic Acids in Aqueous Solution*. 1961, London: Butterworth.
8. Kropf, H., Chem. Ing. Techn., 1964. **36**: p. 759.
9. Ni, N., Japan Chemical Week, 1976: p. 628.
10. Ni, N., Chem. Ind., 1977. **29**: p. 525.
11. Bolton, P.D., F.M. Hall, and J.H. Rece, Spectrochim. Acta, 1966. **22**: p. 1149.
12. Jordan, W. and B. Cornils, *Phenole*, in *Methodicum Chimicum*. 1975, Thieme: Stuttgart. p. 105.
13. Flemming, J.B., J.R. Lambrix, and J.R. Nixon, Hydrocarbon Proc., 1976: p. 185.
14. McNeil, D., *Cresols*, in *Encyclopedia of Chemical Technology*. 1966, Interscience: London.
15. Pujado, P.R., J.R. Salazar, and C.V. Berger, Hydrocarbon Proc., 1976: p. 91.
16. Seubold, F.H. and W.E. Vaugham, J. Amer. Chem. Soc., 1953. **75**: p. 3790.
17. West, R.C., ed. *Handbook of Chemistry and Physics*. 48 ed. 1967, the chemical rubber company: cleaveland.
18. Baekeland, L.H. 1907: US Patent # 942809.
19. Nielsen, D. and K.K. Sudan. International Particleboard/Composite Materials Symposium. 1996. Pullman, WA.
20. Zsvitsas, A.A. and R.D. Beaulieu, Am. Chem. Soc. Div. Org. Coatings and Plastic Reprints, 1957. **27**: p. 100.

21. Grenier-loustalot, M.F., S. Larroque, and P. Grenier, Polymer, 1996. **37**(6): p. 939.
22. Pizzi, A., ed. *Wood Adhesives Chemistry and Technology*. Vol. 2. 1989, Marcel Dekker: New York.
23. Knop, A. and W. Scheib, *Chemistry and Application of Phenolic Resins*. 1979, New York: Springer-Verlag.
24. Werstler, D.D., Polymer, 1986. **27**(5): p. 750-756.
25. Sprengling, G.R. and C.W. Lewis, J. Am. Chem. Soc, 1953. **75**: p. 5709.
26. Ferguson, L.N., Chem. Revs., 1952. **50**: p. 47.
27. Freeman, J.H. and C.W. Lewis, J. Am. Chem. Soc, 1954. **76**: p. 2080-2087.
28. Caesar, P.D.a.A.N.S., Ind. Eng. Chem, 1948. **40**: p. 922-928.
29. Peer, H.G., REc. Trav. Chim., 1959. **78**: p. 851.
30. Peer, H.G., Rec. Trav. Chim., 1960. **79**: p. 825.
31. Zinke, A., J. Appl. Chem. (London), 1951. **1**: p. 257-266.
32. Megson, N.J.L., *Phenolic Resin Chemistry*. 1958, New York: Academic Press.
33. Martin, M.L., J.-J. Delpuech, and G.J. Martin, *Practical NMR Spectroscopy*. 1980, Heyden, London.
34. Yeddanapalli, L.M. and D.J. Francis, Makromol. Chem, 1962. **119**: p. 17.
35. Kim, M., G.Y. Wu, and L.W. Amos, Journal of Polymer Science. Part A: Polymer Chemistry, 1997. **35**: p. 3275-3285.
36. Kim, M.G., G.T. Tiedeman, and L.A. Amos. *Weyerhaeuser Science Symposium*. 1980.
37. Pizzi, A. and T. Walton, *Advanced Wood Adhesives Technology*. 1994, New York: Mercel Dekker, Inc.
38. So, S., et al., Journal of Applied Polymer Science, 1990. **39**(3): p. 531-538.
39. Sellers, T.J., *Plywood and Adhesive Technology :* . 1985, New York: Marcel Dekker, Inc.
40. Kim, M.G., Y. Wu and L.W. Amos, Journal of Polymer Science, Part A. Polymer Chemistry, 1997. **35**(15): p. 3275-3285.
41. Fyfe, C., A.A. Rudin, and W. Tchit, Macromolecules, 1980. **13**: p. 1322-1324.
42. Maciel, G.E., et al., Macromolecules, 1983. **16**: p. 598-604.
43. Johns, W.E., *Chapter 3*, in *Wood Adhesives: Chemistry and Technology.* 1989, Marcel Dekker, Inc.: New York.
44. Pizzi, A., J. Adhes. Sci. Technol, 1990. **4**: p. 589.
45. Pizzi, A. and G. De Sousa, Chem. Phys., 1992. **164**: p. 203.
46. Pizzi, A. and N.J. Eaton, J. Adhes. Sci. Technol, 1987. **1**: p. 191.
47. Mizumachi, M. and H. Morita, Wood Sci., 1975. **7**(3): p. 256-260.
48. Lu, X. and A. Pizzi, Holz als Roh- und Werkstoff, 1998. **56**: p. 339-346.
49. Onic, L., et al., International Journal of Adhesion & Adhesives, 1998. **18**: p. 89-94.
50. Pizzi, A. and R. Garcia, J. Appl. Polym. Sci., 1998. **70**: p. 1111.
51. Pizzi, A., X. Lu, and R. Garcia, J. Appl. Polym. Sci., 1999. **71**: p. 915.
52. Pizzi, A., ed. *Wood Adhesives Chemistry and Technology*. Vol. 1. 1983, Marcel Dekker: New York.
53. Holopainen, T., et al., Journal of Applied Polymer Science, 1997. **66**(6): p. 1183-1193.

54. So, S. and A. Rudin, Journal of Applied Polymer Science, 1990. **41**(1-2): p. 205-232.
55. Deppe, H.J.a.K.E., Holz als Roh-und Werkstoff., 1971. **29**(2): p. 45-50.
56. Sellers, T.J., *Wood Adhesive Innovations and Applications in North America.* Forest Products Journal, 2001. **51**(6): p. 12-22.
57. Marra, A.A., Technology of Wood Bonding: Principles in Practice. 1992: Van Nostrand Reinhold.
58. Galbraith, C.J. and W.H. Newman. *FRI Bulletin No.177. Pacific Rim Bio-Based Composites Symposium*. 1992. Rotorua, New Zealand.
59. Palardy, R.D., et al., *Wood Adhesives 1990*. 1990. p. 124-128.
60. Clark, R.J., J.J. Karchesy and R.L. Krahmer, Forest Products Journal, 1988. **38**(7/8): p. 71-75.
61. Moriarty, C. Proc. of 33rd International Particleboard/Composite Materials Symposium. 1999. Pullman, WA.
62. Twitchett, H.J., Chemical Society Reviews, 1974. **3**(2): p. 209-230.
63. Ranney, M.W., *Isocyanates Manufacture*. 1972, Park Ridge, New Jersey: Noyes Data Corporation.
64. Ulrich, H., *Chemistry and Technology of Isocyanates*. 1996, New York: John Wiley & Sons, Inc.
65. Tennant, G. Comprehensive Organic Chemistry, ed. D.H.R. Barton and W.D. Ollis. Vol. 2. 1979, Oxford: Pergamon Press.
66. Parodi, F., *Isocyanate Derived Polymers*, in *Comprehensive Polymer Science*, G.A. Allen, Editor. 1989, Pergamon Press: New York. p. 387-411.
67. Wispsza, Z., Polyurethanes: Chemistry, Technology and Applications. 1993, New York: Ellis Horwood.
68. Saunders, J.H. and R.J. Solcombe, Chem. Revs., 1948. **43**: p. 203-218.
69. Wirpsza, Z., Polyurethanes: Chemistry, Technology and Applications. 1993, New York: Ellis Horwood.
70. Wurtz, Compt. Rend., 1948. **27**: p. 242.
71. Szycher, M., *Szycher's Handbook of Poyurethanes*. 1999, New York: CRC Press
72. Owen, N.L., W.B. banks, and H. West, J. Molecular Structure, 1988. **175**: p. 389-394.
73. Rowell, R.M. and W.D. Ellis, Wood Sci., 1979. **12**(1): p. 52-58.
74. Rowell, R.M. and W.D. Ellis, ACS Symposium Series, 1981. **172**: p. 264-284.
75. Rowell, R.M., W.C. Feist, and W.D. Ellis, Wood Sci., 1981. **13**(4): p. 202-208.
76. Deppe, H.J.a.K.E. Proc. 11th International Particleboard/Composite Materials Symposium. 1977. Pullman, WA.
77. G.W., B. and R.P. Redman. in Proceedings of the FESYP International Particleboard Symposium. 1978. Hamburg.
78. Wendler, S.L. and C.E. Frazier, Journal of Adhesion, 1995. **50**: p. 135-153.
79. Ni, J. and C.E. Frazier, Journal of Adhesion, 1998. **66**: p. 89-116.
80. Wendler, S.L. and C.E. Frazier, Journal of Applied Polymer Science, 1996. **61**: p. 775-782.
81. Wendler, S.L. and C.E. Frazier, International Journal Of adhesion and Adhesives, 1996. **16**: p. 179-186.

82. Pizzi, A., B. Mtsweni, and W. Parsons, Journal of Applied Polymer Science, 1994. **52**: p. 1847-1856.
83. Das, S. and C.E. Frazier. in *28th ACS National Meeting*. 2004. Philadelphia: ACS.
84. Pratt, B.C. and H.S. Rothrock, *Bonding of laminates by means of isocyanates*. 1947, (E. I. du Pont de Nemours & Co.). US.
85. *Cellular artificial resins*. 1949, (Equipement menager et industriel). FR.
86. Pollock, J.M. and N.H. Ray, *Phenol- and urea-formaldehyde resin-curing agents*. 1963, (Imperial Chemical Industries Ltd.). Application: GB
GB. p. 2 pp.
87. Phillips, T.L., *Phenol-formaldehyde foams*. 1962, (Distillers Co. Ltd.). Application: GB
GB. p. 3 pp.
88. Rosthauser, J.W. and W.D. Detlefsen. 2001: US.
89. Zheng, J., Studies of PF Resol/Isocyanate Hybrid Adhesives, in Wood Science and Forest Products. 2000, Virginia Tech: Blacksburg, VA.
90. Rosthauser, J.W. and H.G. Schmelzer. 2001: US.
91. Miller, T.R., L.D. Creel, and W.D. Detlefsen. (2002): US.
92. Pizzi, A., J. Valenzuela, and C. Westermeyer, Holzforschung, 1993. **47**: p. 68-71.
93. Hsu, W.-H. 2001: US.
94. Hse, C.Y. 1980: US.
95. Haider, K.W., et al. *Wood Adhesives 2000, Extended Abstracts*. 2000. South Lake Tahoe, NV: Forest Products Society.
96. Kresta, J.E., A. Garcia, and K.C. Frisch, ACS Symposium Series, 1981. **172**(27): p. 403-417.
97. Zhuang, M. and S.P. R., Holzforschung, 1993. **47**: p. 425-434.
98. Pizzi, A. and T. Walton, Holzforschung, 1992. **46**(6): p. 541-547.
99. Williams, A., J. Chem. Soc., Perkin Trans, 1972. **2**: p. 808-812.
100. Prime, R.B., *Thermal Characterization of Polymeric Materials*, ed. E.A. Turi. 1997, New York: Academic Press.
101. Wisanrakkit, G., J.K. Gillham, and J.B. Enns, Journal of Applied Polymer Science, 1990. **41**: p. 1895-1912.
102. Campbell, D., R.A. Pethrick, and J.R. White, *Polymer Characterization--Physical Techniques*. 2 ed. 2000, United Kingdom: Stanley Thornes Ltd.
103. Benoit, H., Z. Grusic, and P. Rempp, J. Polym. Sci. B, 1967. **5**: p. 753.
104. Wyatt, D., et al., Am. Lab., 1988. **20**: p. 108.
105. Sellers, T.J. and M.L. Prewitt, J. Chromotogr., 1990. **513**: p. 271.
106. Kim, M.G., et al., Ind. Eng. Chem. Res, 1992. **31**: p. 973-979.
107. Wellons, J.D. and L. Gollob, Wood Sci., 1980. **13**: p. 68.
108. Yazaki, Y., et al., Holzforschung, 1994. **48**: p. 41-48.
109. Kim, M.G. and L.W. Amos, Ind. Eng. Chem. Res, 1991. **30**: p. 1151-1157.
110. Riedl, B., M.-J. Vohl, and L. Calve, J. Appl. Polym. Sci., 1990. **39**: p. 341-353.
111. Cole-Parmer, Chemical Compatability Database. 2006.
112. Myers, G.E., et al., Journal of Applied Polymer Science, 1991. **43**(2): p. 237-250.
113. Welch, S., et al., *Viscotek GPC School Handbook*. 2004, Viscotek Corporation. p. 58.
114. Bain, D.R., Polymer, 1984. **25**: p. 403-404.

115. Mbachu, R., R.G. Schmidt, and B.M. Broline, *Wood Adhesives 2000, Extended Abstracts.* . 2000, South Lake Tahoe, NV: Forest Products Society.
116. Rosen, S.L., *Fundamental Principles of Polymeric Materials*. 1993, New York: John Wiley.
117. Denesuk, M., et al., J. Colloid and Interface Sci., 1993. **158**: p. 114-120.
118. de Meijer, M., K. Thurich, and H. Militz, Holz als Roh- und Werkstoff, 2001. **59**: p. 35-45.
119. Winter, H.H., Polymer Engineering and Science, 1987. **27**(22): p. 1698-1702.
120. Pawlowski, H. and X. Xu. *Anual Technical Conference-Society of Plastic Engineers*. 1999: Society of Plastic Engineers.
121. Kim, M.G., W.L.S. Nieh, and R.M. Meacham, Ind. Eng. Chem. Res, 1991. **30**(4): p. 798-803.
122. Lorenz, L.F. and A.W. Christiansen, Ind. Eng. Chem. Res, 1995. **34**: p. 4520-4523.
123. Umemura, K.A.T.a.S.K., Journal of Wood Science, 1998. **44**: p. 204-210.
124. Umemura, K., A. Takahashi, and S. Kawai, Journal of Applied Polymer Science, 1999. **74**: p. 1807-1814.
125. Laborie, M.-P., *Ph.D. Dissertation*. 2002, Virginia Polytechnic Institute and State University: Blacksburg, VA.
126. Wolcott, M.P., Presentation given at the 55th Forest Products Annual Meeting. Baltimore, MD. 2001.
127. Winter, H.H. and F. Chambon, J. Rheol., 1986. **30**: p. 367-382.
128. *Multiwave Oscillation*. TA Instruments Rheology Applications Notes (2001)
129. Lange, J., et al., Polymer, 2000. **41**: p. 5949-5955.
130. Peng, W. and B. Riedl, Polymer, 1994. **35**(6): p. 1280-1286.
131. Wolcott, M.P. and T.G. Rials, *In situ cure monitoring of adhesives for wood-based composites.* Proceedings of the Washington State University International Particleboard/Composite Materials Symposium, 1995. **29th**: p. 185-193.
132. Harper, D.P., M.P. Wolcott, and T.G. Rials, *Assessment of pMDI cure in saturated steam environments.* Wood Adhesives 2000, [International Symposium], 7th, S. Lake Tahoe, NV, United States, June 22-23, 2000, 2001: p. 73-79.
133. Harper, D.P., M.P. Wolcott, and T.G. Rials, Evaluating cure of a pMDI-wood bondline using spectroscopic, calorimetric and mechanical methods. Journal of Adhesion, 2001. **76**(1): p. 55-74.
134. Harper, D.P., M.P. Wolcott, and T.G. Rials, *Evaluation of the cure kinetics of the wood/pMDI bondline.* International Journal of Adhesion and Adhesives, 2001. **21**(2): p. 137-144.
135. Garcia, P. and S. Wang, Wood and Fiber Science, 2005. **37**: p. 619-698.
136. Reading, M., D. Elliot, and L. Hill, Trends in Polymer Science, 1993. **1**(8): p. 248-253.
137. Reading, M., D. Elliot and L. Hill, Journal of Thermal Analysis, 1993. **40**(13): p. 949-955.
138. Wang, X.M., et al., Polymer, 1994. **35**(26): p. 5685-5692.
139. Vick, C.B. and A.W. Christiansen, Wood and Fiber Science, 1993. **25**(1): p. 77-86.

140. Sebenik, A., I. Vizovisek, and S. Lapanje, European Polymer Journal, 1974. **10**: p. 273-278.
141. Park, B.D. and Riedl, Journal of Applied Polymer Science, 2000. **77**: p. 1284-1293.
142. Kenny, J.M., G. Pisaniello, F. Farina and S. Puzziello, Thermochimica Acta, 1995. **269**(270): p. 201-211.
143. Christiansen, A.W.a.L.G., Journal of Applied Polymer Science, 1985. **30**: p. 2279-2289.
144. Toffey, A. and W.G. Glasser, Journal of Applied Polymer Science., 1999. **73**(10): p. 1879-1889.
145. Das, S., in *Macromolecular Science and Engineering*. 2005, Virginia Tech: Blacksburg.

CHAPTER 3. MORPHOLOGICAL ANALYSIS OF PF/PMDI HYBRID WOOD ADHESIVES

The content of this chapter is presented in the form of a paper which has been submitted to the *Journal of Adhesion Science and Technology.*

Abstract- Simple blends of polymeric methylenebis(phenylisocyanate), pMDI, dispersed in aqueous phenol formaldehyde, PF, were studied to determine how the emulsion structure impacted the resulting solid-state morphology. Shortly after mixing, optical microscopy of the liquid emulsions revealed rapid membrane formation around the dispersed pMDI droplets. This membrane appeared to arise from the pMDI/PF reaction and not the pMDI/H_2O reaction. Field emission scanning electron microscopy (FE/SEM) and atomic force microscopy (AFM) of partially cured blends detected a pMDI-borne dispersed phase exhibiting a sharp phase-boundary. AFM revealed a halo surrounding the dispersed phase. This halo feature extended into the PF continuous phase; it was interpreted as evidence for a copolymeric region, suggesting that pMDI diffused into the continuous phase. Dynamic mechanical analysis of the partially cured blends revealed two overlapping secondary transitions, interpreted as phenolic relaxations from neat PF and separately from a PF/pMDI copolymer. Supporting the putative copolymer formation is the fact that the pMDI dispersed phase is associated with accelerated cure in comparison to neat PF. Collectively, the results indicate that the liquid emulsion morphology is largely preserved in the resulting solid, but that some interdiffusion occurs between phases during cure. The resulting copolymer formation accelerates cure and possibly enhances toughness near the phase boundary.

3.1. Introduction

Alkaline phenol-formaldehyde has been an important wood adhesive since early in the 20th century. Only in the last 35 years has polymeric

methylenebis(phenylisocyanate) emerged as an alternative for the manufacture of certain wood-based composites. By North American standards these two resins (respectively PF and pMDI) remain the only choice for the mass production of exterior grade structural wood composites. No other adhesive has become a significant option.

This work speaks to a possible alternative involving a physical blend of aqueous PF with liquid pMDI. At first glance such a system may hardly seem novel. However, upon blending these immiscible resins interesting possibilities arise from both the structure of the resulting emulsion and from the corresponding solid-state multiphase morphology. Previous results from our laboratory demonstrated that emulsion effects dominated the properties of these blends and that co-reaction between resins provided an added layer of complexity [1]. Therefore, commercial implementation of this system will likely require extensive research on the interactions between emulsion effects and PF resin chemistry. Compelling justification for such development was first provided by Pizzi et al [2]; PF/pMDI blends provided excellent performance for plywood made with difficult-to-bond woods and remarkable resistance to boiling water was also claimed. Since this 1993 report, no significant industrial use of the PF/pMDI blend has occurred in North America. However, there has been recent industrial interest as revealed in the United States patent literature. One invention includes the blending of pMDI with powdered PF [3]. Another involves the preparation of protected phenolics that deprotect during hot-pressing and subsequently react with pMDI [4]. A third patent discusses the simplest method, which is to mix aqueous PF with liquid pMDI just prior to adhesive application [5].

Our research focuses on this latter system, a simple physical blend of aqueous PF and liquid pMDI. Both classes of adhesives are commercially available and hence could provide a cost effective approach toward adhesive development. Fracture cleavage of bonded-wood double cantilever beams revealed that hybrids containing a PF continuous phase were substantially toughened [1]. This toughening was attributed to a putative polyurea/biuret/urethane dispersed phase arising from pMDI. Hybrids containing a dispersed PF phase, however, did not substantially toughen the isocyanate-borne continuous phase [1]. Direct evidence for a solid-state multiphase morphology was not provided in our previous paper; it was instead inferred from the rheology of the liquid

emulsions. The objective of this work is to provide some insight into the solid-state morphology of these hybrid resins.

3.2. Experimental

3.2.1. Materials and Reagents

Commercial OSB resins were used as received; these were liquid PF resol (Core® OSB resin from Dynea) and pMDI (Rubinate® 1840 from Huntsman Polyurethanes). The resols had a viscosity of about 300 mPa•s (25^{o}C), a solids content of 50% and pH = 10.6 or 11.8. The pMDI had a 100% solids content with a viscosity of 166 mPa•s (25^{o}C) and an NCO content of 31%. All neat resins exhibited Newtonian flow.

3.2.2. Blend Preparation

Only one blend ratio was studied, containing 75 parts PF resin solids to 25 parts pMDI resin solids (hereafter referred to as PF75). This blend ratio was chosen because of its substantial toughness at relatively low pMDI loadings [1]. No fillers, extenders or any other additives were used.

Blends were prepared using two different techniques: hand-mixing and mechanical agitation. For each technique, blends were mixed at two different shear rates: "high-shear" and "low-shear"—creating four sample-types. Hand-mixed blends were prepared in 10 gram batches inside a 50 ml glass beaker (i.d. = 40 mm) by stirring at approximately 200 rpm (high-shear) or 30 rpm (low-shear) for one minute using a 9.5 mm diameter glass rod. Hand-mixed blends were used for all analytical methods except optical microscopy. Mechanically-agitated blends were prepared in 45g batches inside a 40 mm diameter glass vessel and agitated at either 1,500 rpm (high-shear) or 200 rpm (low-shear) for one minute using a digital mixer fitted with a one inch diameter, three-blade propeller (Cole Parmer 04553-60). Only mechanically-agitated blends were used for optical microscopy.

3.2.3. Blend Curing

Partially-cured, solid samples were prepared for dynamic mechanical analysis, scanning electron microscopy, atomic force microscopy and infrared spectroscopy. Immediately after blending, the resin mixtures were poured into Teflon molds and cured in a convection oven (60°C, 13.5 hours) yielding flexible non-tacky samples, approximately 6 mm in thickness. Partially-cured neat PF resins were similarly prepared, but cured for 36 hours to achieve a similar degree of rigidity, as judged by manual inspection. Upon cooling to room temperature both the neat PF and the PF75 samples were brittle glasses. Unless noted otherwise, partially-cured samples were stored over dry ice for a maximum of 24 hours prior to analysis.

3.2.4. Optical Microscopy of Liquid Blends

Optical microscope images were obtained for mechanically-agitated PF75. Portions of high-shear and low-shear hybrid resins were immediately diluted with an equal volume of pH 10 buffer (500 mL of 0.025M sodium tetraborate in 183 mL of 0.1M NaOH). The diluted hybrids were pipetted onto glass slides and covered with a transparent slip. Photomicrographs were obtained within 15 minutes of blend preparation.

3.2.5. Dynamic Mechanical Analysis (DMA)

DMA was conducted on a TA Instruments 2980 with dry nitrogen purging of the specimen chamber and liquid nitrogen cooling. Specimens were analyzed in single-cantilever bending (17.65 mm clamp spacing, strain ~ 0.02%, 1Hz, heating rate 5°C/min), with a clamping torque of 0.565 N-m (5 in-lb).

Partially-cured neat PF and hand-mixed (high-shear) PF75 samples were promptly machined into 9 x 6 x 20 mm specimens. These were sanded to remove the "skin" that formed on the atmosphere-exposed surface. The machined specimens were tested in two different states: "undried" and "dried". To prevent additional cure, undried specimens were simply stored in sealed plastic bags over dry ice for a maximum of 7

days. Dried specimens were conditioned at room temperature in a desiccator, over P_2O_5 under 0.1 mm Hg vacuum, for 12 days (neat PF) or 13 days (PF75). Drying caused a 19.5% mass loss in neat PF specimens and a 27.9% reduction in the hybrids; during the last 24 hours of drying all specimens exhibited mass losses of 0.2% or less.

3.2.6. Field-Emission Scanning Electron Microscopy (FE/SEM)

A Leo 1550 field-emission scanning electron microscope operating at 5 kV was used to analyze partially-cured, hand-mixed PF75 high-shear and low-shear specimens. Fracture surfaces intended for analysis were created by pressing a sharp razor into the glassy specimens. Some specimens were further treated by immersing the fracture surface in continuously stirred 1,2-dichloroethane for periods ranging from 1 to 120 minutes. This solvent was selected because it is miscible with liquid pMDI but is a poor swelling agent for cured PF resol [6]. After solvent treatment the specimens were simply allowed to air dry. All specimens were mounted on aluminum stubs and sputter coated with gold (ca. 12 nm thick). In-lens detection was used to produce high-resolution surface specific images.

3.2.7. Infrared (IR) Spectroscopy

A KBr pellet of a partially-cured, hand-mixed (high-shear) PF75 hybrid was prepared by standard methods. Transmission spectra of the pellet were promptly obtained using a Perkin-Elmer 283B spectrophotometer purged with dry nitrogen (resolution 2nm, 32 scans).

3.2.8. Atomic Force Microscopy (AFM)

AFM images were obtained for a partially–cured, hand-mixed (high-shear) PF75 hybrid. Fracture surfaces were created for analysis as mentioned above and imaged in tapping mode with a Digital Instruments Dimension 3000 scope equipped with a Nanoscope IIIa controller using silicon cantilevers and tips.

3.3. Results and Discussion

3.3.1. Optical Microscopy of Liquid Blends

Optical microscope images were obtained for mechanically-agitated PF75 blends; Figure 3.1 shows a high-shear mechanically-agitated blend. These images revealed that co-reaction gave rise to a polymeric membrane surrounding the dispersed pMDI droplets. Membrane formation occurred rapidly and membranes appeared to be fully-developed even in initial images obtained ~90 seconds after mixing. The rapid reaction apparently preserved the shear-induced elongation and deformation of the pMDI droplets, resulting in stabilized dispersed domains whose size was highly dependent on the blending shear rate (images of low-shear blends not shown). As seen in Figure 3.1, some pMDI droplets seemed to form multiple, concentric membranes and may suggest that early formed droplets ruptured and exuded new droplets, leaving behind collapsed, birefringent membranes. The preserved elongation of the pMDI droplets also helped distinguish them from other spherical structures, presumed to be gas bubbles. Microscope images of a blend consisting solely of pMDI and pH 10 buffer (buffer as described previously) did not reveal signs of a membrane (images not shown), suggesting that membrane formation in the PF75 blends was dominated by PF-NCO rather than water-NCO reactions.

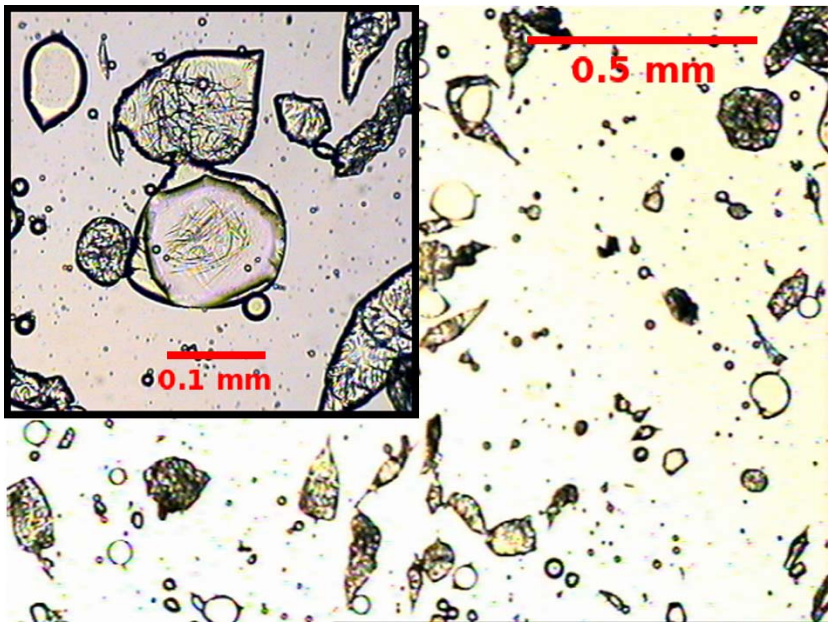

Figure 3.1. **Optical transmission micrographs of liquid PF75 which was mixed using high-shear mechanical agitation at 1500 rpm; image obtained within 15 minutes of blending**

Regarding liquid state rheology, the PF/pMDI blends are known to exhibit an immediate viscosity increase upon mixing, inherent to emulsification [1]. However, the rapid formation of a membrane that preserved the shear induced deformations no doubt also influenced the emulsion's rheology. These images also raise questions about the nature of the resulting solid-state polyphase morphology. Is the shear-dependant liquid emulsion structure preserved or is a derivative morphology developed?

3.3.2. Dynamic Mechanical Analysis (DMA)

Figure 3.2 shows typical DMA thermal scans of partially cured PF and PF75 (hand-mixed, high-shear), undried in both cases. Three major transitions were evident for both specimens: a subambient softening near -55°C, a second softening near 35°C and a high temperature stiffening above 110°C. The softening near 35°C is a glass transition, roughly correlating with the 60°C isothermal cure temperature and indicating that vitrification (during sample preparation) was incomplete.

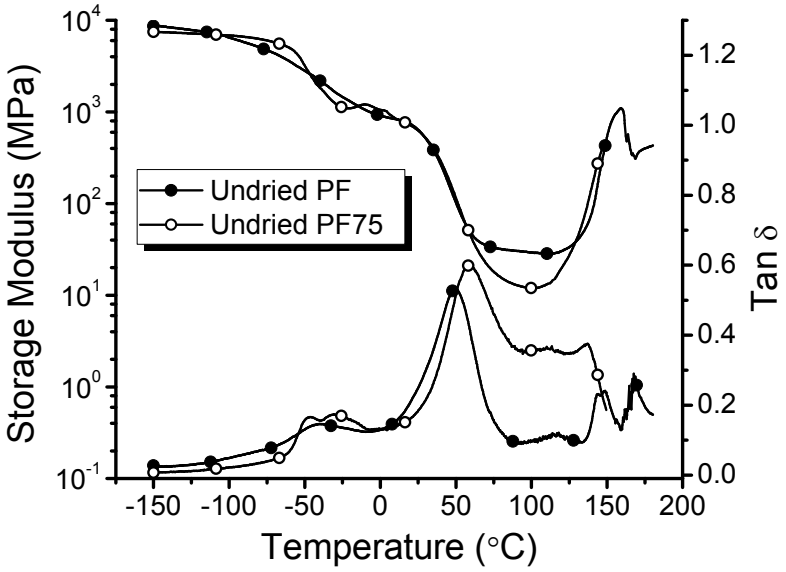

Figure 3.2. DMA thermal scans of undried, partially-cured PF and PF75 (high-shear) which, prior to DMA, was isothermally cured at 60°C for 13.5 or 36 hours, respectively (frequency = 1 Hz; heating rate 5 °C/min)

Notice in both specimens the significant low temperature softening near –55°C. Regarding neat PF resols, we have found no mention of this transition in the literature. However, a moisture sensitive β-transition at –86°C (dielectric analysis) has been reported for novolaks and was attributed to phenolic ring motions [7-9]. The -55°C softenings in Figure 3.2 are presumed to be analogous secondary relaxations. In PF75 the low temperature softening appeared as two overlapping peaks, which were collectively narrower than the broad uniform transition seen in neat PF. This double peak in the hybrid is believed to reflect a dual-phase morphology attributed to PF in both homopolymeric and copolymeric forms. Additionally, the similar intensities of the overlapping peaks suggested that similar quantities of the two materials were present. Regarding the hybrid PF75, we previously suspected that a portion of the low temperature softening was attributable to residual liquid pMDI (Tg = -54°C [10]), but this was not the case as will be discussed later.

Cure resumed above 110°C as seen from the increasing storage modulus in the high temperature region of Figure 3.2. Shortly thereafter the signal degraded because

both specimens deformed and fractured. After heating from 150 to 225°C, the hybrid specimens exhibited small light-brown colored spherical extrusions (~ 1mm dia.), in addition to splits and fissures along the specimen length.

The DMA specimens discussed in Figure 3.2 were not dried beyond the thermal treatment they received during isothermal cure. To investigate the influence of moisture on the observed DMA transitions, several of the partially-cured PF and PF75 specimens were subjected to prolonged desiccation, as described previously. Similar to the literature reports on neat PF novolaks [7-9], a moisture dependence was observed for the secondary transition of both neat PF and PF75: the –50°C softening was no longer present in dried PF; in dried PF75 it was broadened and significantly reduced in magnitude, Figure 3.3. Desiccation also increased the Tg's of both sample types by approximately 25°C and 75°C in PF75 and PF, respectively. This strong moisture dependence is presumed to arise from the hygroscopic sodium phenolates present in the samples. Finally, at the highest temperatures resin cure resumes, although it was not clearly detected in dried PF because of the loss of specimen integrity.

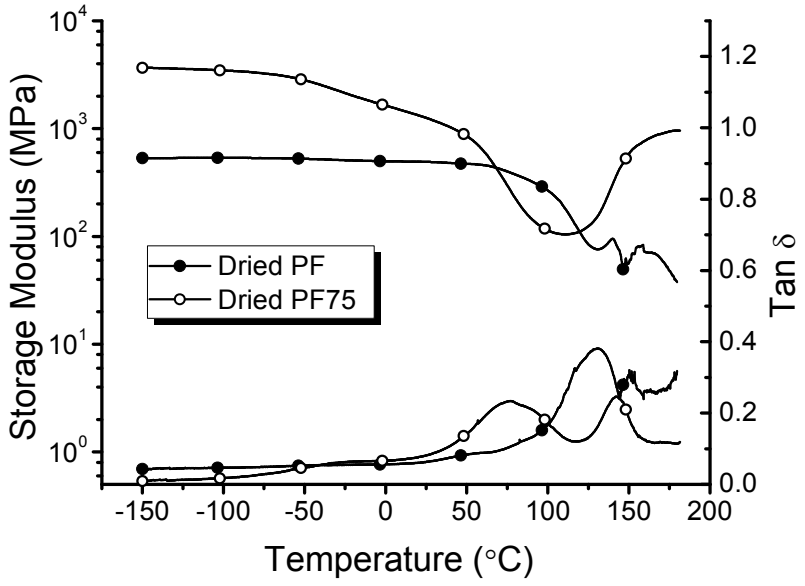

Figure 3.3. DMA thermal scans of dried, partially-cured PF and PF75 (high-shear) which, prior to DMA, was isothermally cured at 60°C for 13.5 or 36 hours, respectively (frequency = 1 Hz; heating rate 5 °C/min)

3.3.3. Field Emission Scanning Electron Microscopy (FE/SEM) of Partially Cured Hybrids

Figure 3.4 shows FE/SEM images of two different fracture surfaces: the left hand image is from a specimen that received no solvent washing; the specimen on the right was subjected to washing with 1,2-dichloroethane. Solvent washing had no perceptible impact on the specimen fracture surfaces and indicated that no large domains of liquid pMDI persisted in the cured hybrids. Both images exhibited large spherical voids that probably arose from water vapor and perhaps also from CO_2. The relative void size differs in the two images but this merely reflects the fact that a void size gradient developed across the thickness in all specimens. Crystalline materials are also present in both images, some being large and well formed while others are much smaller–grained, covering the surface in a blanket fashion. X-ray analysis revealed high concentrations of sodium in these regions, suggesting that these were NaOH crystals. The NaOH crystals, both large and small, appeared most commonly within the voids and are likely associated with the void-forming water. Careful inspection of the continuous phase fracture surface revealed relatively light-colored and often irregularly shaped features ranging from about 5 to 40 microns in size; these were not associated with NaOH crystals. Figure 3.5 shows another specimen (solvent washed for 120 min) that provides a better view of one of these light-colored features. The light color appears to have arisen from localized plastic yielding and it reveals a sharp boundary between the glassy matrix and these dispersed plastic zones. Previous bonded-wood fracture studies suggested that a pMDI-borne dispersed phase substantially toughened the phenolic continuous phase [1]. It follows that the plastic domains (seen in Figures 3.4 and 3.5) correspond to the pMDI-borne dispersed phase. The extended solvent washing did not solvate or otherwise affect these pMDI-borne domains, indicating that these domains existed in an advanced cure-state that did not contain appreciable amounts of liquid pMDI.

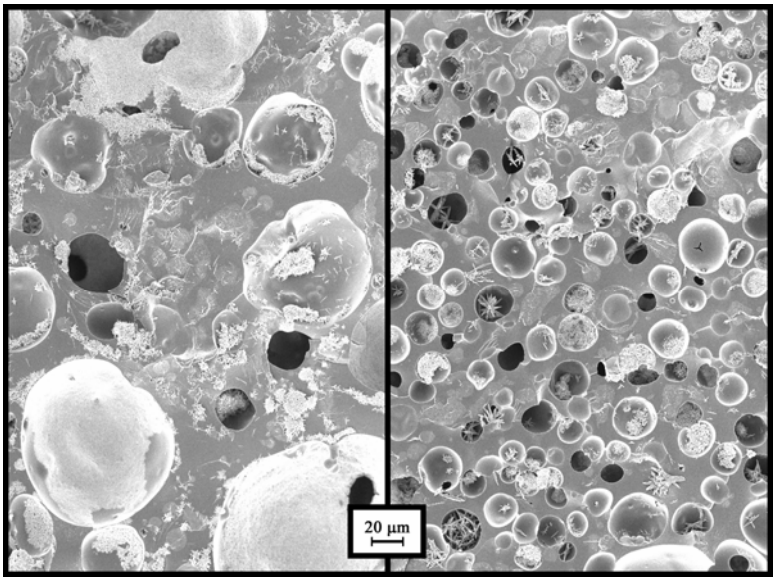

Figure 3.4. **FE/SEM micrographs which show the fracture cleavage surfaces of partially-cured PF75 (high-shear) samples. Left: A typical surface that was not subjected to solvent washing. Right: A typical surface that was exposed to a 5 minute surface washing with 1,2-dichloroethane.**

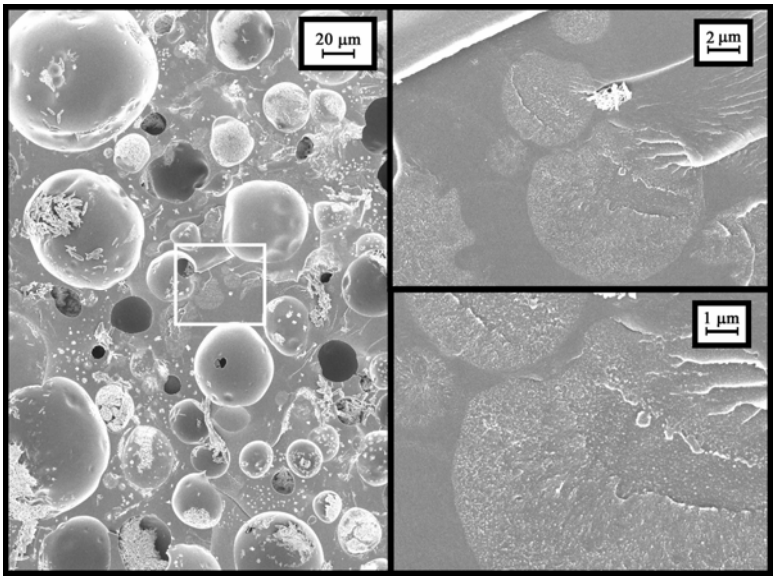

Figure 3.5. **FE/SEM micrographs of the fracture cleavage surface of a partially-cured PF75 (high shear) sample which was subjected to 120 minutes of surface washing with 1,2-dichloroethane. The two images at right are higher magnification views of the region within the white box shown in the left image.**

Similar pMDI-borne domains were also observed in low-shear specimens, but they were much larger than those observed in the high-shear specimens (data not shown). Consequently, it appeared that the shear-rate dependent morphology of the parent emulsion was preserved or otherwise reflected in the cured hybrid resin.

3.3.4 Infrared (IR) Analysis of a Partially Cured Hybrid

Transmission infrared spectra of partially-cured, high-shear PF75 were obtained to determine if residual liquid pMDI may have been present in the partially cured hybrids. Infrared spectroscopy should definitively detect unreacted isocyanate because its signal is both strong and well resolved. The spectrum presented in Figure 3.6 does exhibit a characteristic isocyanate signal at 2270 cm^{-1}, however it is very weak. This demonstrates that partially cured PF75 contained only minor amounts of residual NCO.

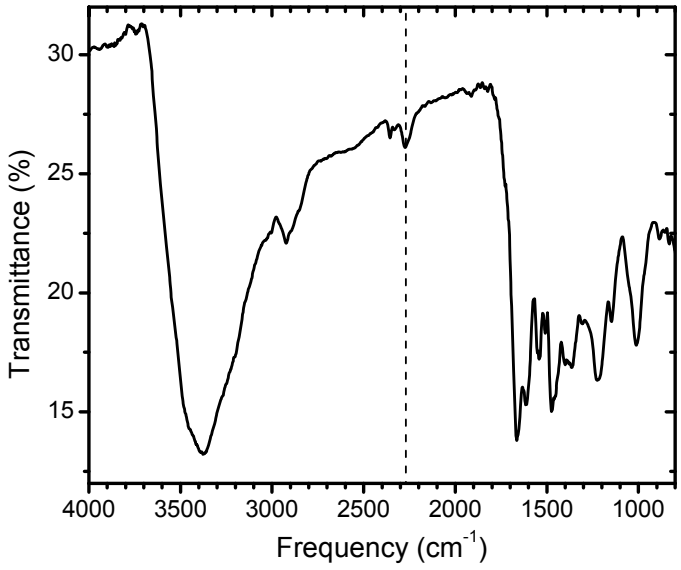

Figure 3.6. Transmission infrared spectrum of a partially-cured PF75 hybrid. The dotted line marks the isocyanate signal maximum occurring at 2270 cm^{-1}.

3.3.5. Atomic Force Microscopy (AFM)

Figure 3.7 shows AFM height (left) and phase (right) images of partially-cured PF75 (hand-mixed, high-shear) in a local continuous-phase region lacking voids and NaOH crystals. The AFM image shows a roughly 2 micron spherical domain delineated by a sharp boundary. The height image reveals a fine, raised texture within the spherical domain and this is consistent with the dispersed plastic-yielding zones seen in the FE/SEM images. Also in the phase image, close inspection reveals a lighter halo surrounding most of the pMDI-borne domain and suggests that the continuous phase was harder in this region. Realizing that texture differences may influence shading in AFM phase images, it could be that this halo reflects a significant area of copolymeric material having a greater hardness than the continuous phase. The double-peaked secondary relaxation observed in DMA of the hybrids also suggested that large amounts of copolymer were present (Figure 3.2; near -55°C). For the AFM image, the area of the copolymeric halo appears smaller than the total area of the PF continuous phase but it is unclear exactly where the lighter copolymeric material ends and the neat-PF continuous phase begins. Whatever its exact extent, both DMA and AFM suggest that copolymerization is not strictly limited to the sharp interface surrounding the dispersed domains. Otherwise, only minuscule amounts of copolymer would form; this would not result in a separate DMA secondary relaxation and would not exhibit a halo in AFM. The previously mentioned accelerated curing of the hybrid samples (see *Section 2.3: Blend Curing*) provides further evidence that pMDI diffused into and copolymerized with the PF continuous phase. Finally, in the AFM phase image the dispersed domain's shade is also somewhat variable, although not to the same extent as in the continuous phase. This may indicate that interdiffusion was bidirectional and that both phases contain copolymeric regions. Whatever the case, the sharp boundary between the dispersed and continuous phases suggests that diffusion was partially restricted by the initial membrane. Since evidence of diffusion is more obvious in the continuous phase, this may indicate that the initial membrane was more permeable to pMDI than to PF, perhaps owing to the small size of the pMDI monomers and oligomers.

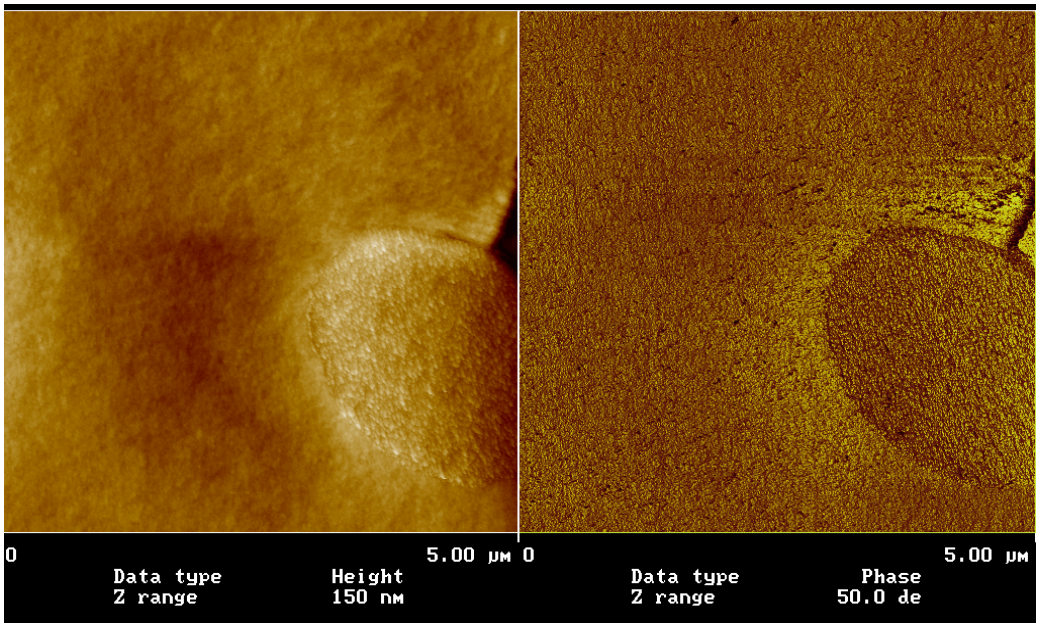

Figure 3.7. Atomic force microscope height (left) and phase (right) images of a partially-cured PF75 (high-shear) hybrid prepared in a fashion similar to Figure 3.2.

Regarding the performance of PF-pMDI hybrid adhesives, this study revealed significantly accelerated curing of PF75 relative to neat PF, suggesting that the hybrid adhesive may facilitate more rapid hot-pressing. Additionally, previous research within our lab demonstrated improved fracture toughness for specimen bonded with PF75 relative to either neat PF of neat pMDI [1]. The morphology of the PF75 blends sheds light on the mechanism for this toughening. It is likely that the spherical dispersed domains themselves act as crack blunting structures. The coploymeric region surrounding these domains is also likely to aid in uniformly distributing stresses into and around the softer dispersed domains. However, one must wonder if the possible benefits of the pMDI-borne dispersed phase extend beyond simple toughening. It will be informative to determine how the properties of the parent emulsion actually influence the hybrid's adhesive performance. Furthermore, since the shear-dependent multiphase emulsion structure is reflected in the solid-state hybrid morphology one could expect that variables influencing the emulsion structure will similarly influence the solid-state performance.

3.4. Conclusions

Emulsions containing liquid pMDI dispersed in aqueous PF resol are unusual because the components are both immiscible and co-reactive. In the liquid state the co-reaction was rapid, forming a polymeric membrane that encapsulated the pMDI dispersed phase and preserved the shear-induced deformations experienced during blending. This membrane appeared to arise from the reaction between pMDI and PF rather than the reaction between pMDI and H_2O.

In the solid state, FE/SEM and AFM detected dispersed pMDI-borne domains separated from the continuous phase by a sharp boundary. Similar to the liquid emulsion, the size of these dispersed domains was a function of the blending shear rate. In addition to the sharp transition between phases, the AFM phase image revealed a lighter halo that surrounded the dispersed domain and extended into the continuous phase. This halo is interpreted as a copolymeric region resulting from the diffusion of pMDI into the continuous phase. It is unclear if PF also diffused in the opposite direction into the dispersed domains. However, the sharp boundary between phases suggests that the overall diffusion was regulated by the initial liquid-state membrane.

DMA of the PF-pMDI hybrids exhibited two partially overlapping low temperature relaxations centered at -55^0C. One of these relaxations is believed to be the secondary transition of homopolymeric PF, the other relaxation is attributed to the analogous relaxation of PF-pMDI copolymer. The intensities of these overlapping transitions suggest that roughly equal proportions of PF and PF-pMDI copolymer were present.

Finally, the accelerated curing of the hybrid adhesive relative to neat PF supports our assertion that pMDI diffused into and copolymerized with PF in the continuous phase. These results indicate that while the liquid emulsion's multiphase morphology is largely preserved, significant interdiffusion occurs between the phases during cure. The resulting copolymer formation accelerates cure and the multiphase morphology likely acts to enhance toughness near the phase boundary.

3.4. References

[1] J. Zheng, S. C. Fox and C. E. Frazier, *Forest Products Journal* **54**, 74 (2004).

[2] A. Pizzi, J. Valenzuela and C. Westermeyer, *Holzforschung* **47**, 68 (1993).

[3] J. W. Rosthauser and W. D. Detlefsen, US Patent No. 6214265 (2001).

[4] T. R. Miller, L. D. Creel and W. D. Detlefsen, US Patent No. 6478998 (2002).

[5] W.-H. Hsu, US Patent No. 6,297,313 (2001).

[6] R. G. Schmidt and C. E. Frazier, *International Journal of Adhesion and Adhesives* **18**, 139 (1998).

[7] M. Reinhardt, A. Schonhals, D. Pfeifer, et al., *Polymers for Advanced Technology* **7**, 791 (1996).

[8] M. Topic and Z. Katovic, *Polymer* **35**, 5536 (1994).

[9] M. Topic and Z. Katovic, *Croatica Chemica Acta* **69**, 1215 (1996).

[10] J. Zheng, STUDIES OF PF RESOL / ISOCYANATE HYBRID ADHESIVES, Ph.D., Department of Wood Science and Forest Products, Virginia Tech. Blacksburg, VA (2002)

CHAPTER 4. INFLUENCE OF PF RESIN CHEMISTRY ON THE CURING OF PF/PMDI HYBRID WOOD ADHESIVES

4.1. Introduction

Earlier studies of PF/pMDI blends employed commercially available resins, so no consideration was given to resin synthetic variables. We could expect that both PF and pMDI synthetic variables would impact the performance of the hybrid system. PF resols have vast formulation flexibility, whereas pMDI wood binders are rather limited in formulation since they are a by-product from higher value materials. Consequently, the performance of the hybrid system should be studied as a function of the major PF variables.

The chemical composition and reactivity of PF/pMDI hybrid adhesives has been studied by several research groups. One study, using model compounds in aqueous alkali, found urethane formation to be significant [1]. Additionally, benzylic methylols were found to be more reactive towards phenyl isocyanate than phenolic alcohols. These results were confirmed by *Zhuang and Steiner* [2] using DSC and kinetic studies of model phenolics. Similarly, using FTIR spectroscopy *Pizzi and Walton* [3] report preferential urethane relative to urea formation along with significant co-reaction even at room temperature. Their study postulates that resols with a high methylol content and low molecular weight (i.e. resins synthesized with a high F/P ratio for short reaction times) will allow for maximum pMDI co-reaction and maximum performance. However, the above studies all relied on model compounds to determine the relative reactivities in solutions. These studies therefore do not take into account the specific multiphase morphology present in actual PF/pMDI hybrids. Furthermore, the above studies also fail to address the possibility that wood exerts a catalytic effect that significantly alters the reaction kinetics. In the study by *Zheng* [4] solid state ^{13}C and ^{15}N NMR was used to characterize the adhesive composition of resin impregnated wood cured under conditions

closely approximating industrial hot-pressing. Urethane linkages were found to be present in only slightly lower concentrations than the predominate urea linkages.

In the present study a series of PF resins of varying formaldehyde to phenol (F/P) ratio and alkali content were synthesized and characterized. These PF resins were then used to probe the effects of PF chemistry and composition on the cure properties of hybrid resins. Since actual PF resins were used instead of model compounds, this study should accurately reflect the influence which the demonstrated PF/pMDI multiphase morphology has on resin curing. Bulk resin characterization was performed using both DSC and parallel plate cure rheology. Finally, the influence of wood on hybrid cure kinetics was studied using in-situ micro dielectric analysis of wood bondlines.

4.2. Experimental

4.2.1. Materials

PF resols were synthesized using 50 wt% NaOH, crystalline phenol, urea (all Fisher ACS), 37 wt% formaldehyde (Aldrich ACS; contains 10-15% methanol stabilizer) and deionized water. The pMDI used in this study was a commercial OSB type resin (Rubinate® 1840 from Huntsman Polyurethanes) with 100% solids content, a viscosity of 166 mPa•s (25^{o}C) and an NCO content of 31%. For free formaldehyde determination, hydroxylamine hydrochloride (25 wt% and 0.1N NaOH), HCl (1N and 0.1N) and 50 wt% methanol (all Fisher ACS) were used. For ^{13}C NMR spectroscopy, D_2O (99.9%, Cambridge Isotope Laboratories) and 30 wt% NaOD (99.5% in D_2O, Cambridge Isotope Laboratories) were used as solvents. For GPC analysis, the mobile phase was THF (OmniSolv, 99.99%) containing BHT (Fisher, 99%) inhibitor; formic acid (Acros Organics 99.5%) was used to neutralize the resols prior to analysis. The GPC universal calibration curve was constructed using a series of polystyrene standards (American Polymer Standards and Viskotek), along with 2 model phenolics: 3,5-di-hydroxybezylalcohol and bis 4-di-hydroxyphenylmethane (both Fisher ACS).

4.2.1. Resol Synthesis

Six different PF resol formulations were synthesized, each with a target formaldehyde to phenol (F/P) mole ratio between 1.8 and 2.5, and an alkali content between 3% and 7% (based on total resin mass). Each formulation was prepared in three separate batches; replicate batches were subsequently combined to reduce the overall variability. As will be discussed later (*Section 4.3.1.1*), quantitative ^{13}C NMR analysis of the synthesized resins revealed that the actual F/P ratios differed from the synthetic targets. The six resin formulations are described in Figure 4.1, as a function of both the target (Figure 4.1A) and the measured (Figure 4.1B) F/P ratio; the NaOH/phenol molar ratios are provided in Table 4.1. Resins will be referred to by their measured F/P ratio followed by the percentage alkali. For example, "PF 2.0/7%" indicates the neat PF resin with a measured F/P ratio of 2.0 (target F/P ratio = 2.5) and an alkali content of 7%.

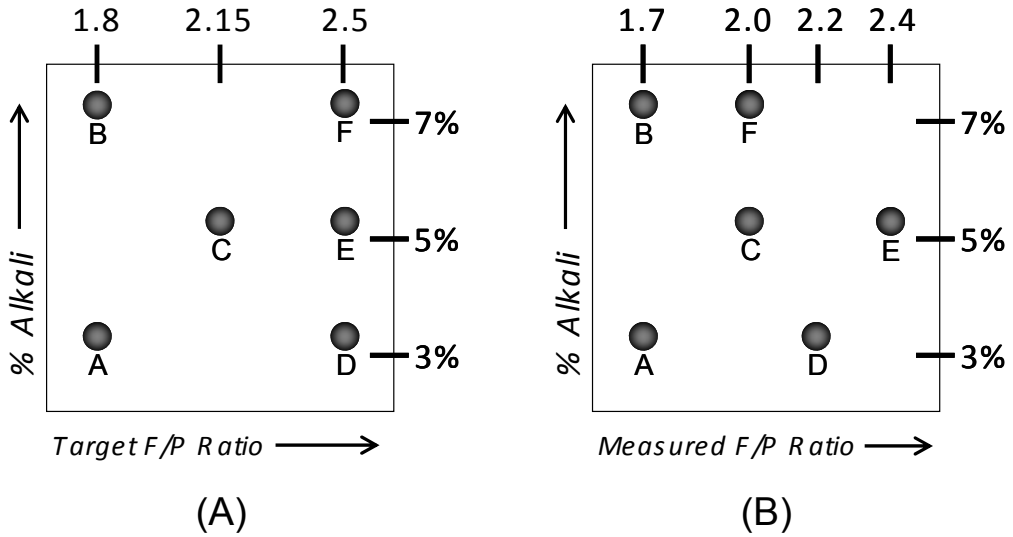

Figure 4.1. Experimental matrix for the preparation of PF resins as a function of: (A) the target F/P mole ratio and alkali content; and (B) the measured (^{13}C NMR) F/P ratio and alkali content.

Table 4.1. NaOH/phenol molar ratios of the six resol formulations.

NaOH/Phenol Mole Ratio			
	Target F/P ratio		
Alkali Content (%)	1.8	2.15	2.5
3%	0.236		0.270
5%		0.441	0.470
7%	0.603		0.689

Resins were synthesized in a 2-litre glass reactor equipped with a reflux condenser, thermocouple, Teflon coated copper heat exchanger, reagent addition/aliquot removal port and a 1.5-inch three-blade propeller attached to a variable-speed overhead mixer. Temperature regimes were carefully maintained at ±1.5 °C using a Barnant 689-0015 temperature controller operating in a previously calibrated proportional-integral-derivative (PID) mode. As necessary, water cooling to the heat exchanger was provided and manually attenuated using an Omega FL-5351ST flow-meter. During reaction, viscosity was measured periodically on 1 ml aliquots using a Brookfield CAP200+ viscometer (30°C, 10,000 s^{-1}, "#3" cone). Plots of viscosity versus reaction time were constructed and extrapolated in real-time to achieve target viscosities.

Reagent quantities were based on a solids content of 50% and a batch size of 960g. A double-caustic charge (split-cook) procedure was employed: phenol, half of the necessary NaOH and 90% of the necessary deionized water were initially charged to the reactor (t = 0 min) and heated to 70 °C with agitation. To minimize the potential exotherm, formaldehyde was metered into the reactor at 8 ml/min using an FMI QVG50 pump with V200 stroke rate controller. Following formaldehyde addition, reflux was initiated (95 °C) and, once the viscosity reached 200 ±50 mPa·s (t ≈ 130 – 164 min, dependant on formulation), the reactor was rapidly cooled and held at 70 °C until the viscosity reached 400 ±50 mPa·s (t ≈ 180 – 310 min). The remaining NaOH and distilled water were subsequently added and the reaction was maintained at 70 °C until the viscosity returned to 400 ±25 mPa·s, at which point the reaction was rapidly quenched to 20 °C. Overall reaction times were between 225 ±10 min for PF 2.2/3% and 650 ±50 min for PF 1.7/7%.

As will be discussed in *Section 4.3.1.2.,* the viscosities of PF 2.4/5% and PF 2.0/7% were originally somewhat higher than those of the remaining four resols.

Therefore, 1.6 and 2.75 wt% de-ionized water (based on total resin mass) was added to these respective resins to more uniformly standardize resin viscosity.

A small portion of each blend was set aside without additive for free formaldehyde, percent solids, NMR and certain DSC analyses. To the remaining portion, two-percent urea (based on total resin mass) was added as a free formaldehyde scavenger typical of industrial resin formulations. Resins were stored frozen at -22 °C. .

4.2.2. Quantitative ^{13}C NMR Spectroscopy of PF Resols

Solutions were dissolved in D_2O with 30 wt% NaOD added to enhance resin solubility and reduce viscosity. Solution concentrations were 1.0**:**0.2**:**3.33 D_2O**:**NaOD solution**:**PF resin. Quantitative ^{13}C NMR spectra were recorded on a Varian Inova 400MHz spectrometer with a 5 mm solution probe, observing at 100.577 MHz using inverse gated proton decoupling to suppress the Nuclear Overhauser Effect. A total of 4,100 scans were averaged for each resin using a 7.3 μs, 90° pulse followed by a 10 s pulse delay. All spectra were referenced to the MeOH already present in the PF resin (as formaldehyde stabilizer) with a δ value of 49.3 ppm.

4.2.3. Resol Viscosity Profile Determination

Following urea addition, neat PF viscosity characterization was performed over a broad stress range using a TA Instruments AR 1000 stress controlled rheometer equipped with a 40 mm diameter 2° steel cone. The temperature was maintained at 30.0 °C via the rheometer's peltier plate. A thin layer of low-viscosity silicon oil was used to seal the edge of the PF resin exposed to the atmosphere, preventing sample drying, which otherwise severely influenced the viscosity measurements. Steady state viscosities were recorded at 60 individual stresses between 5.968×10^{3} and 5.968×10^{-3} Pa. At each stress level, data points were collected and averaged over six second intervals until a steady state was achieved, where three consecutive six second measurements agreed within 5%. Two replicate experiments were preformed on each resin.

4.2.4. Resol Non-Volatile Solids Content Determination

Resin solids contents were determined in a fashion similar to that of ASTM D1489. Approximately 10g of resin (not containing post-added urea) was placed in a glass vial and dried in a 105 °C convection oven for 3 days. Samples were removed from the oven, immediately placed in a sealed N_2 evacuated desiccator and stored over P_2O_5 for another 24 hours. Reported solids contents are the average of two replicate samples.

4.2.5. Resol Free Formaldehyde Determination

Resol free formaldehyde contents were determined for PF resins not containing post-added urea in a fashion similar to the ISO 11402 hydroxylamine hydrochloride procedure. A 10 wt% hydroxylamine hydrochloride solution was prepared and pH adjusted to 4.0 using both 25 wt% and 0.1N NaOH. Between 3 and 30 g of resin were added to a 150 ml glass beaker (the exact amount used was iteratively adjusted as described below). Next, 50 ml of 50 wt% methanol was added to the resin and the solution pH was adjusted to 4.0 using the 1N and 0.1N HCl solutions. Finally, 50 ml of the hydroxylamine hydrochloride solution was added and the solution was stirred for 5 minutes. The liberated HCl was titrated with 0.1004 N NaOH back to a pH of 4.0. The measurement was repeated until 2 valid titrations were accomplished with each requiring between 15 and 30ml of NaOH titrant.

4.2.6. Gel Permeation Chromatography of PF Resols

4.2.6.1. Sample Preparation

BHT inhibited THF containing 0.5wt% formic acid was used to prepare 25 mg/ml PF resin solutions (based on total resin mass). Trace amounts of DMSO were added to each sample as an internal flow rate reference. The formic acid was necessary to solubilize the resins, but resulted in the formation of a white, crystalline precipitate, presumed to be sodium formate. After 24 hours dissolution the liquid portion of the solution was passed through a 0.45µm Teflon syringe filter and the filtrate was analyzed.

4.2.6.2. System

Separation was achieved using Waters HR1 and HR3 columns connected in series. The THF mobile phase containing 0.025 wt% BHT inhibitor was pumped at 0.5ml/min from a Waters 515 HPLC pump connected to a Li-Chrome III flat-coil pulse dampener. Inline solvent degassing was performed with a Phenomenex DG4000 vacuum degasser. A Viscotek TDA 302 Triple Array Detector consisting of right angle and low angle light scattering detectors (RALS and LALS, respectively), an inline viscometer and a differential refractometer (RI) was used for signal detection. Viscotek Omnisec 3.1 Software was used for data analysis. Sample injections (101.0 µl) were delivered using a Rheodyne 7125 injection port. The precise injection volume had been previously calculated using the average integrated RI response of six polystyrene standards of precisely known concentration and a well established dn/dc (0.185 ml/mg).

4.2.6.3. Calibration

Two calibration methods were compared: universal and triple detection. For each method a single 1,050 dalton polystyrene standard was used to calibrate elution time offsets and voltage responses of each detector. In addition, for universal calibration a calibration curve was constructed using 15 polystyrene standards (MP= 1,870k, 400k, 170k, 89.3k, 64.5k, 30.1k, 13.4k, 6.04k, 2.79k, 1.32k, 1.05k supplied by Viskotek; MP=765, 510, 370, 250 supplied by American Polymer Standards) and two model phenolics (3,5-di-hydroxybezylalcohol and bis 4-di-hydroxyphenylmethane). Supplier intrinsic viscosity (IV) values were used for the polystyrene samples. Viscometer response was used to determine the IV of the model phenolics. The Log(molecular weight * IV) versus elution volume calibration curve was modeled with a 5^{th} order polynomial.

4.2.6.4. dn/dc Determination

The dn/dc value for phenol formaldehyde resol in THF has been reported as 0.176ml/mg [6]. However, this value resulted in calculated sample recoveries (based on total RI response areas) well above 100%. Using Bis(4-hydroxyphenyl)methane as a

model PF compound, a dn/dc of 0.2068 ml/mg was measured and used for all subsequent resol analyses.

4.2.7. PF/pMDI Hybrid Blend Preparation

Only one blend ratio was examined, containing 75 parts PF resin solids to 25 parts pMDI resin solids. This blend ratio was chosen because of its substantial toughness at relatively low pMDI loadings [1]. Blends were prepared in small 10 g batches inside a 22 mm diameter glass vessel. Liquid pMDI was added to the PF and then agitated at 900 rpm for 1.5 minutes using a digital mixer fitted with a standard type R-I radial flow impeller [5] of 16 mm maximum diameter (custom fabricated). Each hybrid blend will hereafter be referred to in a manner analogous to the PF resins; i.e. "Hybrid 1.7/3%" denotes a PF/pMDI hybrid adhesive produced from the neat PF 1.7/3% resol.

4.2.8. Differential Scanning Calorimetry (DSC) of Resol and Hybrid Adhesives

All DSC measurements were conducted on a TA Instruments Q100 DSC equipped with a refrigerated cooling system. Nitrogen was used as the purge gas (50 ml/min). Sapphire was used to calibrate the heat capacity (Cp) response. Hybrid samples were blended immediately prior to analysis. Resin samples (approximately 25 mg) were analyzed in sealed, stainless steel high-volume DSC pans (TA Instruments). The DSC pans effectively suppressed volatilization and, unlike aluminum pans, were inert towards the alkali resins. The sealed sample pans were weighed before and after analysis to determine both the precise resin mass and to verify that no mass loss occurred.

4.2.8.1. Thermal Scans

DSC thermal scans were preformed from 50 °C to 200 °C with a heating rate of 10 °C/min. Following the initial scan, the samples were quench cooled and rescanned under the same conditions. Two replicate measurements were preformed for each resin with <5% peak height deviations between measurements.

4.2.8.2. Quasi-Isothermal Modulated DSC (MDSC) Curing

Resins were quench cooled to -90 °C and heated at 10 °C/min to 86.85 °C (300K) without modulation. Then, using a temperature modulation amplitude of 1.5 °C/200 s, samples were cured in a quasi-isothermal state for 120 – 400 minutes until vitrification was complete, as determined from inspection of the Cp signal. Following vitrification the samples were quench cooled and re-scanned twice from -90 °C to 200 °C at 10 °C/min without modulation. Multiple replicates were conducted for each of the analyzed resins.

4.2.9. Parallel Plate Oscillation Cure Rheology of Hybrid and Neat Resol Adhesives

Hybrid and neat PF resins were cured in oscillation mode on TA Instruments AR 1000 and AR 2000 series rheometers equipped with blended liquid-gas nitrogen cooling and ETC furnaces. All settings, including temperature, were calibrated to be equivalent on each instrument. Resins were cured isothermally at 65 °C using a 25 mm stainless-steel parallel-plate geometry. To prevent drying, the resins were immersed in silicon oil throughout cure using a custom fabricated immersion cup. During the experiments the normal force was maintained between -1 and 1 N by adjusting the instrument gap.

Liquid resin samples (0.25 ml) were placed between preheated parallel plates of the rheometer and the gap was adjusted for proper geometry filling (approximately 500 μm). The immersion cup was then filled with silicon oil pre-heated to 65 °C. Samples were tested in controlled strain mode using the iterative precision strain control feature of the otherwise stress controlled rheometer. Multiple oscillation strains were used, with the applied strain increasing in a stepwise fashion as cure progressed; this ensured an adequate stress response while still remaining within the curing adhesive's previously established linear viscoelastic region (LVR). The initial oscillation strain was 10%. This was automatically reduced to 2% once the storage modulus (G') exceeded 50 Pa and finally, to 0.5% once G' rose above 10,000 Pa. To analyze the frequency dependence of resin cure, four different oscillation frequencies were used: 0.2, 0.6, 2 and 5 Hz. Individual data points were averaged over 10 seconds of oscillation at a given frequency and the oscillation frequency was cyclically varied between the four values throughout

the entire experiment. This allowed four flow curves to be constructed from a single experiment, each flow curve corresponding to a different oscillation frequency. Cure was monitored until vitrification was complete or until sample delimitation occurred (due to prolonged silicon oil exposure).

4.2.10. Dielectric Analysis (DEA) of Resin Cure within Wood Bondlines

In-situ curing of selected hybrid and neat PF adhesives was monitored between 10 mm thick yellow-poplar laminates. The adhesive was spread at 25g/mm^2 onto each laminate face using a hard rubber roller. An Idex conductivity sensor was sandwiched within the assembly and cure was monitored using a Micromet Eumetric System III Microdielectrometer with High-Con interface while hot pressing at 100 psi and 200 °C.

4.3. Results and Discussion

4.3.1. Resol Characterization

4.3.1.1. Quantitative ^{13}C NMR analysis of PF resols

^{13}C NMR spectra were obtained for relatively concentrated resol samples dissolved in a D_2O/NaOD solution. Unlike DMSO, D_2O has no carbon resonances and therefore did not overlap with the resol spectra. The added NaOD and the high PF concentration also avoided problems with poor resol solubility associated with neat D_2O [7, 8]. However, the high sample concentration made the solutions quite viscous and this resulted in significant spectral line broadening (Figures 4.2 and 4.3). This broadening did prevent differentiation of certain functional groups (discussed below), but was an acceptable tradeoff for reduced acquisition time.

Peak assignments are presented in Figure 4.2 and summarized in Table 4.2. Comparative spectra of the six PF formulations are overlaid in Figure 4.3. All peak assignments were based on previous literature [7-10] except the extreme downfield peak (~173 ppm) visible in Figure 4.2, also appearing in the high F/P, high alkali resols of Figure 4.3. No mention of this peak was found in the literature. Instead, based on its chemical shift, its appearance in high alkali resins and the already alkaline nature of the

solvent, this peak was attributed to the C_1 of deprotonated phenols. Also, as noted in Figure 4.2, a portion of the hemiformal moieties (namely those connected to an aromatic phenolic) overlap with the methylol resonance. It is assumed that the total hemiformal content was relatively minor. Therefore, this aromatic hemiformal resonance was neglected and treated as part of the methylol resonance—an acknowledged minor source of error.

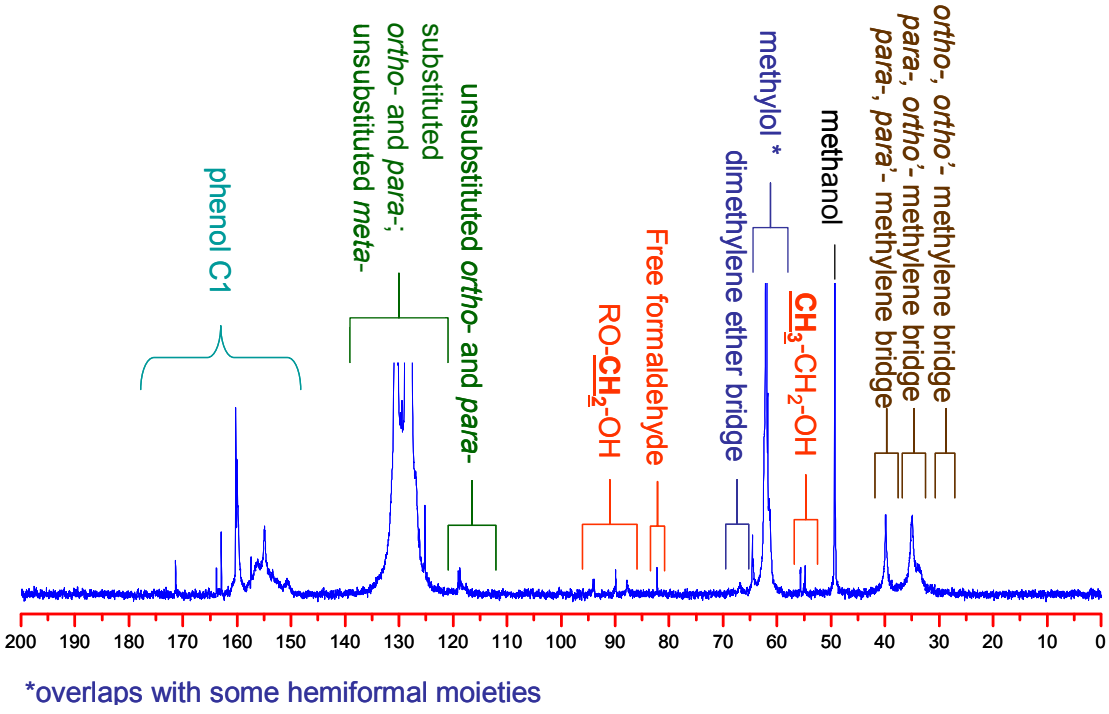

Figure 4.2. Representative ^{13}C NMR spectrum of PF 2.0/5% with peak assignments

Table 4.2. PF resol chemical composition by ^{13}C NMR. The reported peak integration areas are relative to the total phenol *o-,m- and p-* peak area, which was set equal to 5.

Chemical Group	δ		PF Formulation					
			PF 1.7/3%	PF 1.7/7%	PF 2.0/5%	PF 2.2/3%	PF 2.4/5%	PF 2.0/7%
		Target F/P	1.8	1.8	2.15	2.5	2.5	2.5
		% Alkali	3%	7%	5%	3%	5%	7%
		NaOH/Phenol	0.236	0.603	0.441	0.270	0.470	0.689
Measured F/P ratio			**1.73**	**1.69**	**1.98**	**2.24**	**2.43**	**2.01**
Phenol *o-,m-,p-*	112.5-140 *ppm*		5	5	5	5	5	5
Phenol C_1	146.5-172 *ppm*		0.98	0.94	0.93	0.97	0.97	0.94
Unsubstituted Ph *o-,p-*	112.5-121.5 *ppm*		0.5	0.38	0.08	0.03	0.02	0.06
Total Formaldehyde Moieties			0	0.04	0.07	0.43	0.68	0.39
Free Formaldehyde	83.2 *ppm*		0	0	0.01	0.07	0.12	0.06
Hemiformal	52.5-56.5 & 86.5-95.5 *ppm*		0	0.04	0.06	0.36	0.56	0.33
Total Crosslinks			0.66	0.74	0.74	0.70	0.84	0.75
o/p Methylene Bridge Ratio			0.54	0.51	0.5	0.49	0.56	0.57
p-p' Methylene Bridges	38-42 *ppm*		0.22	0.24	0.24	0.21	0.21	0.19
o-p' Methylene Bridges	30.5-37.5 *ppm*		0.39	0.49	0.48	0.41	0.53	0.51
o-o' Methylene Bridges	27.5-30.5 *ppm*		0.03	0	0	0	0	0
Dimethylene Ether Bridges	65.5-69 *ppm*		0.015	0.005	0.015	0.075	0.1	0.045
Methylol	59-65.6 *ppm*		1.07	0.91	1.17	1.11	0.91	0.87

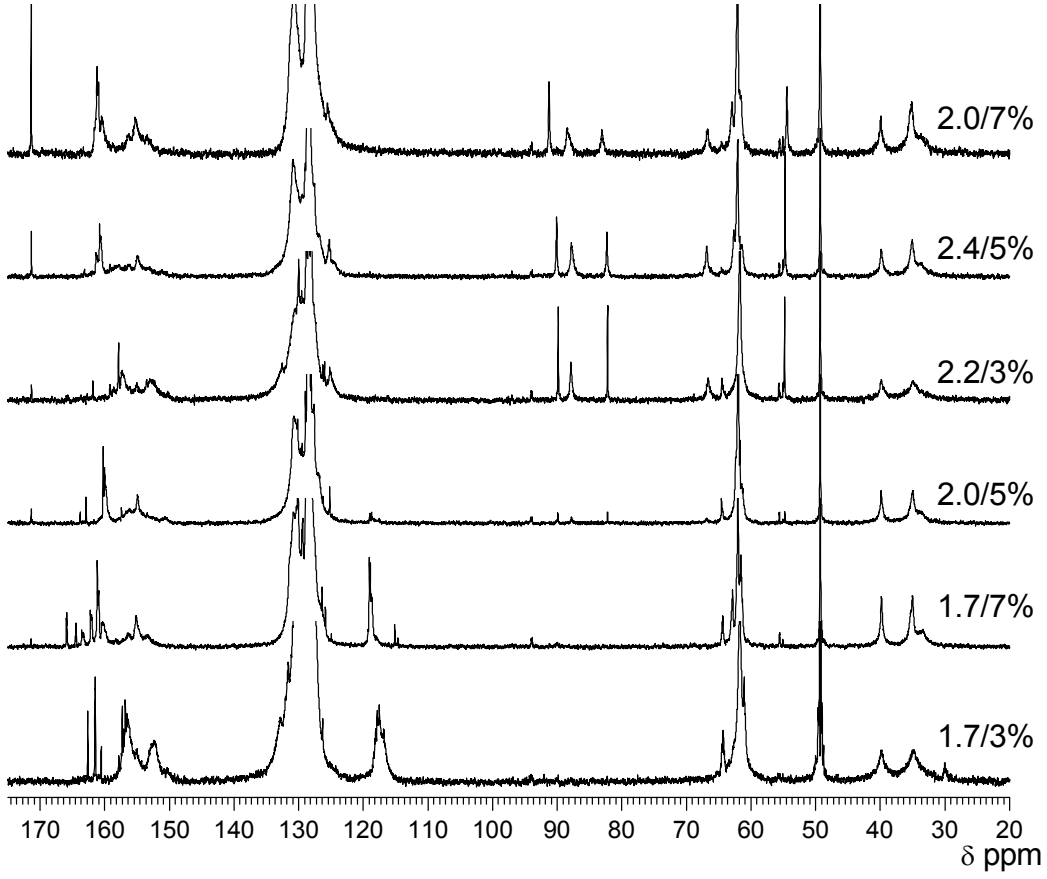

Figure 4.3. Overlay of PF resol ^{13}C NMR spectra

Most values in Table 4.2 were obtained simply by integrating across the indicated chemical shift range(s). For the dimethylene ether bridges (DMEBs), integration results were reduced by a factor of two to account for both methylene resonances. The measured F/P ratios were obtained by dividing the sum of all non-aromatic peak areas by that of the aromatic peak areas. Likewise, the "total formaldehyde moieties" value is the sum of the free formaldehyde and hemiformal resonances. The term "total crosslinks" is simply the sum of all methylene bridges (MBs) and DMEBs. The ratio of ortho to para methylene bridges was calculated as: *o/p* MB = (2 · (*o-o'* MB) + (*o-p* MB)) ÷ (2 · (*p-p'* MB) + (*o-p'* MB)).

Regarding the quantitation of the acquired spectrum, the intensity of the phenolic C_1 given in Table 4.2 relative to the other five aromatic carbons compares favorably with its actual value of 1.0. This indicates reasonably good quantitation, comparable to the majority of published PF resol studies [7, 8, 10], though not quite as good as the more recent method developed by *Gelan et. al.* [9]. In fact, the degree of quantitation is quite notable given that a pulse delay of only 10 s was used without any paramagnetic relaxation agent. Typically it has been held that the T_1 decay time for the non-protonated aromatic carbons was on the order of 15 s, and that this necessitates a preparation delay of at least 75 s to completely eliminate proton Nuclear Overhauser Effects (NOEs) [9]. However, preliminary experiments in which the recycle delay was doubled did not seem to improve spectrum quality. Furthermore, using variable concentrations of either chromium(III) acetlyacetonate or iron(III) diethylenetriaminepentaacetaacetonate paramagnetic relaxation agents also failed to improve the apparent quantitation.

Note that the measured F/P ratios given in Table 4.2 are lower than the target synthetic ratios. This is not likely related to the spectrum quality; most studies reveal a decreased F/P ratio following synthesis [7-10] suggesting that some formaldehyde volatilization is common during synthesis. However, the large discrepancy between the target and measured FP ratios of PF 2.0/7% is surprising. While high alkali levels significantly lengthened the reaction times and could possibly contribute to increased formaldehyde volatilization, other high alkali resins did not show evidence of this effect. Furthermore, although the paraformaldehyde content of aqueous formalin is known to be somewhat variable, the synthesis order was randomized and each PF formulation was

prepared in three separate batches—minimizing any potential negative impacts of reagent instability and variability.

From Table 4.2 it is evident that the proportion of unsubstituted aromatic ortho and para positions decreased as the measured F/P ratio increased, as expected. Also in agreement with previous literature [7] is the observed increase in free formaldehyde moieties in high F/P resins. Although it has been reported that high alkali content leads to preferential ortho substitution through the formation of a chelate structure [11], significant line broadening hindered separation of the ortho and para substituted phenol resonances, making direct observation of this effect impossible. The relative proportion of ortho to para methylene bridges was relatively uniform across all formulations, with methylene bridge formation at the para position being roughly twice as common as at the ortho position; ortho-ortho' methylene bridges were only detected in PF 1.7/3%. Such selectivity towards the para position (despite its lower relative abundance) has been attributed to steric effects [12]. Also in agreement with previous literature [13-17] was the preferential formation of DMEB's in the highly substituted, high F/P resins; no clear trend was observed between DMEB formation and alkali content. Finally, the total amount of crosslinks seemed to correlate well with increasing F/P ratio and alkali content.

Since isocyanates are known to react rapidly with resol methylols to form urethane bonds, the amount of methylol substitution may be of importance for PF/pMDI blends [3]. From Table 4.2 it is evident that low alkali resins have a greater proportion of free methylols. In contrast, F/P ratio appeared to have only a variable, indirect influence on methylol content. In any case, PF 2.0/5% had the highest methylol content while PF 2.0/7% has the lowest.

4.3.1.2. Viscosity, Solids and Free Formaldehyde Determination

Results of the steady-state viscosity, percent solids and free formaldehyde measurements are given in Table 4.3. The variation in viscosity between replicate experiments was less than 3% and all resins exhibited almost perfectly Newtonian behavior over the selected shear rate range (standard error $\leq$ 3%). Consequently only a single viscosity value is reported, averaged across all shear rates for the two replicate

experiments. As mentioned previosly, the viscosities of PF 2.4/5% and PF 2.0/7% were originally somewhat higher than those of the remaining four resols. Therefore, 1.6 and 2.75 wt% de-ionized water (based on total resin mass) was added to these respective resins to more uniformly standardize resin viscosity. Also note in Table 4.3 that all resins' viscosities are substantially lower than the 400 mPa·s end-point viscosity targeted during resin synthesis. Upon cooling, vapor within the reactor condensed and reduced the viscosities of the resins by approximately 20 mPa·s. The remaining reduction in viscosity is due to the thinning effect of the 2% post-added urea.

Table 4.3. Viscosity, solids and free formaldehyde content of blended PF resins (formaldehyde and solids contents are of neat resins. Viscosities are of resins after 2% urea addition)

		η (mPa•s)	% Solids	% Free CH_2O
Number of Measurements		*2*	*2*	*2*
COV ≤		*3%*	*1.50%*	*10%*
Resin	**1.7/3%**	223.5	43.3	0.086
	1.7/7%	220.7	44.4	0.013
	2.0/5%	229.3	43.3	0.33
	2.0/7%	237‡	42.39‡	2.4
	2.2/3%	254.6	43.6	2.7
	2.4/5%	242.5‡	41.34‡	3.7

‡ The viscosity/% Solids of resins 2.0/7% and 2.4/5% were reduced post synthesis. Respectively, orginal values were 275.05 mPa•s, 42.0% and 308.1 mPa•s, 43.6%.

While the solids content of each resin is lower than the target solids content of 50%, there is little variation between individual resins. Similar to the ^{13C} NMR analysis, resol F/P ratio appears to have a strong effect on the percent free formaldehyde in each resin formulation. In contrast, no clear trend is evident regarding alkali's effect on free-formaldehyde.

4.3.1.3. Gel Permeation Chromatography (GPC) of PF Resols

PF resol's low solubility in organic solvents presents an obstacle to conventional, organic mobile phase GPC analysis. While resols can be directly solubilized and

analyzed using an alkaline aqueous mobile phase [18, 19], aqueous GPC systems are relatively specialized and uncommon in most polymer laboratories. Consequently, various techniques are typically employed to modify the resol and make it soluble in a given organic GPC solvent. One commonly used method is to first acetylate the resol resin; however, this derivatization is believed to advance resol cure and, when using organic solvents, the resulting solution may still contain high molecular weight aggregates [20, 21]. An alternative method attempts to neutralize and solubilize PF resols using a THF mobile phase that has been additized with either acetic [22] or trichloroacetic acid (TCAA) [23, 24]. However, the ability of this technique to fully solubilize the resol without altering its molecular weight distribution is subject to controversy [20]. Furthermore, preliminary experiments within our lab found TCAA additized mobile phases to be unsuitable for use in most GPC systems; stainless steel is not entirely resistant to TCAA [25] and this caused leaks to regularly develop in our system.

In this study an alternative neutralizing agent, formic acid, was chosen for investigation because of its relatively high pK_a and its compatibility with stainless steel. As an added benefit, significantly longer resol-THF solution stability was observed using formic acid relative to TCAA: while formic acid neutralized resol-THF solutions did not visibly precipitate until 10+ days of storage, TCAA neutralized solutions showed precipitation after only 2-3 days, making it difficult to allow samples to fully dissolve (possibly taking up to 24 hours [26]) while also ensuring that they did not significantly advance.

RI traces for the six PF resins are shown in Figure 4.4, overlaid with the universal calibration curve. Note the prominent shoulder in the high molecular weight fraction of PF 1.7/7%, PF 2.4/5% and PF 2.0/7%, along with the bimodal behavior of the remaining three resols in this region. This broadened molecular weight distribution reflects the intended result of double caustic charge (split cook) synthetic procedure [27, 28] and, as would be expected, the effect is most prominent for the high alkali resins. As a precaution, however, it should be mentioned that the presence of high molecular weight aggregates remains a largely unexplored possibility [20], and this could also be artificially broadening the resol chromatograms.

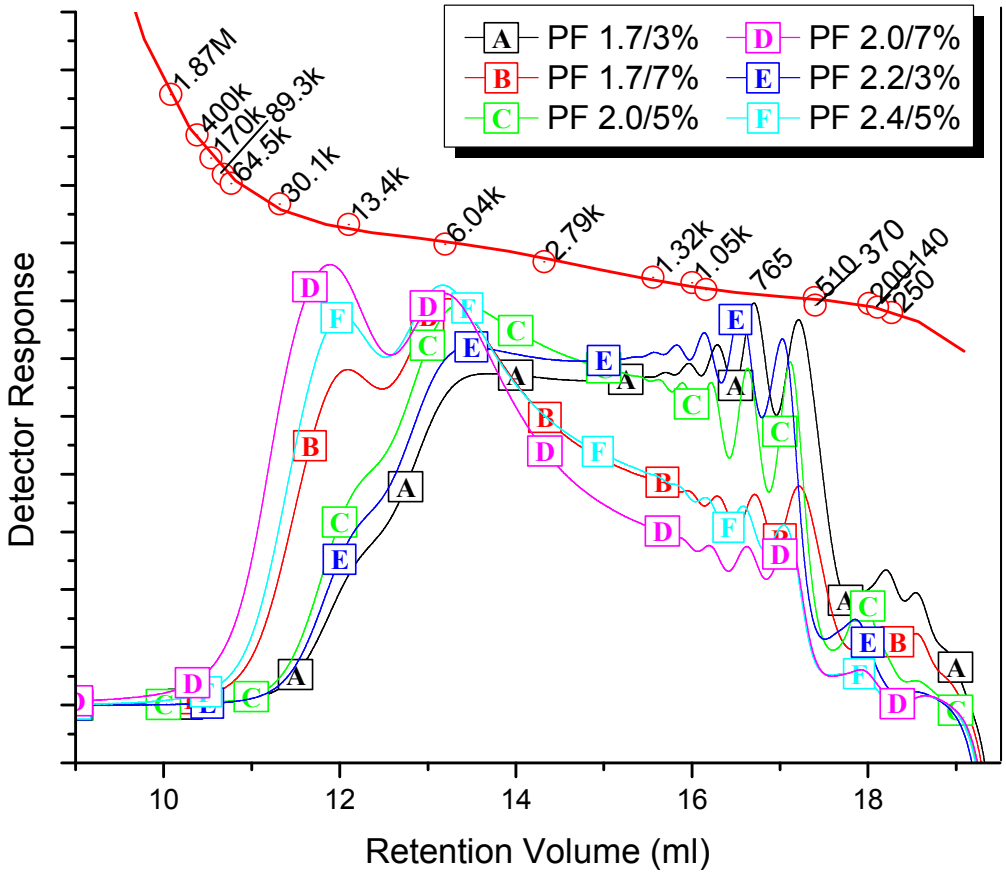

Figure 4.4. Refractive index (RI) chromatograms of PF resols overlaid with 5th order universal calibration curve

Qualitatively, from Figure 4.4 it is readily apparent that the resins synthesized with high F/P ratios and high alkali contents contained a greater proportion of high molecular weight material. More detailed, quantitative comparisons of the six resins were made using both universal and triple detection calibration methods. For both methods, analysis was complicated by the negative RI response of residual sodium formate, which obscured any unsubstituted phenols present in the solution. The overlapping sodium formate peak also made it impossible to accurately integrate the total RI response of each chromatogram and directly determine each resol's dn/dc. However, using 0.176 ml/mg as the literature dn/dc value for PF in THF resulted in calculated sample recoveries (based on total RI response areas) well above 100% for the formic acid neutralized resols. Therefore, a formic acid-THF solution of the model compound, bis(4-hydroxyphenyl)methane, was prepared in the same fashion as the resols and its measured

dn/dc of 0.2068 ml/mg was used in place of the actual resol dn/dc for both calibration methods. Using this dn/dc value resulted in calculated sample recoveries (based on the total RI response and corrected for resin solids) of 100 +/-2%, suggesting 0.2068 ml/mg to be a good approximation of the actual resol dn/dc.

For universal calibration, the calibration curve (Figure 4.4) appears relatively linear across the region of interest, although its slope is more strongly negative prior to ~11 ml, resulting in reduced resolution towards the very highest molecular weight fraction of the PF resins studied. IV detector responses of the six resins are presented in Figure 4.5 and results of the universal calibration molecular weight calculations are summarized in Table 4.4. The universal calibration M_w values mirror the trend which visual inspection of Figures 4.4 and 4.5 suggests, with M_w increasing with increasing F/P ratios and alkali contents. The universal calibration M_n values also generally increase with increasing F/P ratios and alkali contents, with the notable exception of PF 2.0/7%. Owing to its exceptionally large polydispersity, PF 2.0/7% actually had the 3rd lowest M_n despite having the largest M_w. Examining the universal polydispersity values in Table 4.3, especially those of PF 2.0/7%, PF 2.4/5% and PF 1.7/7%, suggests that high alkali contents resulted in relatively broader molecular weight distributions, as would be expected for split cook resol formulations.

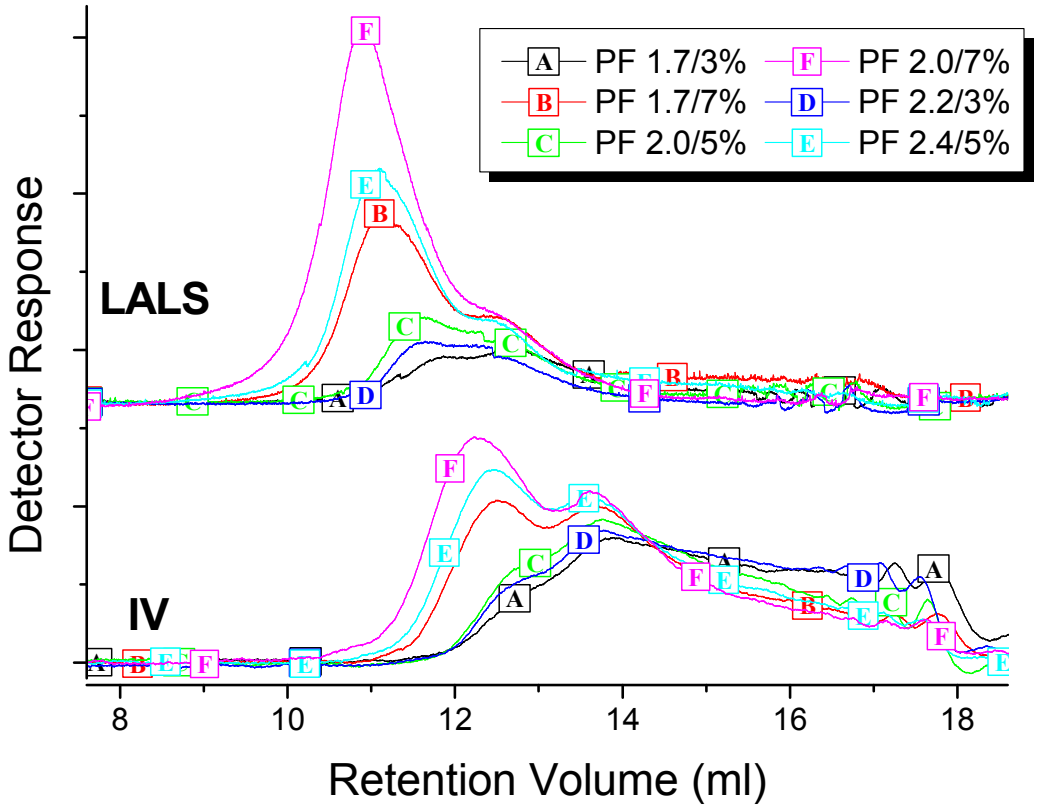

Figure 4.5. **Intrinsic viscosity (IV) and low angle light scattering (LALS) chromatograms of PF resols**

Table 4.4. **PF molecular weights using GPC universal and triple detection calculation**

Resin	Universal			Triple Detection		
	M_n	M_w	M_w/M_n	M_n	M_w	M_w/M_n
1.7/3%	689	3668	5.32	913	3282	3.59
1.7/7%	1047	13832	13.21	3372	8475	2.51
2.0/5%	2214	11338	5.12	1764	4447	2.52
2.0/7%	1630	72509	44.48	3221	14811	4.60
2.2/3%	2155	9765	4.53	998	3657	3.66
2.4/5%	3969	64363	16.22	3034	9801	3.23

For comparative purposes, the chromatograms of the six resols were also analyzed using triple detection; these results are summarized alongside the universal calibration results in Table 4.4. The triple detection M_w values follow the same trend as the

universal calibration data but are significantly lower in magnitude. Recall that the slope of the universal calibration curve (Figure 4.4) rose sharply at high elution volumes, providing poor resolution towards the high molecular weight resol fractions. Unlike universal calibration, triple detection does not rely on a calibration curve; instead, the polymer M_w is calculated directly from the LS signal. As is evident in Figure 4.5, LS detectors are especially sensitive to high molecular weight fractions. As an added benefit, since calculations are not based on calibration standards, triple detection results are largely unaffected by both flow rate fluctuations and polymer-column interactions. For these reasons, it is likely that the triple detection M_w values in Table 4.4 more accurately reflect the true M_w of the resols. In contrast， and as evident in Figure 4.5, LS detectors have an inherent low sensitivity to low molecular weight species and offer poor resolution at high elution volumes. Indeed, the relative trend of the triple detection M_n values bears little resemblance to the corresponding universal M_n data. Because of the low sensitivity of triple detection to low molecular weight species, in this case it is presumed that the universal M_n values more accurately reflect the actual resol M_n's.

4.3.2. Hybrid and Neat PF Cure Characterization

4.3.2.1. DSC Thermal Scans of PF Resols and Hybrids

First heating DSC thermal scans of the six neat PF resins are presented in Figure 4.6. Depending on the formulation, between one and three distinct exotherms were present. When present, the lowest temperature exotherm was centered below 142°C, the middle exotherm occurred between 142 °C and 165 °C, and the high temperature exotherm appeared above 165 °C.

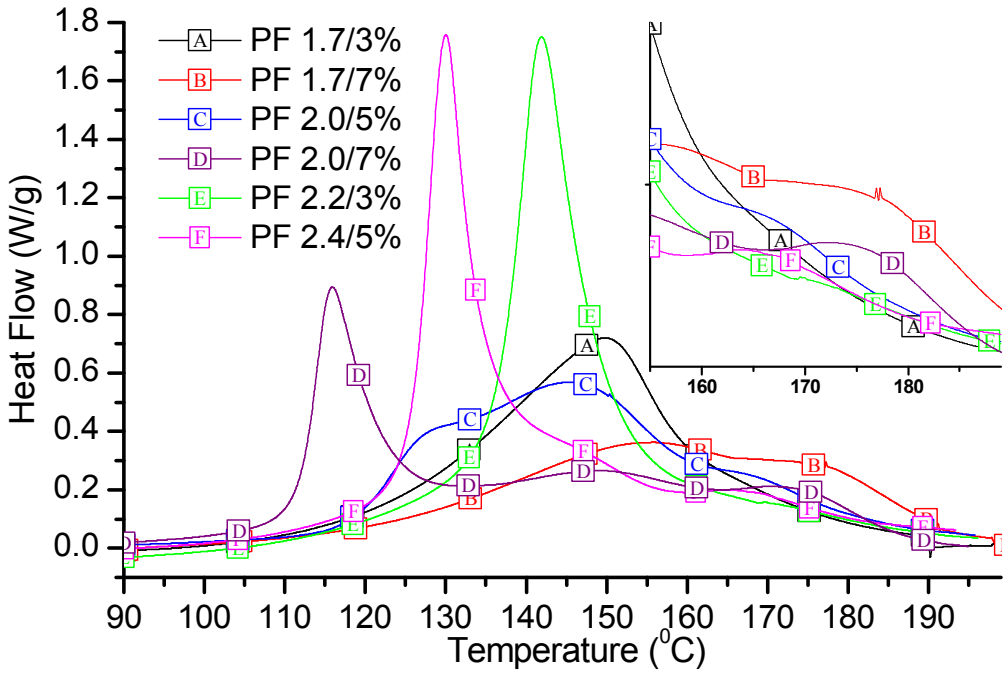

Figure 4.6. Single heating DSC thermograms of PF resins (heating rate: 10 °C/min; results are the average of two experiments)

The mid-range exotherm (142-165 °C) was present in all resins—with the possible exception of PF 2.2/3%; in PF 2.2/3% the exotherm may also have been present, but if this was the case it was obscured by a large, lower temperature exotherm (discussed below). Although subject to controversy [29, 30], exotherms in this temperature region have generally been attributed to crosslinking reactions involving the condensation of methylols [31-34]. Consistent with this explanation, the intensity of the mid-range exotherm appears to correlate fairly well with the resol methylol contents previously summarized in Table 4.2.

Although absent in the F/P 1.7 resins, the remaining resols exhibited a low temperature exotherm appearing somewhere between 115 and 142 °C. The intensity and precise location of this lower temperature exotherm is consistent with previous literature which assigns the peak to hydroxymethylation reactions [31-34]: the peak intensity increased with increasing F/P ratios while the onset temperature decreased as the amount of NaOH catalyst increased.

In addition to the two main exotherms observed below 165 °C, a generally minor, high temperature exotherm was apparent, centered at 170-175 °C. This peak's intensity appears to be related to resin alkali content, being virtually non-existent in the 3% alkali resins and maximum in the 7% alkali samples. In resol thermograms the highest temperature peak is often associated with conversion of DMEBs into simple MBs [35]. However, at least for the initial DMEB contents given in Table 4.2 there is no correlation with this peak's intensity. Furthermore, Figure 4.7 compares the effect of urea addition on PF 1.7/3% and on PF 2.0/7% and reveals that the high temperature peak was only present in high alkali resins that also contain post-added urea. Based on these findings it seems unlikely that this high temperature peak arises from conversion of DMEB's into simple MB's. Instead, the exact identity of this peak remains uncertain, although it appears to be related to both alkali and urea content.

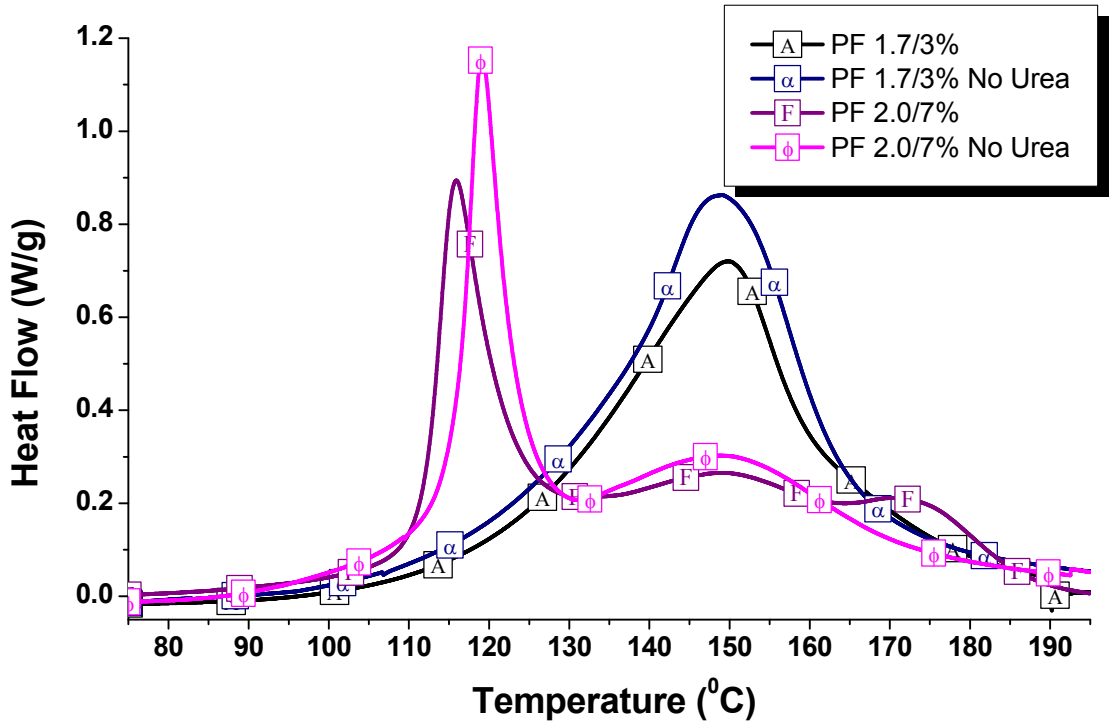

Figure 4.7. **Single heating DSC thermograms of two PF resols with and without post added urea. (Heating rate: 10 ^{0}C/min; results are the average of two experiments)**

In Figure 4.8 the previously presented DSC thermograms of three neat PF resins are compared with thermograms of three analogous hybrid resins**.** All three hybrid samples exhibit an exotherm not present in the neat PF samples and centered at ~105 °C. Although the identity of this peak is uncertain, its intensity appears to increase with increasing alkali and F/P ratios. Self polymerization of the pMDI phase is a possibility, although if this were the case all three hybrid peaks would be expected to be of roughly equal intensities. Co-reaction with the PF phase may be more likely. It has been suggested that urethane formation between pMDI and both phenolic hydroxyls and methylols will be significant in typical hybrid curing reactions [1]. At first glance the exotherm intensities do not seem to relate to the amount of methylol in each PF (detected using NMR, Table 4.2). However, it has been reported that urethane formation is strongly favored under alkaline conditions [1]. Perhaps the increased alkali content of Hybrid 2.0/7% accounts for the proportionally greater intensity of this first exotherm despite PF 2.0/7%'s low methylol content.

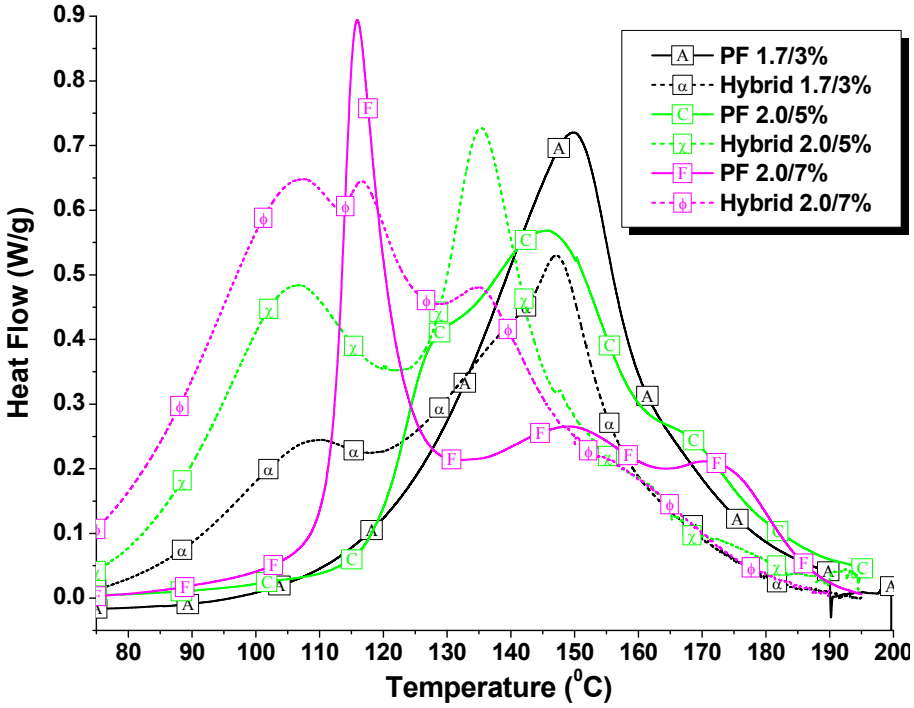

Figure 4.8. **Single heating DSC thermal scans of three PF resols and three corresponding hybrid resins (Heating rate: 10 °C/min; results are the average of two replicate experiments)**

Further examination of the 2.0/7% thermograms reveals a peak centered at 115 °C present in both the neat PF and the hybrid sample. This seems to indicate that whatever the corresponding reaction is in the neat resin, perhaps hydroxymethylation, the reaction also occurred unaltered in the hybrid resin. Otherwise, the remaining high temperature portions of these two thermograms are notably dissimilar. The peak centered at 150 °C in PF 2.0/7% is either absent in Hybrid 2.0/7% or has shifted to 135 °C with a concomitant increase in intensity. The high temperature 175 °C peak associated with urea in PF 2.0/7% is altogether absent in Hybrid 2.0/7%. Were the pMDI born domains to remain strictly segregated one would expect most of the corresponding neat PFs cure behavior to remain evident in the hybrid thermograms. Instead, curing of the hybrid resin was substantially altered and accelerated; both cure onset and cure completion occurred at lower temperatures in the hybrid and the location and/or intensity of the characteristic neat PF cure peaks changed significantly.

Cure acceleration and altered cure kinetics were also evident in the Hybrid 2.0/5% and Hybrid 1.7/7% resins. Whereas two overlapping cure exotherms were observed in PF 2.0/5% (centered at 135 °C and 150 °C), only a single exotherm was observed in Hybrid 2.0/5%. Hybrid 1.7/3% shows somewhat more similarity with its corresponding neat PF thermogram in that the dominant exotherm occurred at 147 °C in both samples. However, in Hybrid 1.7/3% the intensity of the main exotherm was reduced and concluded at a somewhat lower temperature than in PF 1.7/3%. Furthermore, a lower temperature shoulder centered at 135 °C is observed for the exotherm of the hybrid but not the neat PF sample.

By itself, DSC is quite limited in its ability to clarify the precise mechanism with which pMDI alters the phenolic phase's cure in hybrid samples. However, such studies do reveal that the individual hybrid phases, rather than remaining strictly segregated, interact significantly. The DSC thermal studies also suggest the value of a more detailed analysis of these resins using techniques capable of discerning the underlying chemical reactions occurring during hybrid cure.

4.3.2.2. Quasi Isothermal MDSC Curing of Hybrid Resins

Methods of studying thermoset cure using quasi-isothermal MDSC were pioneered by *Assche and Mele* [36]. MDSC provides the same heat flow information as a conventional isothermal DSC experiment but has the unique additional ability to measure heat capacity (Cp) continuously during exothermic curing processes [37]. Vitrification can therefore be readily monitored using quasi-isothermal MDSC: vitrification restricts the polymer's mobility and this results in an observable, stepwise decrease in heat capacity. Studies of epoxy amine systems confirm that the time to vitrification measured by the midpoint of the MDSC Cp transition is in agreement with vitrification measured using rheological techniques [36]. Analysis of the heat flow during such experiments provides further information on the reaction kinetics. Systems such as the epoxy amine system studied by *Assche and Mele* exhibit autocatalytic reaction kinetics. In auto-catalyzed reactions the maximum in heat flow does not occur until 30-40 percent conversion, resulting in a mostly symmetric heat flow peak. This is in contrast to n^{th} order reactions in which the heat flow is maximal at the beginning of the reaction and then steadily declines during cure [38].

Studies of neat PF resols have demonstrated that these resins follow n^{th} order kinetics [39]. Indeed, quasi-MDSC curing of neat PF2.0/7% (shown in Appendix A.1.1) confirmed this behavior. Figure 4.9 provides Cp and heat flow measurements for three selected hybrid resins. In Hybrid 1.7/3% a clear step decrease in Cp is centered at 100 min and indicates vitrification. Furthermore, the shape of the heat flow signal is typical of simple n^{th} order reaction kinetics (the erratic heat flow behavior at low cure times is an experimental artifact occurring while the temperature amplitude stabilized). The Cp trace for Hybrid 2.0/7% is similar to that of Hybrid 1.7/3%, although vitrification occurs significantly earlier, at approximately 60 min. The heat flow signal for Hybrid 2.0/7%, however, is quite unusual. Initially, the reaction does follow n^{th} order kinetics. But, approximately 60 minutes into cure and coincident with vitrification, a second heat flow event is observed with a peak shape characteristic of an autocatalytic event. The precise time of vitrification for this resin was actually somewhat variable, ranging from 40 to 60 min for three replicate samples, but for each replicate the second exothermic event was

coincident with vitrification. Apparently, cure in Hybrid 2.0/7% proceeded for a substantial amount of time following n^{th} order kinetics in which the rate of reaction steadily declined. Then, at a somewhat variable point during isothermal cure a second reaction was initiated and coincided with vitrification. Analysis of Hybrid 1.7/7% reveals behavior intermediate to Hybrid 1.7/3% and Hybrid 2.0/7%. Although the step decrease in Cp is somewhat broadened for this resin, it is centered at approximately 80 min. Additionally, although a latent exothermic event is apparent as a shoulder in the heat flow signal, the event is low in magnitude and only partially resolved from the initial n^{th} order kinetic event. Whatever the cause of the latent reactivity observed in Hybrids 1.7/7% and 2.0/7%, it appears to be strongly influenced by F/P ratio and, to a lesser extent, by alkali content. Furthermore, the noted variability in the onset time of this exotherm suggests that it is sensitive to slight differences in blend preparation, perhaps reflecting slight variations in the emulsion structure.

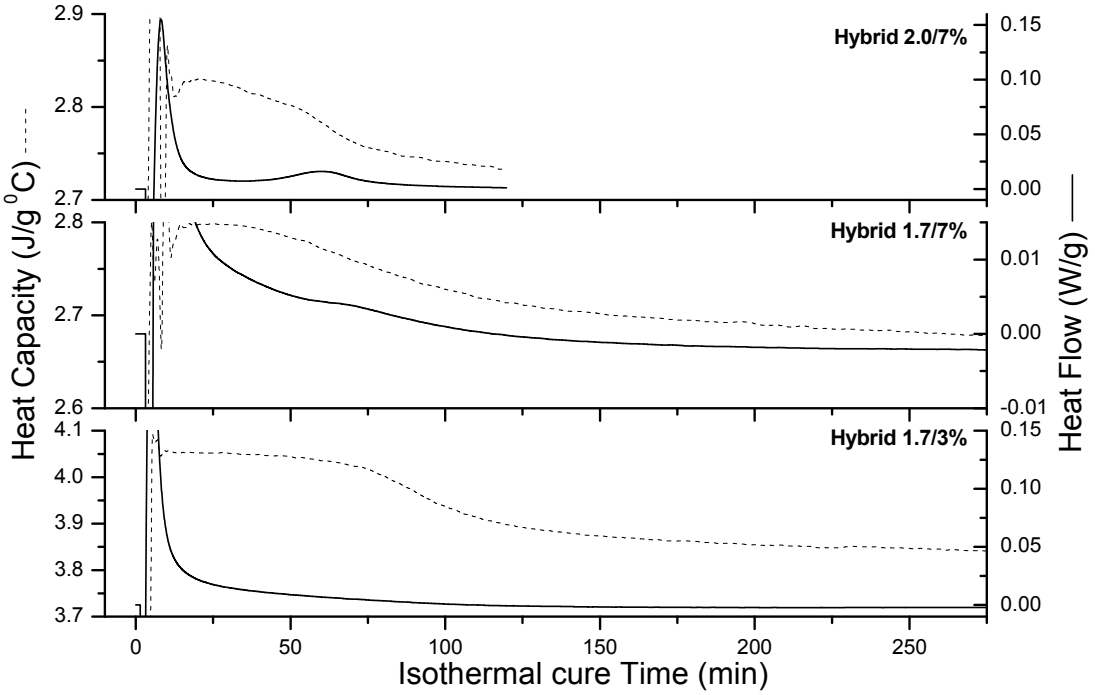

Figure 4.9. MDSC quasi-isothermal curing of three hybrid resins (T=86.85 °C; amplitude=1.5 °C/200s)

Immediately following isothermal curing, each resin was scanned twice from -90 to 200 °C using conventional DSC. A portion of these two scans from 25 to 200 °C is

presented in Figure 4.10. In the first heats of Hybrid 1.7/3% and 1.7/7% a broad, very slight glass transition is perhaps evident near the isothermal cure temperature. In all three resins a subsequent exotherm is then observed beginning at approximately 115–125 °C. This exotherm may represent residual curing, although its onset is significantly higher than the previous isothermal cure temperature. Urethane decomposition may be a more likely explanation; urethane structures formed between PF and pMDI are known to be thermally unstable at temperatures exceeding 120 ^{0}C [40], and this corresponds to the exotherm onset temperature.

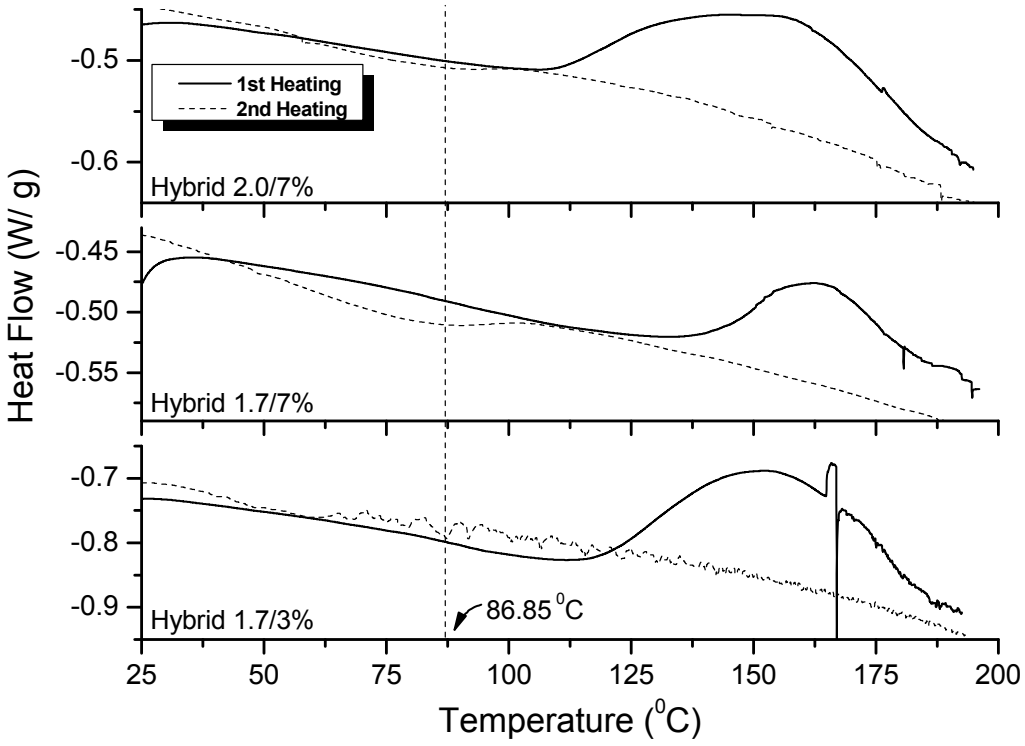

Figure 4.10. Conventional DSC 1st and 2nd heatings of three hybrid resins following quasi-isothermal MDSC curing (heating rate=10 °C/min). The prior isothermal cure temperature is indicated by the dotted vertical line.

The behavior observed in the second heating of Figure 4.10 is more unusual. In Hybrids 2.0/7% and 1.7/7% a slight exotherm is again resolved, only in this case the onset temperature does correspond with the isothermal cure temperature. Hybrid 1.7/3% also exhibits a minor exotherm, but the poor signal makes it difficult to accurately establish its onset. It is quite surprising that any residual reactivity would remain in these

three hybrid systems following the high temperatures reached during the first thermal scan. Unfortunately, DSC alone is not able to provide insight into the chemical significance of this unusual curing behavior. However, given the complex, multiphase morphology of the hybrid resins one must wonder if this event is somehow related—perhaps indicating that diffusion is somewhat restricted between the individual blend components.

4.3.2.3. Parallel Plate Cure Rheology

Cure rheology was monitored isothermally at 65 °C. The low temperature was necessary to prevent near instantaneous partial gelation and agglomeration of some hybrid resins (observed when temperatures were greater than ~75°C) and to prevent the boiling of all resin types (resulting in sample overflow) at temperatures greater than 95 °C. As described previously, to prevent drying during cure the resins were immersed in silicon oil. For the hybrid resins, the pMDI seemed to be well encapsulated within the hybrid continuous phase and did not appear to mix with the silicon oil. Representative results of the isothermal curing experiments are shown for PF 2.0/7% and PF 2.0/5% in Figure 4.11. Each of the four G', G" and tan δ traces represent one of the four applied frequencies. As discussed by *Winter* [41, 42], the gel point of a thermosetting material is rigorously defined as the point at which the loss tangent (tan δ) becomes independent of the frequency of dynamic oscillation. While the intersection of the G' and G'' is more commonly used as an indicator of gelation this is only valid for stoichometrically balanced thermoset chemistries far away from their glass transition. In Figure 4.11 a distinct point of frequency independence is clearly present in the tan δ of PF 2.0/7%, occurring approximately 81 min into cure (coincidently this point partially overlaps with a gap in data collection during which the strain level changed). Also note that for PF 2.0/7% the G'/G" crossover does not occur until 90-103 min (depending on frequency). However, a distinct tan δ crossover like that shown for PF 2.0/7% was only observed in a few instances; the behavior displayed in Figure 4.11 for PF 2.0/5% was more typical. Here, perhaps due to the poor signal and large amount of scatter, no definite tan δ crossover exists. Consequently, it was necessary to use the intersection of G' and G" as

an approximate indicator of the actual gel point when making comparisons between resins.

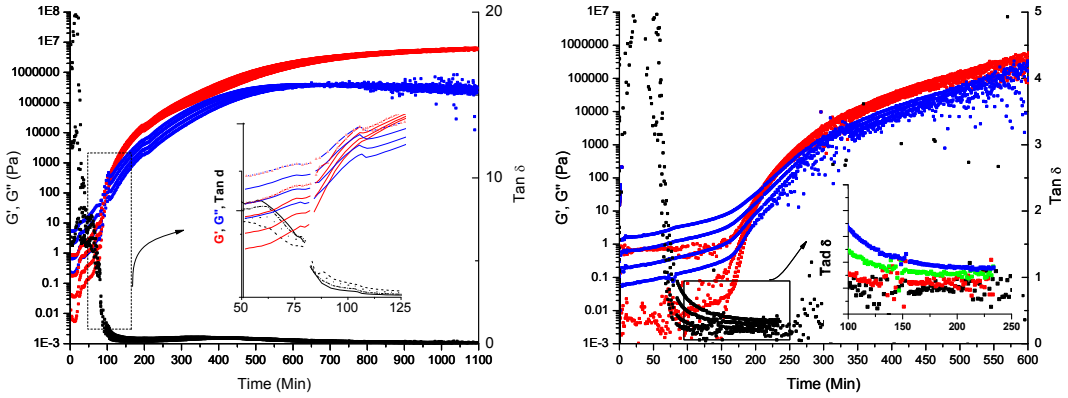

Figure 4.11. Multi-frequency isothermal parallel plate cure rheology of PF 2.0/7% (left) and PF 2.0/5% (right). Only the former exhibits a frequency independent crossover in tan δ. (Temp = 65 °C; frequency = 0.2, 0.6, 2, & 5 Hz; oscillation strain varied during cure)

Approximate gel times of the neat resols, based on the G'/G'' crossover, are summarized in Figure 4.12; these values were averaged from the 5 Hz signal of two replicate cure experiments. A clear effect of both F/P and alkali is noted, with gel time increasing in response to increased F/P ratio and alkali level. The complete 5 Hz G' curing behavior for all six PF resins is presented in Figure 4.13. In all cases the modulus remained relatively constant before reaching an inflection point, after which the modulus climbed rapidly. This inflection occurs before the gel point and likely indicates the point of polymer chain entanglement. Regarding the time of vitrification, cure stresses and prolonged exposure to the silicon immersion oil led to sample delamination, necessitating that the experiments be terminated prior to cure completion. Therefore, the vitrification times of the resols can only be approximated by extrapolating the storage modulus traces presented in Figure 4.13. Despite differences in final moduli, visual extrapolation of the curves in Figure 4.13 suggests that resol vitrification follows the same relative trend as the gel times: cure of PF 1.7/3% clearly progressed the slowest; PF 1.7/7%, PF 2.2/3% and PF 2.0/5% all approach vitrification at an intermediate rate; and finally, PF 2.0/7% and PF 2.4/5% approach vitrification the fastest.

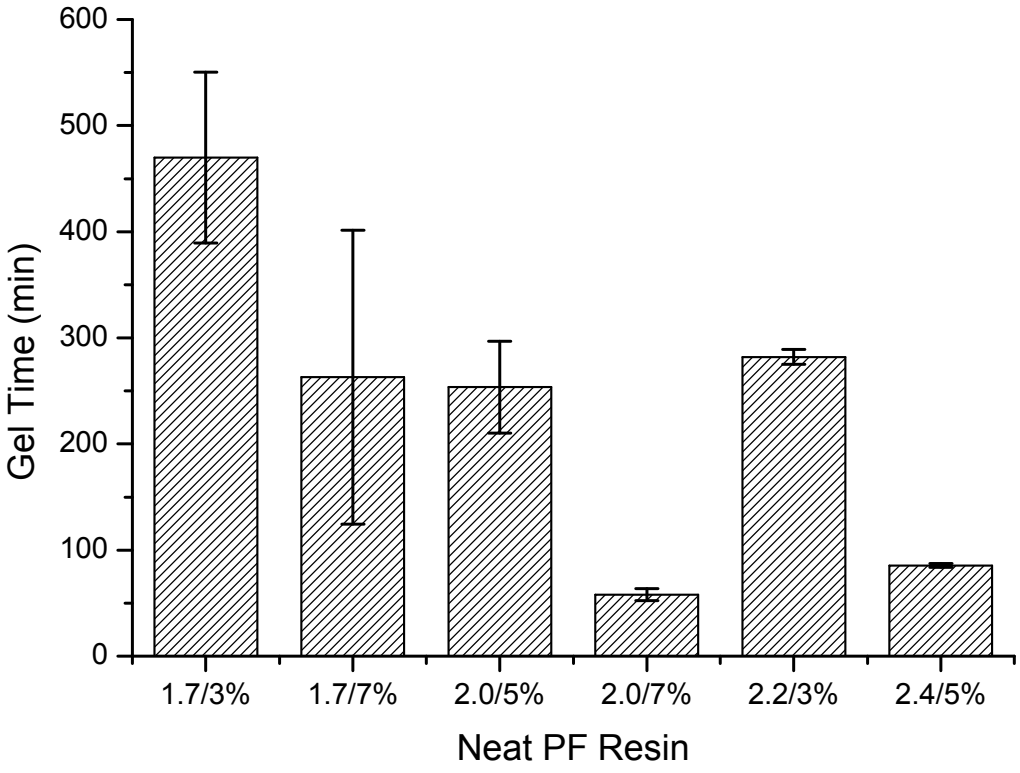

Figure 4.12. **Approximate gel times (intersection of 5 Hz G' & G") of PF resins as measured by parallel plate oscillation rheology (Error bars represent $^{+}$/- one standard deviation)**

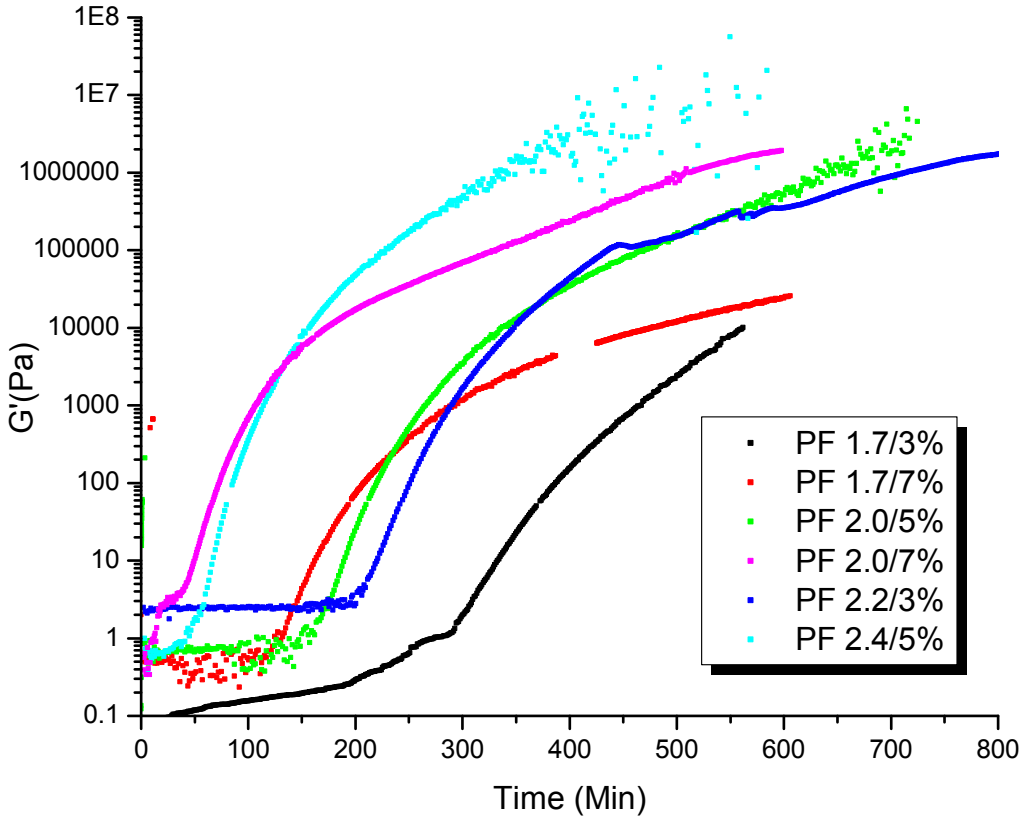

Figure 4.13. Isothermal parallel plate cure rheology of PF resins (Temperature = 65 °C; frequency = 5 Hz; percent strain was varied during cure)

For hybrid resins it was also necessary to use the crossover of the 5 Hz G' and G" signals as an approximate indicator of gelation. These approximate gel times are presented in Figure 4.14, again averaged for two replicate experiments. The relative trend mirrors what was observed for the neat PF resins. However, in all cases gelation of the hybrid resins was significantly accelerated relative to the neat PF resins. The 5Hz G' curing behavior of the six hybrid resins is displayed in Figure 4.15. The rapid curing of the hybrids allowed the curing behavior to be monitored all the way to vitrification without sample delaminating occurring. The relative cure speed of the hybrid resins again matches the general trend observed for the neat PF resins although the overall cure speed was significantly reduced. This indicates that while pMDI effectively accelerates curing of the hybrid resins the relative cure speed still reflects that of the parent PF formulation.

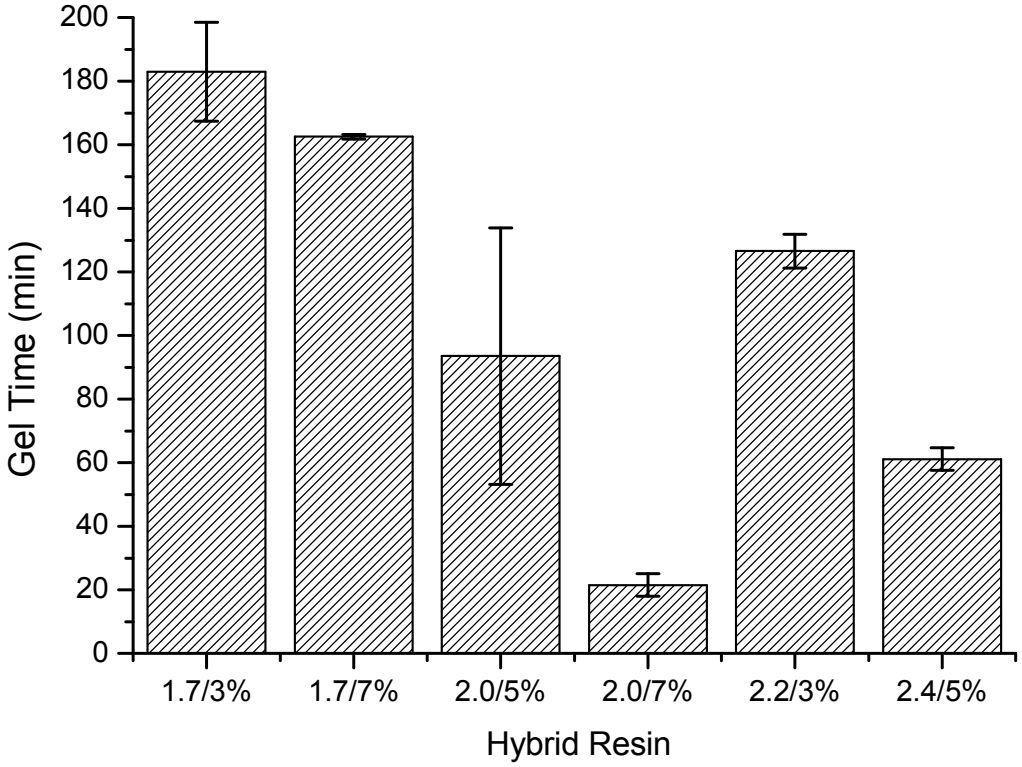

Figure 4.14. Approximate gel times (intersection of 5 Hz G' & G") of hybrid resins as measured by parallel plate oscillation rheology (Error bars represent $^{+}$/- one standard deviation)

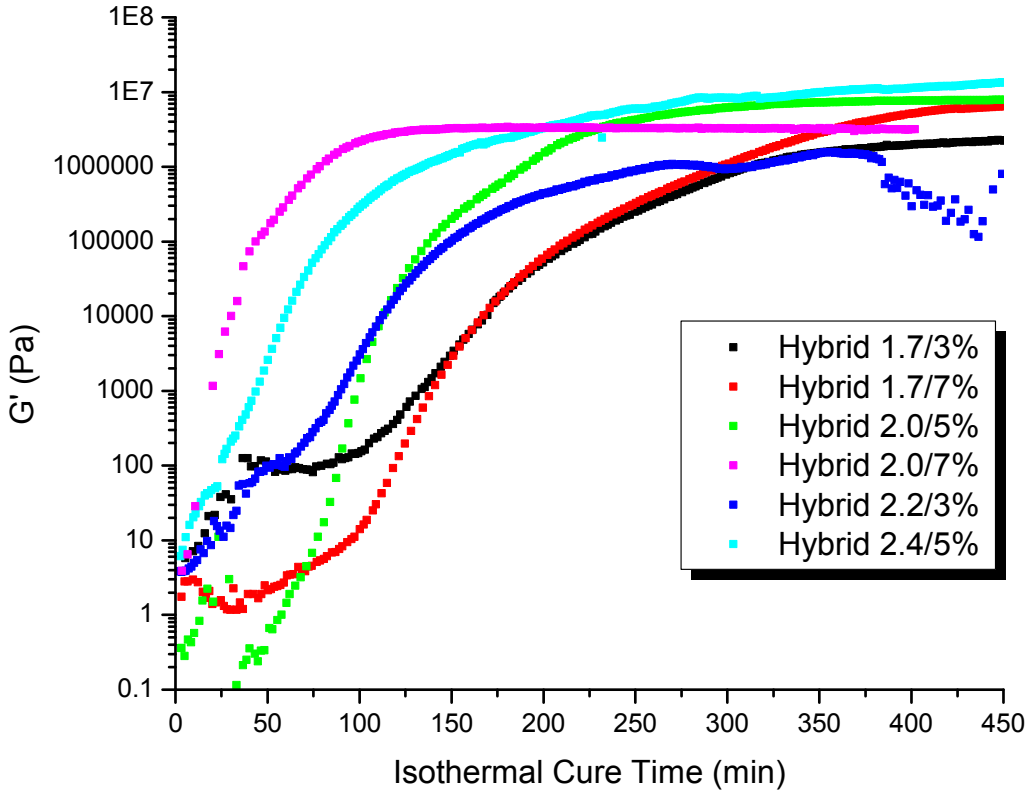

Figure 4.15. Isothermal parallel plate cure rheology of hybrid resins (Temperature = 65 °C; frequency = 5 Hz; percent strain was varied during cure)

The shape of the G' response for the low alkali hybrids is also noteworthy. Especially for Hybrid 1.7/3%, the modulus initially increased rapidly but reached a temporary plateau of ~100 Pa after 25 minutes. Only at 100 min did the modulus again begin to increase rapidly. To a lesser extent this same behavior is noted in Hybrid 2.2/3% and Hybrid 2.4/5%. The cause of this behavior is not clear. However, visually it was noted that when hybrid resins were cured at 75 °C in an open container a brittle agglomerate rapidly formed. This brittle structure seemed to be limited to the dispersed phase, with the non-agglomerated continuous resin phase remained a liquid. Perhaps the previously noted storage modulus plateau represents the formation of such an agglomerate gel. If this were the case, it seems plausible that the overall modulus would subsequently remain relatively constant until the modulus of the liquid phase advanced enough to be detectable over the dominant response of the more advanced aggregate.

4.3.2.4. Dielectric Analysis of Resin Cure within Wood Bondlines:

The in-situ curing of three hybrid adhesives and a neat PF control were studied using dielectric analysis. It should be noted that the resins were applied to the wood surfaces using a hard rubber roller and it is possible that this application method perhaps altered the liquid-state morphology. Plots of log ion viscosity and bondline temperature during 200 °C hot pressing are shown for each adhesive in Figure 4.16. Each trace is the average of two replicate experiments. Due to instrument limitations, the temperature signal below 100 °C was extremely erratic, fluctuating from below room temperature to well above 200 °C. To simplify Figure 4.16, the erratic temperature response prior to 15 minutes has been omitted. Surprisingly, the significant acceleration of hybrid resins which was noted in rheological studies of the bulk resins is not observed in the in-situ dielectric specimen. In fact, in Figure 4.16 the neat PF resin vitrified faster than all but Hybrid 1.7/3%, which itself was the slowest curing of all the hybrid resins in the bulk state. Similarly, Hybrid 2.0/7%, which exhibited the fastest curing in rheological measurements, is actually the slowest curing resin within the wood bondline. Comparison of bond line temperatures can not explain this trend; all resins followed a relatively uniform heating profile and Hybrid 1.7/3%'s temperature actually increased the slowest in spite of the fact that this resin exhibits the fastest in-situ curing.

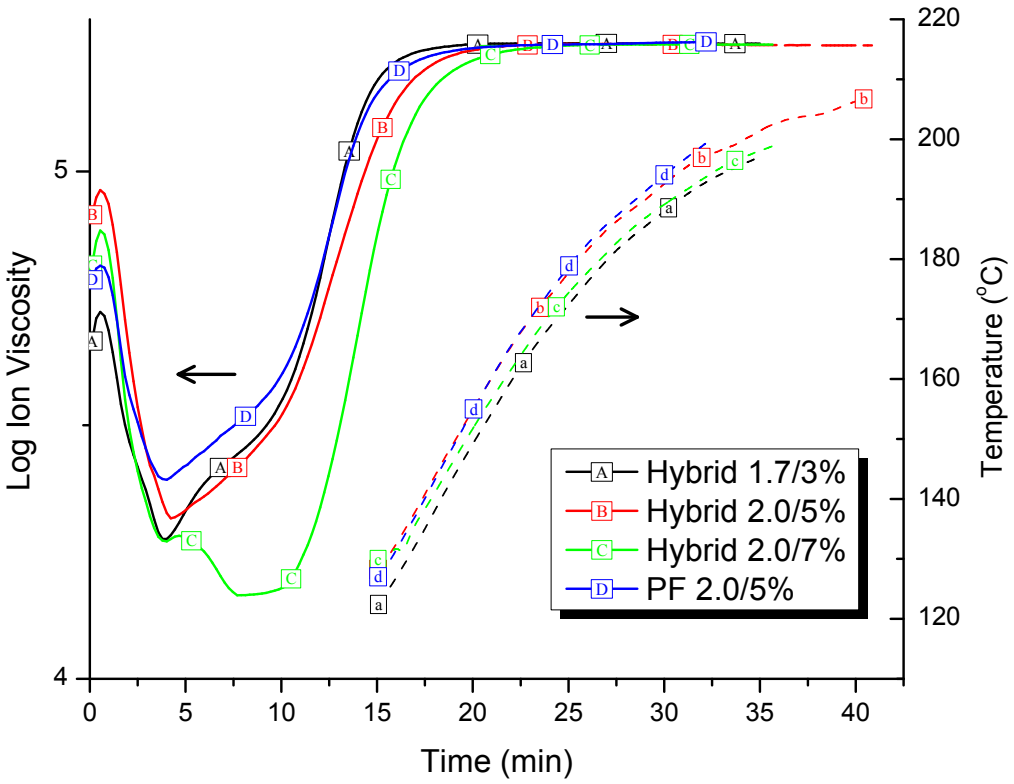

Figure 4.16. In-situ dielectric cure analysis of bonded southern yellow pine laminates (Cure temperature = 200 °C; frequency = 1 Hz; each curve is the average of two specimen)

The dielectric data emphasizes that experiments of bulk resin properties are not necessarily representative of adhesive performance within an actual bonded wood composite. For instance, experimental conditions employed to study the bulk resin properties often poorly replicate the precise temperature, pressure, shear rate and moisture environment experienced by an adhesive within a wood bondline. Furthermore, in certain instances, such as the curing of neat PF resols, wood is known to play an active catalytic function in altering resin cure kinetics [43-47]. Although experiments of bulk resin properties may not be analogous to the resins in-situ properties, the simplified bulk resin system may still provide valuable information regarding underlying cure processes which may not otherwise be experimentally accessible in the more complex composite system.

4.4. Conclusions

Six PF resins of varying F/P ratio and alkali concentration were successfully synthesized at a uniform viscosity and solids content. These resins were characterized using quantitative ^{13}C NMR spectroscopy. Although the properties of the high F/P, high alkali resin were somewhat anomalous, NMR otherwise revealed that increased alkali resulted in an increased number of crosslinks and increased methylol content. Similarly, increased F/P ratio appeared correlated with increased free formaldehyde, increased PF substitution, slightly increased crosslinking and increased methylol content. GPC further revealed a positive relationship between M_w and both F/P ratio and alkali content.

DSC thermal scans of hybrid resins demonstrated that the dispersed pMDI phase significantly altered and accelerated curing of the PF continuous phase. This indicates that significantly more interaction occurs between the pMDI and PF phases of hybrid resins than their multiphase morphology would initially suggest. Quasi-isothermal MDSC curing was useful for monitoring cure kinetics and detecting vitrification of the hybrid resins. Similar to the neat PF formulations, all hybrids initially exhibited n^{th} order reaction kinetics. In the high F/P, high alkali hybrid resins an additional exothermic event was observed partway through cure and was accompanied by rapid vitrification. The cause of this latent reactivity is unknown, but perhaps relates to the complex, multiphase morphology of the hybrid specimens. Initial thermal scans following isothermal curing only showed evidence of a high temperature exotherm believed to be evidence of either residual cure or urethane degradation. However, a second thermal scan following this initial heating revealed a slight exotherm whose onset was coincident with the original isothermal cure temperature. This residual exotherm further indicates that the overall hybrid reactivity remains somewhat restricted, even after thermal scanning up to 200 ^0C.

Similar to the DSC thermal scans, parallel plate cure rheology demonstrated substantially accelerated curing of the hybrid resins relative to neat PF. Furthermore, the precise cure speed of the various hybrid resins reflected that of their parent neat PF formulation. Despite the differences in cure speed observed for the bulk resins, dielectric analysis revealed that within bonded wood specimens all resin formulations, both hybrid and neat PF, cured at roughly the same speed. The in-situ dielectric curing results

highlight the fact that studies of bulk resin properties are not necessarily indicative of the same resin properties within a cured wood bondline. Despite this difference, the previous studies of the bulk resin properties may still allow for better understanding of the type and complexity of interactions occurring within hybrid PF/pMDI adhesives.

4.5. References

1 K. W. Haider, M. A. Wittig, J. A. Dettore, et al., *Wood Adhesives 2000* Forest Products Society, South Lake Tahoe, NV, 2000, p. 85.

2 M. Zhuang and P. R. Steiner, *Holzforschung* **47**, 425 (1993).

3 A. Pizzi and T. Walton, *Holzforschung* **46**, 541 (1992).

4 J. Zheng, Studies of PF Resol/Isocyanate Hybrid Adhesives, PhD, Wood Science and Forest Products, Virginia Tech. Blacksburg, VA (2000)

5 J. Y. Oldshue, *Fluid Mixing Technology* Mcgraw-Hill, Texas, (1983).

6 P. Li, D. W. Coleman, K. M. Spaulding, et al., *J. Chromotogr. A* **914**, 147 (2001).

7 T. Holopainen, L. Alvila, J. Rainio, et al., *Journal of Applied Polymer Science* **66**, 1183 (1997).

8 P. Luukko, L. Alvila, T. Holopainen, et al., *J. Appl. Polym. Sci.* **69**, 1805 (1998).

9 R. Rego, R. Adriaensens, R. Carleer, et al., *Polymer* **45**, 33 (2004).

10 T. Holopainen, L. Alvila, P. Savolainen, et al., *J. Appl. Polym. Sci.* **91**, 2942 (2004).

11 A. Pizzi (Ed.), Wood Adhesives Chemistry and Technology Marcel Dekker, New York, (1989).

12 M. G. Kim and L. W. Amos, *Ind. Eng. Chem. Res* **30**, 1151 (1991).

13 A. Pizzi and T. Walton, *Advanced Wood Adhesives Technology* Mercel Dekker, Inc, New York, (1994).

14 M. G. Kim, L. W. Amos and E. E. Barnes, *Ind. Eng. Chem. Res* **29**, 2032 (1990).

15 M. Kim, G. Y. Wu and L. W. Amos, *Journal of Polymer Science. Part A: Polymer Chemistry* **35**, 3275 (1997).

16 So.S., J. W. Teh, A. Rudin, et al., *Journal of Applied Polymer Science* **39**, 531 (1990).

17 D. D. Werstler, *Polymer* **27**, 750 (1986).

18 M. G. Kim, W. L. Nieh, T. J. Sellers, et al., *Ind. Eng. Chem. Res* **31**, 973 (1992).

19 T. J. Sellers and M. L. Prewitt, *J. Chromotogr.* **513**, 271 (1990).

20 J. D. Wellons and L. Gollob, *Wood Sci.* **13**, 68 (1980).

21 K. G. Moon, W. L. Nieh, T. Sellers, et al., *Ind. Eng. Chem. Res.* **31**, 973 (1992).

22 G. E. Myers, A. W. Christiansen, R.L.Geimer, et al., *Journal of Applied Polymer Science* **43**, 237 (1991).

23 B. Riedl, M.-J. Vohl and L. Calve, *J. Appl. Polym. Sci.* **39**, 341 (1990).

24 R. Mbachu, R. G. Schmidt and B. M. Broline, *Wood Adhesives 2000, Extended Abstracts.* Forest Products Society, South Lake Tahoe, NV, (2000).

25 Cole-Parmer Chemial Compatability Database, 2006.

26 S. Welch, D. Austin, M. Murphy, et al., (Viscotek Corporation, 2004), p. 58.

27 R. A. Haupt and T. Sellers, *Ind. Eng. Chem. Res.* **33**, 693 (1994).

[28] T. J. Sellers, *Plywood and Adhesive Technology :* Marcel Dekker, Inc, New York, (1985).
[29] T. Holopainen, L. Alvila, J. Rainio and T.T. Pakkanen, *Journal of Applied Polymer Science* **66**, 1183 (1997).
[30] A. Toffey and W. Glasser, *Journal of Applied Polymer Science.* **73**, 1879 (1999).
[31] J. M. Kenny, G. Pisaniello, F. Farina and S. Puzziello, *Thermochimica Acta* **269**, 201 (1995).
[32] P. W. King, R. H. Mitchell and A. R. Westwood, *Journal of Applied Polymer Science* **18**, 1117 (1974).
[33] C. B. Vick and A. W. Christiansen, *Wood and Fiber Science* **25**, 77 (1993).
[34] A. W. Christiansen and L. Gollob, *Journal of Applied Polymer Science* **30**, 2279 (1985).
[35] P. Luuko, L. Alvila, T. Holopainen, et al., *Journal of Applied Polymer Science* **82**, 258 (2001).
[36] G. Assche, A. V. Hemelrijck, H. Rahier, et al., *Thermochim Acta* **268**, 121 (1995).
[37] B. V. Mele, in TA Instruments Application Note, Vol. 2006.
[38] R. B. Prime, in: *Thermosets*, E. Turi (Ed.), pp. 435. Academic Press, New York (1981).
[39] Y. Lei, Q. Wu and K. Lian, *J. Appl. Polym. Sci.* **100**, 1642 (2006).
[40] A. Williams, *J. Chem. Soc., Perkin Trans* **2**, 808 (1972).
[41] H. H. Winter and F. Chambon, *J. Rheol.* **30**, 367 (1986).
[42] H. H. Winter, *Polymer Engineering and Science* **27**, 1698 (1987).
[43] X. Lu and A. Pizzi, *Holz als Roh- und Werkstoff* **56**, 339 (1998).
[44] M. Mizumachi and H. Morita, *Wood Sci.* **7**, 256 (1975).
[45] L. Onic, V. Bucur, M. P. Ansell, et al., *International Journal of Adhesion & Adhesives* **18**, 89 (1998).
[46] A. Pizzi and R. Garcia, *J. Appl. Polym. Sci.* **70**, 1111 (1998).
[47] A. Pizzi, X. Lu and R. Garcia, *J. Appl. Polym. Sci.* **71**, 915 (1999).

CHAPTER 5. FRACTURE PERFORMANCE OF PF/PMDI HYBRID ADHESIVES: INFLUENCE OF PF CHEMISTRY

The content of this chapter is presented in the form of a paper which has been submitted to *Wood and Fiber Science.*

5.1. Introduction

Resol phenol formaldehyde, PF, and polymeric methylenebis(phenylisocyanate), pMDI, are the only adhesives economically suitable for the production of exterior grade wood composites. Recent research has focused on a potential alternative consisting of a physical blend of aqueous PF with liquid pMDI. Although such a system may hardly seem novel, a unique feature is that the blend components are both immiscible and co-reactive. As a result, interesting possibilities arise from the structure of the resulting emulsion and from the corresponding solid-state multiphase morphology. Compelling justification for such research was first provided by Pizzi et al [1]. PF/pMDI blends were reported to provide excellent performance for industrial plywood manufacture using difficult-to-bond woods and showed remarkable durability following six-hour boiling water treatment [1]. Blends of PF with pMDI have also attracted industrial interest, as documented by the US patent literature [2-4].

Previous results from our laboratory demonstrated that emulsion effects dominated the rheological properties of liquid blends and that reaction between resins provided an added layer of complexity [5, 6]. When PF was the continuous phase, substantial toughening was provided by the pMDI dispersed phase, but the reverse was not true; PF did not significantly toughen a pMDI continuous phase [7]. However in contrast to Pizzi et al [1], accelerated weathering drastically reduced hybrid performance [6].

A later study found that the blend components reacted rapidly upon blending, encapsulating the pMDI dispersed phase in a polymeric membrane [5]. In the cured solid

state, FE/SEM and AFM detected dispersed pMDI-borne domains exhibiting a sharp phase boundary. However, there was evidence of interdiffusion: 1) dispersed pMDI accelerated gelation in comparison to neat PF, 2) mechanical spectroscopy detected two transitions that were interpreted as secondary relaxations in neat PF and in a PF-pMDI copolymer and 3) AFM provided evidence of copolymer formation in both the continuous and dispersed phases [5].

Those earlier studies employed commercially available resins, so no consideration to resin synthetic variables was given. We could expect that both PF and pMDI synthetic variables would impact the performance of the hybrid system. PF resols have vast formulation flexibility, whereas pMDI wood binders are rather limited in formulation since they are a by-product from higher value materials. Consequently, the performance of the hybrid system should be studied as a function of the major PF variables. In the present study of PF/pMDI hybrid adhesives, the influence of PF alkali and of the F/P mole ratio is studied with respect to the mode-I fracture toughness of bonded-wood dual cantilever beams (DCB).

5.2. Experimental

5.2.1. Materials

The pMDI used was Rubinate® 1840 (Huntsman Polyurethanes), with viscosity (25 °C) of 166 mPa•s and NCO content of 31%. PF resols were synthesized using 50 wt% NaOH, crystalline phenol, urea (Fisher ACS), 37 wt% formaldehyde (Aldrich ACS containing 10-15% methanol) and deionized water. Flat-sawn southern yellow pine (*Pinus spp.*) was machined into laminae (250x150x11mm, LxTxR) with a grain angle of 3 to 5° with respect to the tangential bonding surface. The laminae were planed to a final thickness of 10 mm. Surfaces to be bonded were matched together and equilibrated to an equilibrium moisture content (EMC) of approximately 12%.

5.2.2. Methods

Resol synthesis. – Six different PF resol formulations were synthesized, each with a target formaldehyde to phenol (F/P) mole ratio between 1.8 and 2.5, and an alkali content

(based on total resin mass) between 3% and 7%. Each formulation was prepared in three separate batches; replicate batches subsequently combined to reduce the overall variability. Quantitative ^{13}C NMR analysis of the resols (*Section 4.3.1.1*) revealed that the actual F/P ratio varied somewhat from the synthetic target. The six resin formulations are described in Figure 5.1, as a function of both the target F/P ratio (Figure 5.1A) and the measured F/P ratio (Figure 5.1B);). Note in Figure 4.1B that the precise F/P ratios of PF 2.3/3% and PF 2.5/5% were 2.24 and 2.43, respectively. Given the similarity in the measured F/P ratios of these two resins, they will be grouped together and modeled using a common F/P ratio of 2.3. NaOH/phenol molar ratios of each formulation are provided in Table 5.1. Resins will be referred to by their measured F/P ratio followed by their percent alkali. For example, "PF 2.0/7%" indicates the neat PF resin with a measured F/P ratio of 2.0 (target F/P ratio = 2.5) and an alkali content of 7%.

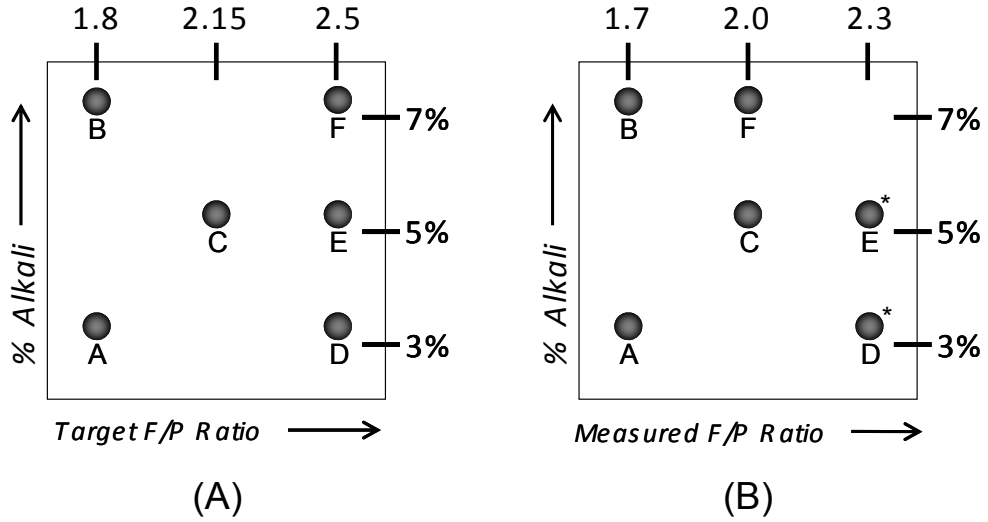

* The measured F/P ratios of PF 2.3/3% and PF 2.3/5% were 2.24 and 2.43, respectively. These resins will referred to and analyzed using a common F/P ratio of 2.3.

Figure 5.1. Experimental matrix for the preparation of PF resins as a function of: (A) the target F/P mole ratio and alkali content; and (B) the measured (^{13}C NMR) F/P ratio and alkali content.

Table 5.1. NaOH/phenol molar ratios of the six resol formulations.

NaOH/Phenol Mole Ratio			
	Target F/P ratio		
Alkali Content (%)	1.8	2.15	2.5
3%	0.236		0.270
5%		0.441	0.470
7%	0.603		0.689

Resins were synthesized in a 2-litre glass reactor equipped with a reflux condenser, thermocouple, Teflon coated copper heat exchanger and overhead mixer. Temperature regimes were carefully maintained at ±1.5 °C. During reaction, viscosity was measured periodically on 1 ml aliquots using a Brookfield CAP200+ viscometer (30 °C, 10,000 s^{-1}). Plots of viscosity versus reaction time were constructed and extrapolated in real-time to achieve target viscosities.

Reagent quantities were based on a solids content of 50% and a batch size of 960 g. A double-caustic charge (split-cook) procedure was employed: phenol, half of the necessary NaOH and 90% of the necessary deionized water were initially charged to the reactor and heated to 70 °C with agitation. All formaldehyde was metered into the reactor (8 ml/min) and then reflux was initiated (95 °C). Once the viscosity reached 200 ±50 mPa·s, the reactor was rapidly cooled and held at 70 °C until the viscosity increased to 400 ±50 mPa·s. The remaining NaOH and distilled water were subsequently added and the reaction was maintained at 70 °C until the viscosity returned to 400 ±25 mPa·s, at which point the reaction was rapidly quenched to 20 °C. Overall reaction times were between 225 ±10 min for PF 2.3/3% and 650 ±50 min for PF 1.7/7%.

Originally, the viscosities of PF 2.3/5% and PF 2.0/7% were somewhat higher than the viscosities of the remaining four resols. Therefore, 1.6 and 2.75 wt% de-ionized water (based on total resin mass) was added to these respective resins to more uniformly standardize resin viscosity. Two-percent urea (based on total resin mass) was then added to each resin as a free-formaldehyde scavenger typical of industrial resol formulations. Following urea addition, all resols had Newtonian viscosities between 220 and 255 mPa·s and solids contents between 41.3% and 44.4%. Detailed characterization of the resols is provided in a separate publication [8]. Resins were stored frozen at -22 °C.

Blend preparation. – Only one blend ratio was examined, containing 75 parts PF resin solids to 25 parts pMDI resin solids. This blend ratio was chosen because of its substantial toughness at relatively low pMDI loadings [7]. Immediately prior to fracture-specimen bonding (described below), PF/pMDI blends were prepared in small 10 g batches inside a 22 mm diameter glass vessel. Liquid pMDI was added to the PF and then agitated at 900 rpm for 90 seconds using a digital mixer fitted with a standard type R-I radial flow impeller [9] of 16 mm maximum diameter (custom fabricated). Hybrid resins are referred to in a manner analogous to the PF resins; i.e. "Hybrid 1.7/3%" denotes a PF/pMDI hybrid adhesive prepared from the neat PF 1.7/3% resol.

Mode-I fracture testing. – A neat-PF 2.0/5% control along with six hybrid resins were investigated. The adhesive was applied onto each laminate face with a hard rubber roller (50 g/m^2 per bonding surface) and the bonded assembly was hot-pressed at 0.69 MPa (100 psi) and 200°C for 20 minutes. The pressing time was selected based on the micro-dielectric analysis of bondline cure [8], which demonstrated that both neat PF and hybrid resins vitrified within approximately 17-20 minutes under the stated cure conditions. No correction was made for the slight differences in cure speed of individual resins. After hot-pressing, the bonded laminates were cooled to room temperature and machined into fracture specimens 20mm wide and approximately 240 mm long, as in [10]. Four laminates were prepared for each resin; typically, six specimens were obtained from each laminate. All fracture specimens were equilibrated to 10% EMC.

The 1st, 3rd and 5th specimens machined from each laminate were tested in an unweathered condition. The remaining three specimens were subjected to simulated weathering (two-hour water boil followed by overnight drying at 105°C). Weathered specimens were re-equilibrated to an EMC of 12% before testing.

Fracture testing was conducted according to the method of Gagliano and Frazier [10]. An initial pre-crack was created by pressing a razor approximately 10mm into the bondline. The specimens were initially tensioned with 5-10 N of preload and the instrument displacement was then set to zero. Specimens were then loaded cyclically in mode-I cleavage in a fashion similar to [10]. Initiation (G_I) and arrest (G_A) strain energy release rates (SERRs) were calculated using linear elastic beam theory employing the corrected compliance method; each specimen's effective flexural rigidity and crack

length offset were obtained from a linear fit of the cube root of compliance versus crack length plot [10]. From 5 to 16 crack extensions were obtained for each specimen, resulting in 5 to 16 values of G_I and G_A per specimen.

5.3. Results and Discussion

The load versus displacement curve for a single unweathered specimen of Hybrid 1.7/3% is given in Figure 5.2 and is typical of the behavior observed for all specimens. Figure 5.2 is overlaid with computer generated slopes, and points of crack initiation and arrest for each cycle. In the algorithm used to analyze the loading curves, crack initiation was identified as the point when the load-displacement curve deviated from linearity by 3%. However, occasionally the peak load occurred at less than 3% deviation, in which case the peak load was substituted as the point of crack initiation. In a few rare instances this criterion erroneously resulted in an initiation load that was less than the arrest load of the previous cycle. In these instances a correction was made by setting the initiation load equal to the arrest load of the previous cycle. Cycles with crack lengths occurring within the first or last 45 mm of the specimen were omitted to avoid beam-end effects. Also note in Figure 5.2 that the slope-lines of cycles 2 through 12 all intersect at a common point, but the slope-line of cycle 1 is incongruent because of the relaxation of the 5-10 N tensioning preload. This is presumably due to wood inelasticity during early cycles when the short effective beam length resulted in the greatest loads. Cycles exhibiting this behavior were excluded from analysis. Typical compliance and SERR plots are overlaid in Figure 5.3 (the corresponding plots of additional specimens are provided in Appendix A.1.2.). Linear regression coefficients (R^2) of all compliance curves were generally greater than 0.99. In those few instances when R^2 was less than 0.99, the specimens were excluded from this study.

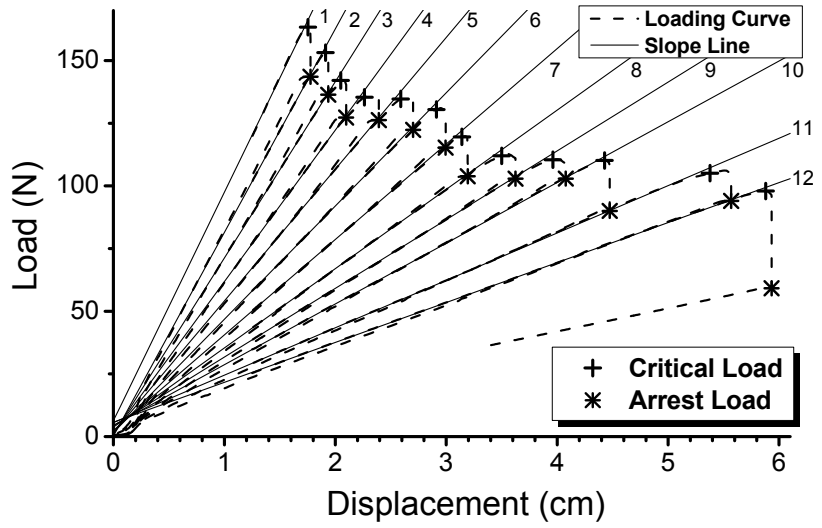

Figure 5.2. A typical load versus displacement curve with fitted slope lines for a flat sawn southern yellow pine specimen.

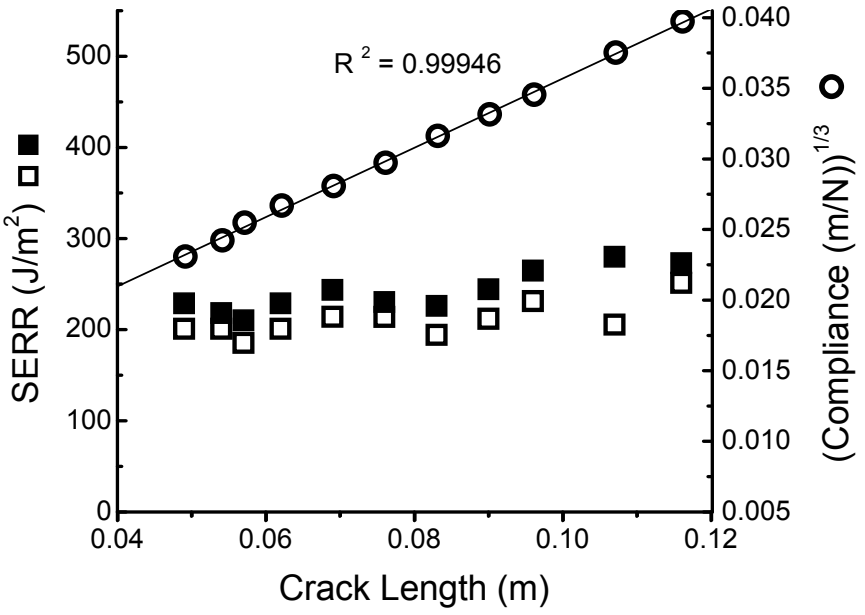

Figure 5.3. Typical cube root of compliance (○) and SERR (□■) plots for this study; this particular plot is for the loading curve depicted in Figure 5.2.

5.3.1. Hybrid Relative to Neat PF Performance

Average G_I and G_A values are summarized in Table 5.2 and presented in Figure 5.4**.** Reported values are simple means of the individual crack extensions averaged oveer

all specimens prepared for each formulation. The unweathered G_I values of all hybrid specimens were between 260 and 370 J/m^2, and this is substantially less than for similar specimens reported by Zheng, et al. [7], in which the substrate was yellow-poplar (*Liriodendron tulipifera*) and the resol was of commercial origin. The discrepancy is not related to the different woods and resols (unpublished data), but might arise from differences in blending methods; Zheng et al. [7] blended the hybrid resins by hand (~200 rpm) and this may have resulted in a different emulsion structure compared to the mechanical agitation (900 rpm) used in this study.

Table 5.2. Initiation (G_I) and arrest (G_A) strain energy release rates for dry and weathered DCB specimens.

	1.7/3%		1.7/7%		2.0/5%		2.0/7%		2.3/3%		2.3/5%		Neat PF	
	Unweathered	*Weathered*	*Unweathered*	*Weathered*	*Unweathered*	*Weathered*	*Unweathered*	*Weathered*	*Unweathered*	*Weathered*	*Unweathered*	*Weathered*	*Unweathered*	*Weathered*
Number of laminates:	*4*	*4*	*4*	*4*	*3*	*2*	*4*	*4*	*4*	*4*	*4*	*4*	*4*	*4*
Number of specimen:	*11*	*12*	*12*	*12*	*11*	*6*	*11*	*12*	*11*	*12*	*12*	*12*	*10*	*12*
G_I (J/m^2)	**279.0**	**265.3**	**371.0**	**354.3**	**359.5**	**294.4**	**276.8**	**245.8**	**282.3**	**274.4**	**309.2**	**297.1**	**259.7**	**285.2**
Standard Dev	51.3	51.2	70.6	71.2	89.5	59.1	43.9	44.4	92.6	86.6	44.3	48.0	89.0	90.9
Number of data points (Cycles)	104	107	89	92	81	52	93	94	85	100	102	118	83	80
G_A (J/m^2)	**253.1**	**232.8**	**324.9**	**305.4**	**315.2**	**256.6**	**250.0**	**214.0**	**243.3**	**232.7**	**268.9**	**260.1**	**232.0**	**237.8**
Standard Dev	45.9	44.0	67.8	67.5	91.5	56.1	37.6	39.6	82.6	78.4	45.2	42.6	82.8	68.6
Number of data points (Cycles)	104.0	105.0	89.0	91.0	81.0	52.0	94.0	95.0	84.0	100.0	104.0	118.0	77.0	80.0

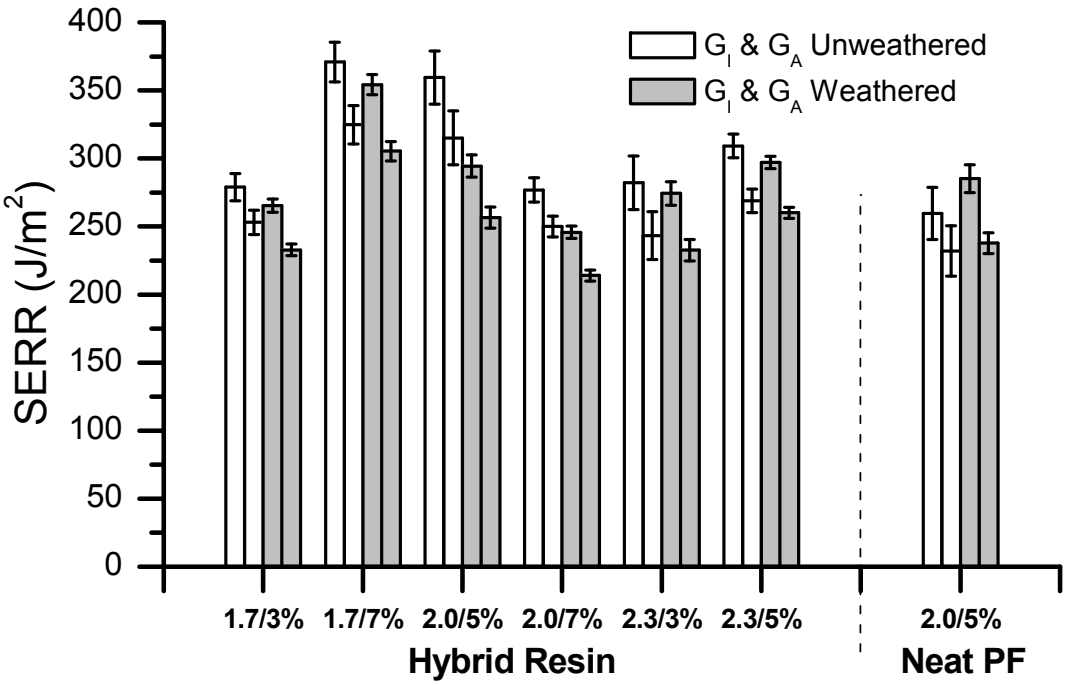

Figure 5.4. Mean initiation (G_I) and arrest (G_A) strain energy release rates for unweatherd and weathered DCB specimens (error bars represent a 95% confidence interval about the mean).

In the unweathered state the mean G_I of Hybrid 2.0/5% was 38% greater than that of the corresponding neat PF 2.0/5% (Satterthwaite *t*-test; P<0.0001) and, like previous studies [7], demonstrates that the dispersed pMDI phase significantly toughens the continuous PF matrix. Following weathering, G_I values of both Hybrid 2.0/5% and the corresponding PF were not significantly different (P = 0.4821). Note that weathering actually increased the mean G_I of PF 2.0/5% by 10%. Increased toughness following weathering has been reported elsewhere [6, 11] and may be due to a relaxation of cure stresses. For Hybrid 2.0/5%, weathering resulted in 26% decrease in G_I toughness, substantially less than that reported in [6]. Relative to the corresponding PF formulation, the overall performance of Hybrid 2.0/5% is promising, corroborating the initial findings reported by Pizzi et al. [1].

5.3.2. Effect of F/P Ratio and Percent Alkali on Hybrid Adhesive Performance

Full factorial models of both G_I and G_A indicated significant binary interaction between F/P and percent alkali ($P < .0001$). Binary interaction between percent alkali and weathering and ternary interaction between F/P, percent alkali and weathering were non-significant ($P = 0.127$ and 0.163, respectively). Therefore, a reduced factorial model that neglected the non-significant interaction effects was used to examine the influence of F/P ratio and alkali content in detail.

Regarding the combined effect of F/P ratio and alkali level on unweathered G_I's, least square means and the related mean difference *P*-values from the reduced factorial model are given in Table 5.3. Significant differences were observed in G_I along the sequence: Hybrid 1.7/7% > Hybrid 2.0/5% > Hybrid 2.3/5% > Hybrid 2.3/3%. The G_I values of Hybrids 1.7/3% and 2.0/7% were statistically equivalent to that of Hybrid 2.3/3%. Table 5.4 gives the corresponding least squares mean and difference values of G_A. The G_A values followed a similar statistical trend as the G_I values: Hybrid 1.7/7% > Hybrid 2.0/5% > Hybrid 2.3/5% > Hybrid 1.7/3% = Hybrids 2.3/3% = 2.0/7%. The interaction effects between F/P ratio and percent alkali prohibit a simple relation of these individual variables to unweathered fracture performance. For example, at the F/P 2.0 level there was an inverse relationship between percent alkali and G_I, but at the F/P 1.7 level this trend was reversed.

Table 5.3. Unweathered crack initiation (G_I) least square means and difference probability (*P*) values based on the reduced factorial model.

	LS Mean	272.2	362.6	329.2	261.3	278.4	303.1
	Resin	Hybrid 1.7/3%	Hybrid 1.7/7%	Hybrid 2.0/5%	Hybrid 2.0/7%	Hybrid 2.3/3%	Hybrid 2.3/5%
Resin	***LS Mean***						
Hybrid 1.7/3%	*272.2*	X	<0.0001	<0.0001	0.0944	0.3336	<0.0001
Hybrid 1.7/7%	*362.6*	<0.0001	X	<0.0001	<0.0001	<0.0001	<0.0001
Hybrid 2.0/5%	*329.2*	<0.0001	<0.0001	X	<0.0001	<0.0001	0.0003
Hybrid 2.0/7%	*261.3*	0.0944	<0.0001	<0.0001	X	0.0106	<0.0001
Hybrid 2.3/3%	*278.4*	0.3336	<0.0001	<0.0001	0.0106	X	0.0001
Hybrid 2.3/5%	*303.1*	<0.0001	<0.0001	0.0003	<0.0001	0.0001	X

Table 5.4. Unweathered crack arrest (G_A) least square means and difference probability *(P)* values based on the reduced factorial model.

	LS Mean	242.9	315.1	287.4	232.1	238.0	264.5
	Resin	Hybrid 1.7/3%	Hybrid 1.7/7%	Hybrid 2.0/5%	Hybrid 2.0/7%	Hybrid 2.3/3%	Hybrid 2.3/5%
Resin	***LS Mean***						
Hybrid 1.7/3%	*242.9*	X	<0.0001	<0.0001	0.0694	0.4095	0.0002
Hybrid 1.7/7%	*315.1*	<0.0001	X	<0.0001	<0.0001	<0.0001	<0.0001
Hybrid 2.0/5%	*287.4*	<0.0001	<0.0001	X	<0.0001	<0.0001	0.0005
Hybrid 2.0/7%	*232.1*	0.0694	<0.0001	<0.0001	X	0.3401	<0.0001
Hybrid 2.3/3%	*238.0*	0.4095	<0.0001	<0.0001	0.3401	X	<0.0001
Hybrid 2.3/5%	*264.5*	0.0002	<0.0001	0.0005	<0.0001	<0.0001	X

5.3.3. Effect of Weathering on Hybrid Adhesive Performance

Both the full and reduced factorial models demonstrate that weathering significantly reduced Hybrid G_I and G_A values ($P < 0.0001$ in all cases). A durability

ratio was calculated for each adhesive as the average weathered G_I value divided by the average unweathered G_I value. These durability ratios are given in Table 5.5. All Hybrid formulations resisted the two-hour water boil quite well, retaining between 82% and 97% of there unweathered G_I toughness. From Table 5.5 it appears that Hybrid 2.3/3% was the most durable while Hybrid 2.0/5% was the least durable. Regarding the influence of F/P ratio on durability, at the two lower alkali levels increasing the F/P ratio led to an increase in durability. However, at the 7% alkali level this trend was reversed. The influence of alkali content on hybrid durability was also variable: at the F/P 1.7 level alkali content had only a minor effect on durability, at the F/P 2.0 level, durability increased with increasing alkali content, and at the F/P 2.3 level durability decreased with increasing alkali content. It is surprising that increased alkali did not consistently decrease hybrid durability; urethane hydrolytic stability is known to be related to alkali content [12], leading *Zheng, Fox and Frazier* [6] to postulate that alkali catalyzed urethane hydrolysis contributed to the poor durability which they observed. Instead, the interaction between durability, F/P ratio and alkali content highlights the complexity of the multiphase hybrid system.

Table 5.5. Fracture toughness G_I durability ratios for each of the six hybrid adhesive formulations (durability = average $G_{I,Weathered}$/average $G_{I,Unweathered}$).

		F/P Ratio		
		1.7	2.0	2.3
% Alkali	3	0.951		0.972
	5		0.819	0.961
	7	0.955	0.888	

5.4. Conclusions

In this study a moderate increase in unweathered fracture toughness was observed for a representative hybrid formulation relative to that of the corresponding neat PF formulation. Regarding the effect of resol chemistry on hybrid fracture toughness, both the F/P ratio and alkali content of the parent PF formulation significantly affected unweathered hybrid performance. However, interaction between hybrid F/P ratio and

alkali content made it impossible to uncouple the effects of F/P ratio from the effects of alkali content. In any case, Hybrid 1.7/7% was determined to have the highest unweathered fracture toughness while Hybrid 2.0/7% had the lowest toughness. Following accelerated weathering, all hybrid formulations retained between 82% and 97% of their original unweathered fracture toughness; this resulted in a weathered hybrid toughness which was statistically equivalent to that of a corresponding weathered neat PF formulation. Both the F/P ratio and the alkali content of the hybrid seemed to influence durability, although the nature of this influence was again highly variable. Overall, the performance of PF/pMDI hybrid adhesives appears heavily influenced by the parent resol's formulation; however, the hybrid system is complex and adhesive development will likely be best accomplished by considering the major resol synthetic variables in aggregate.

5.5. References

1 A. Pizzi, J. Valenzuela and C. Westermeyer, Holzforschung 47, 68 (1993).
2 W.-H. Hsu, US Patent No. 6,297,313 (2001).
3 T. R. Miller, L. D. Creel and W. D. Detlefsen, US Patent No. 6478998. (2002).
4 J. W. Rosthauser and W. D. Detlefsen, US Patent No. 6214265 (2001).
5 D. R. Riedlinger and C. E. Frazier, Journal of Adhesion Science and Technology In Press (2008).
6 J. Zheng, Studies of PF Resol/Isocyanate Hybrid Adhesives, PhD Dissertation, Wood Science and Forest Products, Virginia Tech. Blacksburg, VA (2000)
7 J. Zheng, S. C. Fox and C. E. Frazier, Forest Products Journal 54, 74 (2004).
8 D. R. Riedlinger, Characterization PF reosl-pMDI hybrid adhesives, M.S. Thesis, Department of Macromolecular Science and Engineering, Virginia Tech. Blacksburg, VA. (In Press)
9 J. Y. Oldshue, Fluid Mixing Technology Mcgraw-Hill, Texas, (1983).
10 J. M. Gagliano and C. E. Frazier, Wood and Fiber Science 33, 337 (2001).
11 R. G. Schmidt, Aspects of Wood Adhesion: Applications of 13C CP/MAS NMR and Fracture Testing, Ph.D. Dissertation, Wood Science, Virginia Tech. Blacksburg, VA (1998)
12 B. Van Mele, G. Van Assche and A. Van Hemelrijck, Journal of Reinforced Plastics and Composites. 18, 885 (1999).

CHAPTER 6. CONCLUSIONS

Blends consisting of liquid pMDI dispersed in aqueous PF resol are unusual in that the components are both immiscible and co-reactive. In the liquid state co-reaction was rapid, resulting in a copolymeric membrane which encapsulated the pMDI dispersed phase and preserved the shear-induced deformations experienced during blending.

Following curing, a multi-phase morphology was present and reflected the shear dependent structure of the liquid emulsion. Individual phases appeared to be separated by a sharp phase boundary, but there was also evidence of interdiffusion and co-reaction. For instance, both conventional DSC and oscillation cure rheology demonstrated that within the hybrid systems curing of the PF continuous phase was substantially altered and accelerated. Additionally, mechanical spectroscopy detected two hybrid transitions that were interpreted as secondary relaxations in neat PF and in a PF-pMDI copolymer. MDSC results suggest that overall reaction in the hybrid was somewhat restricted: in most hybrid formulations a latent exothermic event emerged at a somewhat variable time during isothermal curing; furthermore, subsequent conventional DSC analysis of the isothermally cured hybrids detected some residual reactivity even after thermal scanning to 200 ^{0}C.

Although substantially accelerated, bulk resin cure speeds of the various hybrid formulations reflected that of the parent resol formulation. However, within actual wood bondlines dielectric analysis detected little variation in cure speed between any of the formulations, both hybrid and neat PF.

Regarding the bonded wood mode-I fracture performance of hybrid resins, a moderate increase in unweathered fracture toughness was observed for hybrid formulations relative to neat PF. Following accelerated weathering all hybrid formulations retained between 82% and 97% of their original unweathered fracture toughness; this resulted in a weathered hybrid toughness which was statistically equivalent to that of a corresponding weathered neat PF formulation. While the resol F/P

ratio and alkali content appeared to influence hybrid toughness, statistical modeling revealed significant interaction between these variables: the influence of hybrid alkali content depended heavily on each formulation's specific F/P ratio, and vice versa. As such, tailoring of the hybrid adhesive properties is likely to be best accomplished by considering the major resol synthetic variables in aggregate.

Although a preliminary examination of hybrid morphology was provided in this study, further research is necessary to better understand how the hybrid emulsion structure influences blend curing and overall performance. Indeed, the observed isothermal MDSC vitrification times of hybrid resins varied considerably between replicate experiments and this may indicate that hybrid curing is sensitive to subtle differences in emulsion structure. Compared to previous literature reports, the reduced hybrid toughness and improved hybrid durability reported here may also be related to differences in blend preparation and hybrid morphology. While the blended PF/pMDI system is substantially more complex than either neat adhesive, with a greater understanding of this complexity significant formulation flexibility could be realized, allowing the properties of the hybrid system to be custom tailored for specific end-use applications.

APPENDIX

A1. Supplemental Data

A.1.1. Quasi-isothermal MDSC curing of neat PF

As described in section 4.3.2.2., a single neat PF resol was cured using quasi-isothermal MDSC. The thermogram is presented in Figure A.1. Once the temperature modulation stabilizes (at ~10min), the heat flow signal reveals n^{th} order reaction kinetics. However, no step-wise decrease, indicative of vitrification, is observed in the heat capacity signal. This may have been due to either the weak signal or that cure was monitored for an insufficient amount of time.

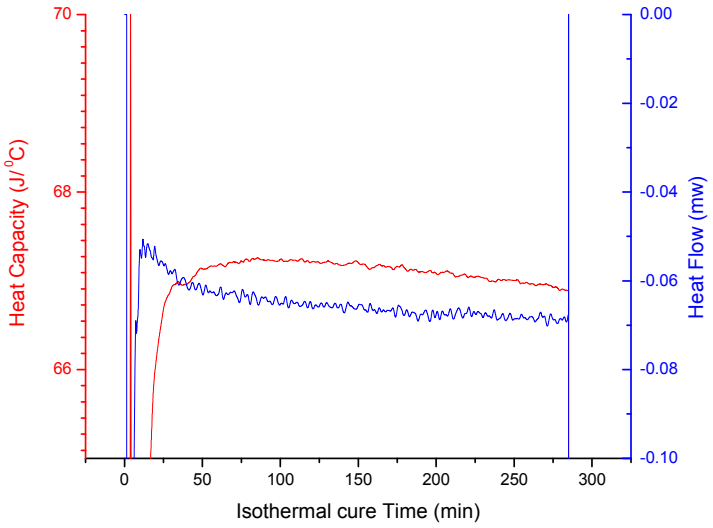

Figure A.1.1 Quasi-isothermal MDSC cure of neat PF 2.5/7% (T = 86.85 ^{0}C; amplitude = 1.5 ^{0}C/200 s)

A.1.2. Supplemental Fracture Toughness Data

The following pages provide a representative sample of the range of behavior exhibited in the cube root compliance and SERR graphs for several fracture specimen. R^2 values are for the compliance fit line.

A.1.2.1. Hybrid 1.7/3% Unweathered Laminate "A"

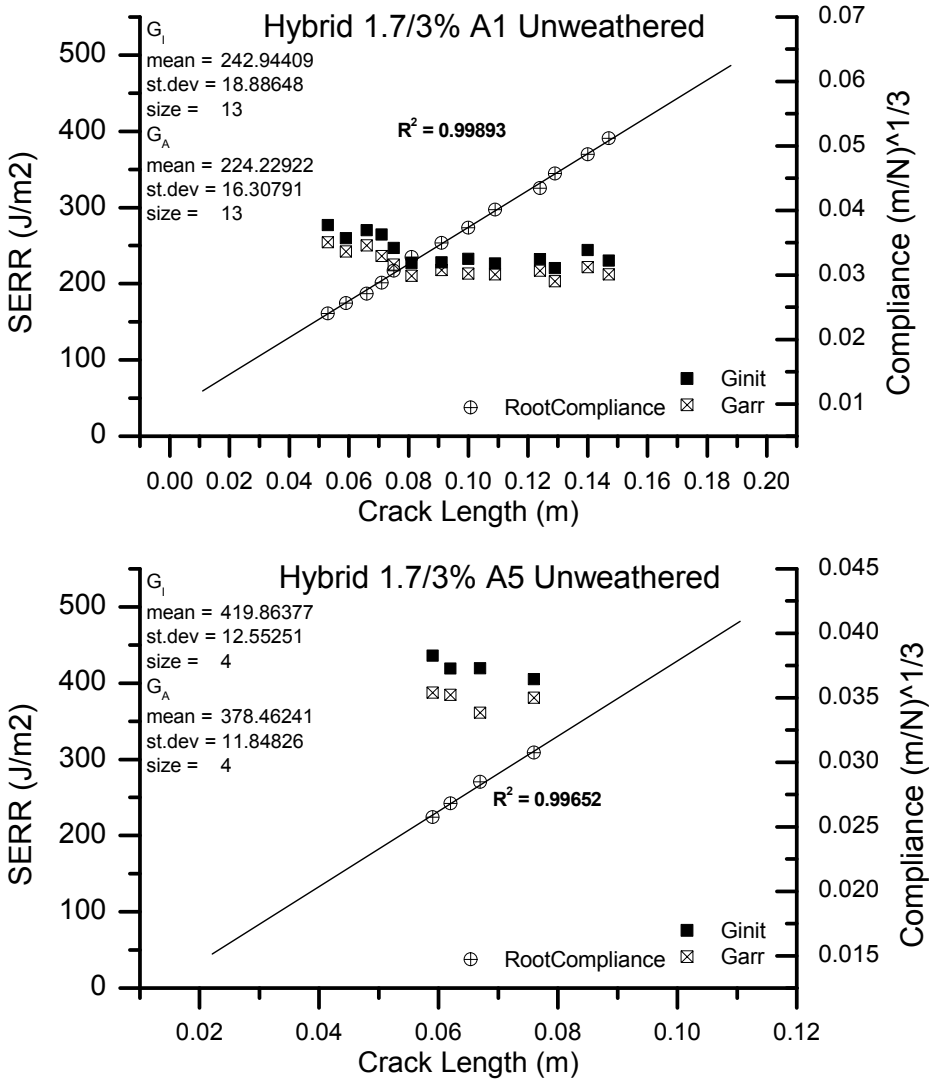

A.1.2.2. Hybrid 1.7/7% Weathered Laminate "B"

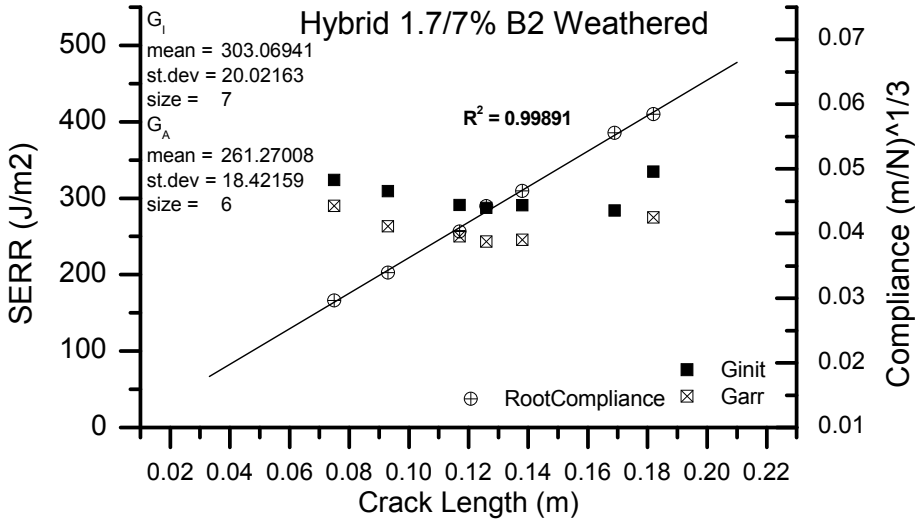

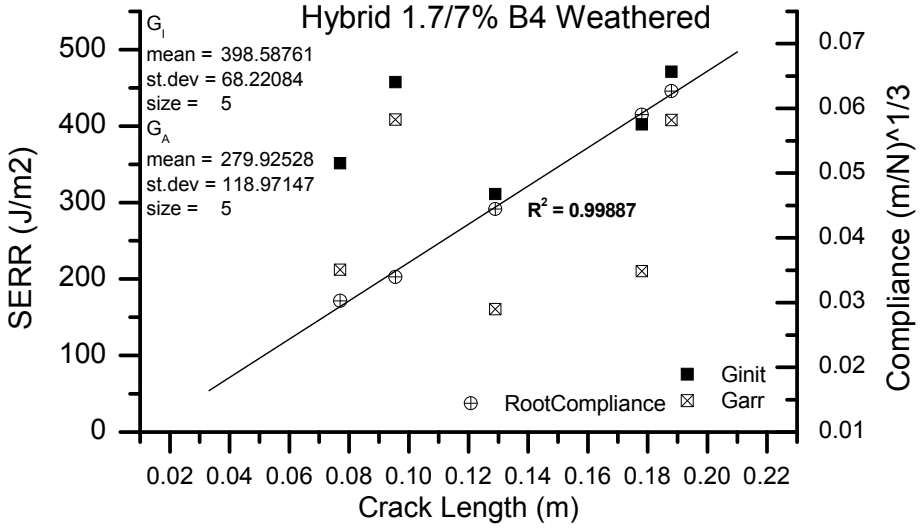

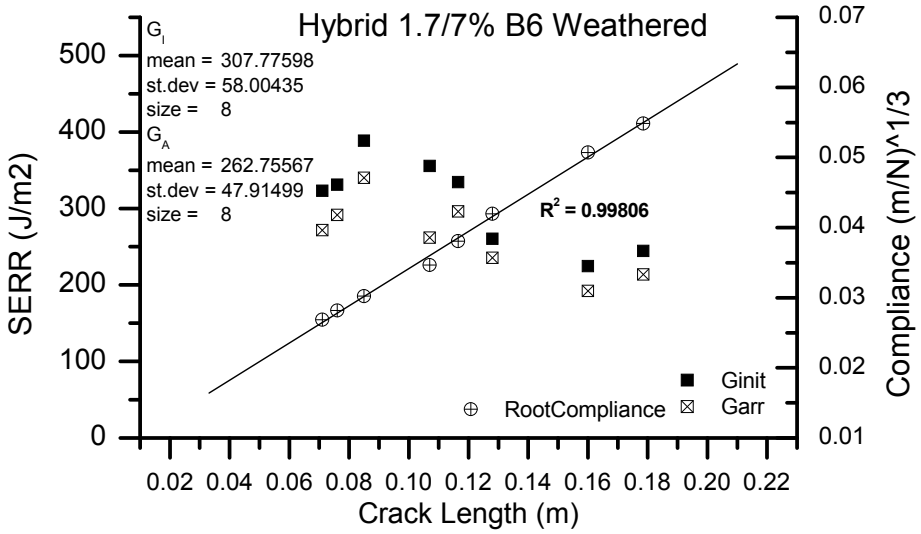

A.1.2.3. Hybrid 2.0/5% Weathered Laminate "A"

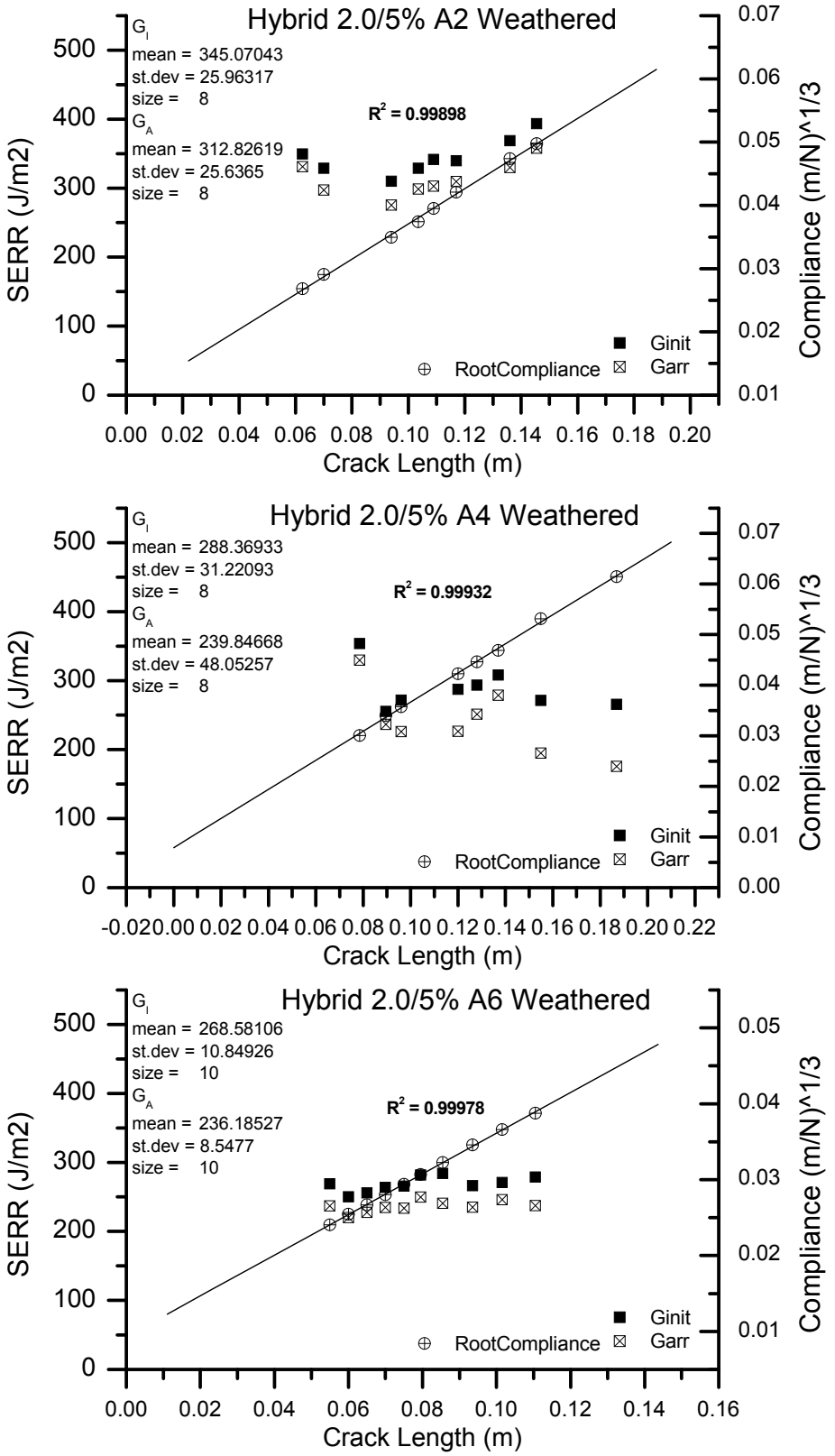

A.1.2.4. PF 2.0/5% Weathered Laminate "B"

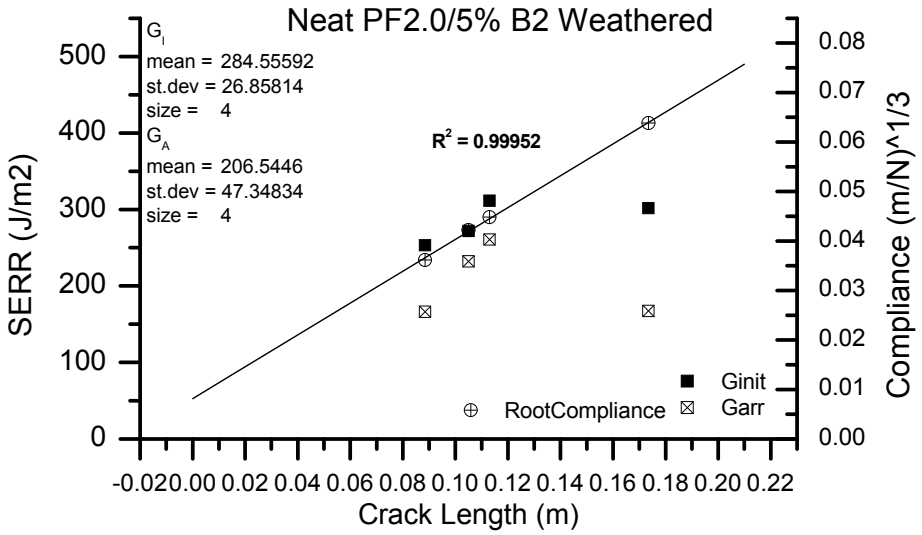

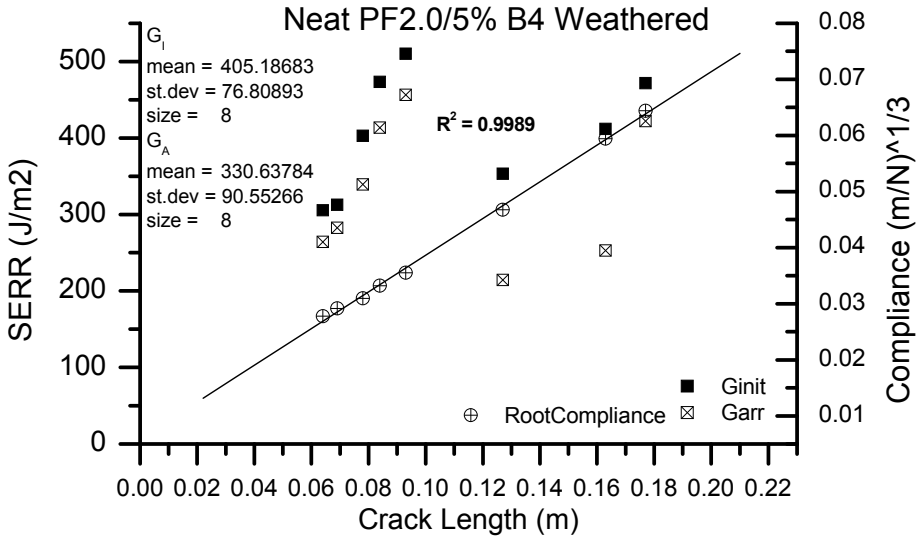

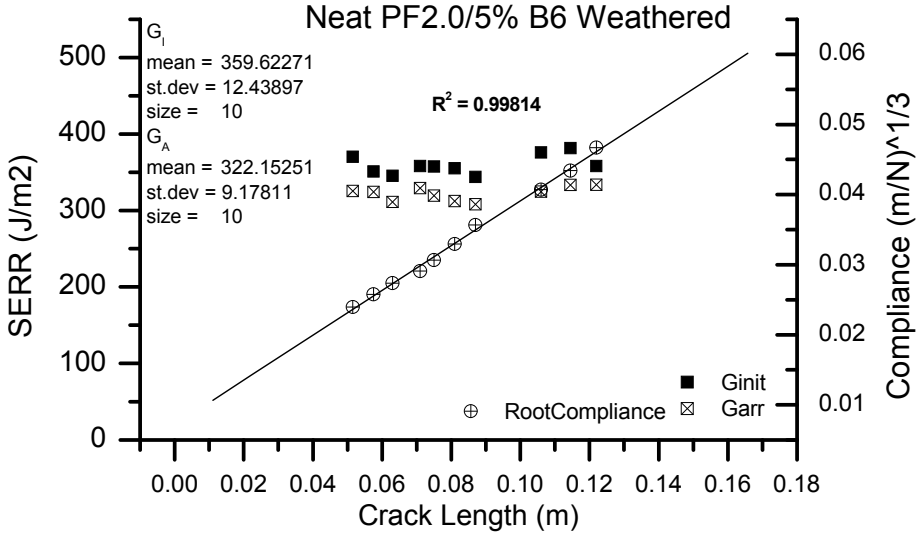

A.2. Tg AS AN INDEX OF CONVERSION IN PMDI-IMPREGNATED WOOD

The following research effort is unrelated to the previous investigation of PF/pMDI hybrid blends and is presented in the form of a paper which has been published in BioResouces 2(4), pg. 605-615. Approximately 40% of the experiments were conducted by a post-doctoral student, Dr. Nanjian Sun; the remaining 60% of the experiments were conducted by the author.

Darren A. Riedlinger,[a] Nanjian Sun,[b] and Charles E. Frazier[c*]

Contact information: a: Department of Macromolecular Science and Engineering,, Virginia Tech, 230 Cheatham Hall, Blacksburg, VA 24060 USA; b: DuPont China R&D Center, 600 Cailun Rd, Zhangjiang Hi Tech Parkm Podung New District, Shanghai 201203 China; c: Department of Wood Science and Forest Products,, Virginia Tech, 230 Cheatham Hall, Blacksburg, VA 24060 USA; Corresponding author: cfrazier@vt.edu

Abstract: It is well established that the glass transition temperature (T_g) is a sensitive measure of cure in neat thermosets. As cure advances, network mobility declines and the T_g rises in a systematic fashion. This study sought to determine if such a relationship exists for polymeric isocyanate adhesives (pMDI) cured in the presence of wood. Yellow-poplar (*Liriodendron tulipifera*) specimens were impregnated with neat pMDI and then isothermally cured for various periods in two different differential scanning calorimeters (DSCs). After this isothermal cure period, the T_g and residual heat of cure were determined. These thermal scans were performed using either constant (conventional) or modulated (MDSC) heating rates. For both methods, the degree of resin cure varied significantly under identical isothermal curing conditions; nevertheless, a strong relationship was found between the degree of resin cure and the associated T_g. While the conventional DSC method yielded slightly improved sensitivity and reproducibility, results from both methods compared favorably.

Article submitted: August 20, 2007; First round of peer-reviewing completed: Sept. 12, 2007; Article accepted: Sept. 12, 2007; Published Oct. 17, 2007.

A.2.1. Introduction

The classic work by Gillham and coworkers (Wisanrakkit and Gillham 1990) established that the glass transition temperature (T_g) is a sensitive measure of cure in thermosets. As cure advances, network mobility declines and the T_g rises in a systematic fashion. For the neat epoxy system studied by Gillham, the relation between T_g and percent conversion was found to be independent of the isothermal cure temperature. This fundamental relationship has since been demonstrated for a variety of other thermosets (Cook et al. 2004; Cook et al. 1997; Harismendy et al. 2000; Li et al. 2000; Malkin et al. 2005; Park et al. 2002; Scott et al. 2002; Teil et al. 2004; Toffey and Glasser 1997).

Modeling of polymeric methylenebis(phenylisocyanate), pMDI, wood adhesive cure has significant importance for optimizing industrial hot-pressing (Harper et al. 2001). Unfortunately, reliable modeling is complicated by the fact that pMDI requires moisture to undergo cure, yet pMDI is itself water immiscible. Although pMDI will cure in the presence of water or water vapor, in such a scenario pMDI's access to water is markedly different from that of pMDI impregnated in a wood substrate. In the latter scenario the water sorbed on wood promotes reaction, but wood's complicated surface is expected to influence the cure state. For instance, it has been demonstrated that the precise moisture content of wood and, in some instances, the wood species itself affect the reaction kinetics (He and Yan 2005; He and Yan 2007). Furthermore, competing reaction pathways exist for the isocyanate conversion and the exact nature of the pMDI-wood bond is not fully understood. The relative proportion of polyurea, biuret/polyuret, allophanate and polyurethane bonds are strongly influenced by wood moisture, cure temperature and wood species (Das et al. 2007; Harper et al. 2001; Owen et al. 1988; Weaver and Owen 1995; Wendler and Frazier 1996). As such, the cure of neat pMDI and of pMDI impregnated wood will likely differ, and this necessitates the development of *in situ* cure monitoring. The method developed by Gillham appears to lend itself to the study of pMDI-impregnated wood specimens and may be useful for developing kinetic based hot-pressing models for wood-pMDI systems. However, the fundamental relationship between T_g and isothermal cure time has only been demonstrated for neat adhesives and it is unknown if this relationship is valid for pMDI-impregnated wood.

Therefore, this study was intended to determine if the wood/pMDI system will conform to the classic relationship between T_g and the degree of cure.

Yellow-poplar (*Liriodendron tulipifera)* specimens were treated with neat pMDI and then isothermally cured for various times and temperatures inside a differential scanning calorimeter, DSC. After this isothermal cure period the samples were cooled and thermally scanned to detect both the T_g and the residual heat of cure of the partially cured resin.

A.2.2. Experimental

Separate DSC experiments were conducted using modulated (MDSC) and constant (conventional DSC) heating rates. In each case a commercial pMDI (Rubinate® 1840 from Huntsman Polyurethanes) was used: viscosity 166 mPa•s (25°C), NCO content 31%. Yellow-poplar flakes 0.3-0.5mm (conventional DSC) or 1.5 mm (MDSC) in thickness were sliced from the tangential wood surface using a disk flaker. The flakes were equilibrated to 7-8% moisture content over saturated aqueous K_2CO_3. Disks 3 mm in diameter were punched from the equilibrated wood specimen and soaked in pMDI for 5 min (conventional DSC) or 1 min (MDSC). For the MDSC specimen the excess resin was simply wiped off with tissue paper. For the conventional DSC specimen the excess resin was removed by placing the impregnated disks between tissue papers and pressed under a 10kg mass for 1 minute. The average weight increase from resination (based on the moisture equilibrated wood mass) was 52 +/-2% for the MDSC specimens and 32 +/-11% for the conventional DSC specimens. While these resin loadings were far in excess of those used in commercial applications, they approached the minimum necessary to obtain adequate heat flow responses for all DSC experiments. All specimens were analyzed immediately following impregnation.

MDSC experiments were conducted on a TA Instruments 2920 DSC equipped with a nitrogen purge (50 cm^3/min) and a refrigerated cooling system. Sapphire was used for the heat capacity calibration; indium was used for the temperature and cell constant calibrations. The resin impregnated disks were sealed in hermetic aluminum DSC pans and isothermally cured within the DSC at 80, 60 or 50°C for prespecified times between 0

and 16 hours. The partially cured specimens were then quench cooled to -90°C and thermally scanned at 2°C/min with a modulation amplitude of 0.4°C and a period of 60s.

Conventional DSC experiments were conducted on a TA Instruments Q100 DSC equipped with a nitrogen purge (50 cm^3/min) and a refrigerated cooling system. Indium was used for the temperature and cell constant calibrations. The resin impregnated disks were sealed in stainless steel high volume sample pans and isothermally cured at 80, 60 or 40°C for prespecified times between 0 and 24 hours. The partially cured specimens were then quench cooled to -90°C and thermally scanned at a constant heating rate of 20°C/min to 200°C. After this initial scan the sample was again quench cooled and rescanned over the above temperature range. This latter scan served as a fully-cured baseline and was subtracted from the initial scan, providing more reproducible measurements of the T_g and the heat of reaction. For both methods, heat of reaction calculations were made with TA Instruments Universal Analysis 2000 software using the sigmoidal baseline fit model. Reported T_g's are for the transition's midpoint.

A.2.3. Results and Discussion

A.2.3.1 Detection of T_g and Residual Cure Using MDSC

Typical MDSC thermograms for specimens precured for 0, 4 and 6 hrs (60°C) are shown in Figure A.2.1. The non-reversible heat flow exhibits the respective cure exotherms.

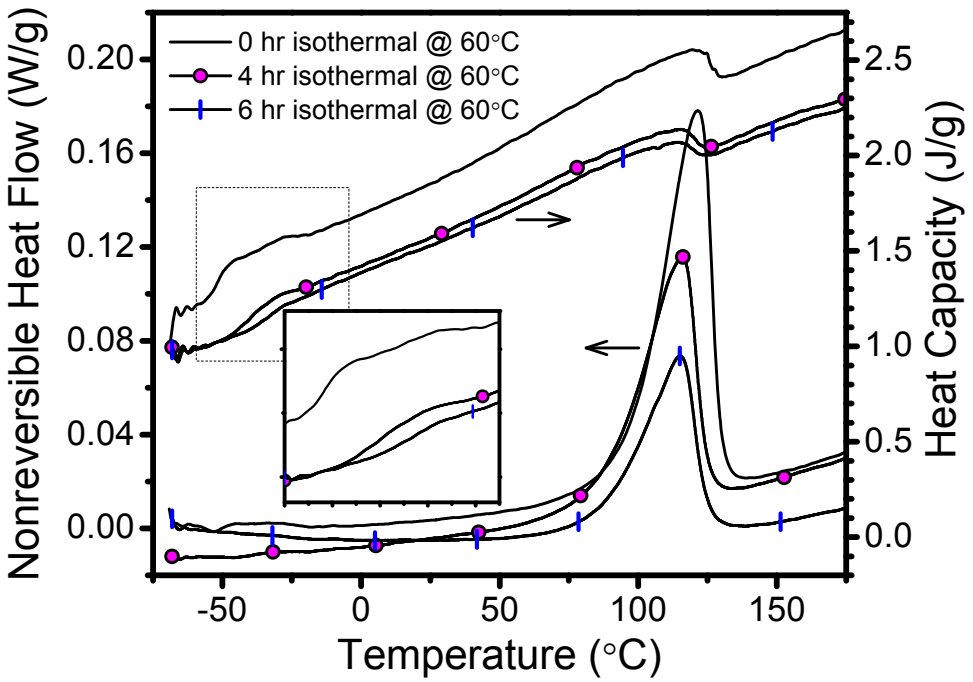

Figure A.2.1. MDSC thermograms of pMDI impregnated yellow-poplar previously cured for various times at 60°C (Heating Rate = 2°C/min; amplitude = 0.4°C; period = 60s). Inset shows an expanded view of heat capacity (Tg traces).

The residual heat of reaction (ΔH_R) decreased with increasing isothermal cure time, relative to the total heat of reaction (ΔH_T) measured for the uncured specimen. The heat flow trace does not clearly show the resin glass transition. The heat capacity curve does reveal the T_g (near -50°C), and vitrification is also seen in the high temperature region corresponding with the heat flow exotherm. As expected, the Tg rose following isothermal pre-curing. However, as the T_g rose its magnitude was proportionately reduced, making accurate detection more difficult.

The fractional conversion, *x*, defined as

$$x = 1 - \frac{\Delta H_R}{\Delta H_T} \qquad (1)$$

is plotted versus isothermal cure time at various temperatures in Figure A.2.2. Using the MDSC method, T_gs were unambiguously detected for fractional conversion only below approximately 0.6. Figure A.2.2 shows significant variation between fractional conversion and isothermal cure time. For example, the 60°C, 4 hr cure data varied about

the mean value by as much as +/- 50%. Similarly, the 50°C fractional conversions were somewhat uniform, but the corresponding cure times ranged from 6 to 15 hours. The reason for this great variation was unknown, nor was it investigated. With a 52% resin content, the MDSC specimens likely contained both adsorbed and free liquid pMDI. Perhaps the data scatter reflects differential degrees of resin adsorption and penetration. However, the corresponding plot of T_g versus fractional conversion (Figure A.2.3) displays a clear trend that is not discerned in Figure A.2.2. While some scatter remains, the T_g rises in a systematic fashion with increasing fractional conversion. Furthermore, this relation between T_g and fractional conversion was independent of the isothermal cure temperature. While Figure A.2.2 exhibits a complex relationship between fractional conversion and isothermal cure time, Figure A.2.3 demonstrates that T_g is an accurate indicator of resin cure. Furthermore, Figure A.2.3 validates the accuracy of the fractional conversions that varied so drastically with isothermal cure time.

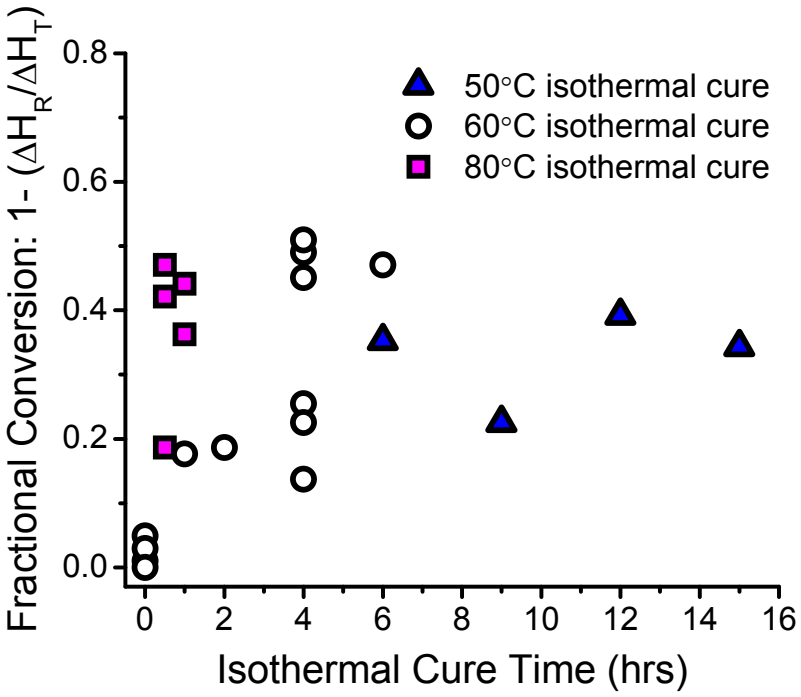

Figure A.2.2. Comparison of fractional conversion versus isothermal cure time at different temperatures analyzed using MDSC.

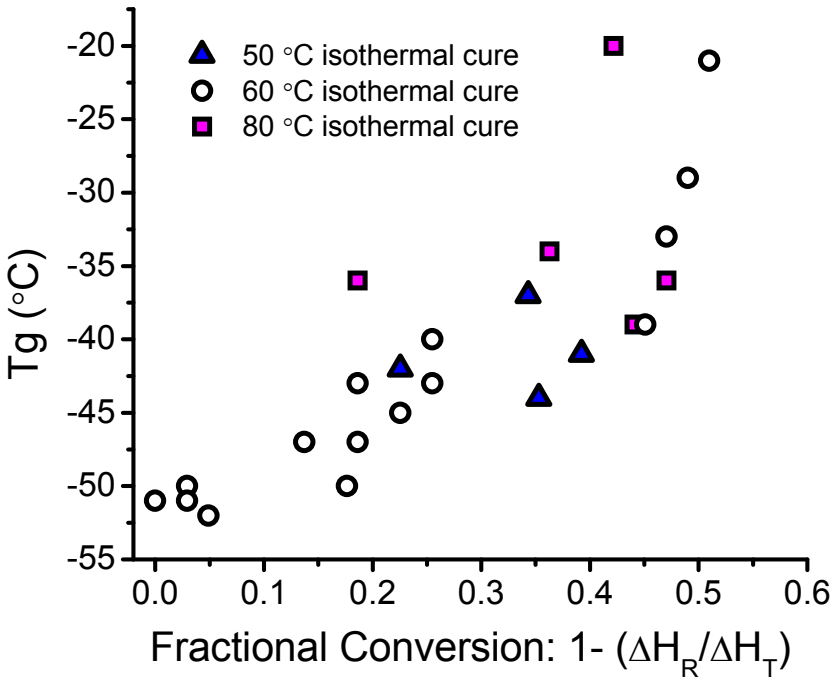

Figure A.2.3. Comparison of Tg versus fractional conversion for MDSC specimens.

A.2.3.2. Detection of Tg and Residual Cure Using Conventional DSC

Using conventional rather than modulated heating it was possible to use a significantly greater heating rate (20°C/min vs. 2°C/min). This larger heating rate and, to a lesser extent, the greater sensitivity of the Q100 DSC increased the intensity of the observed Tg's. As such, using the conventional DSC method the Tg's were unambiguously detected in the heat flow signal even at fractional conversions greater than 0.9.

Typical conventional DSC 1st and 2nd heating scans are shown in Figure A.2.4 along with the difference (subtraction) of these two scans. The subtraction trace exhibits an improved baseline relative to the 1st heating scan, and this made the definition of the Tg and the heat of reaction more reproducible.

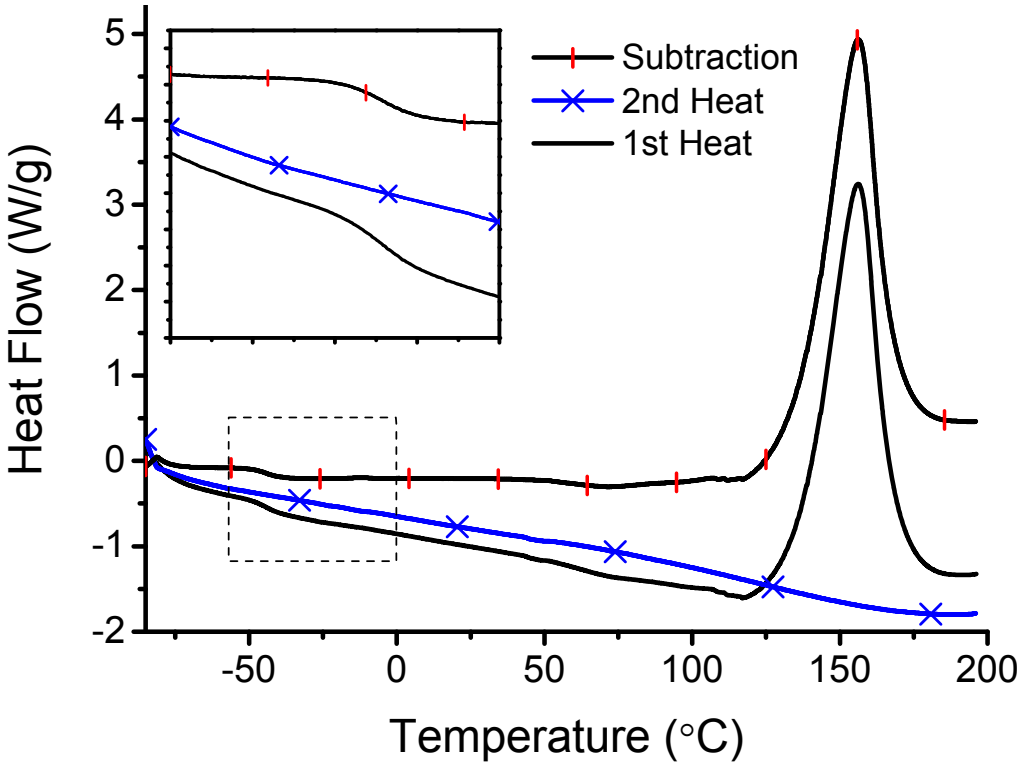

Figure A.2.4. Typical conventional DSC 1st and 2nd heats and the difference thereof (subtraction) for pMDI impregnated yellow-poplar (heating rate = 20°C/min)

Analogous to Figure A.2.2, the plot of fractional conversion versus isothermal cure time for the conventional DSC specimens is presented in Figure A.2.5. Despite some improvement relative to the data in Figure A.2.2, Figure A.2.5 still shows significant variation (e.g. the 80° data at 0.66 hours and the 60°C data at 3 hrs isothermal cure). With a 32% resin content, the conventional DSC specimens should contain mostly adsorbed pMDI, in comparison to the MDSC specimens that had 52% resin. Again, it is unknown why the relationship between fractional conversion and isothermal cure time was so varied. As previously mentioned, perhaps the micro- and nanoscale penetration varied and influenced the cure rate. While the wood specimens were very small, yellow-poplar has a very uniform grain. Perhaps during wood preparation (punching from a flake) the specimens experienced different degrees of compression and damage that could influence resin penetration.

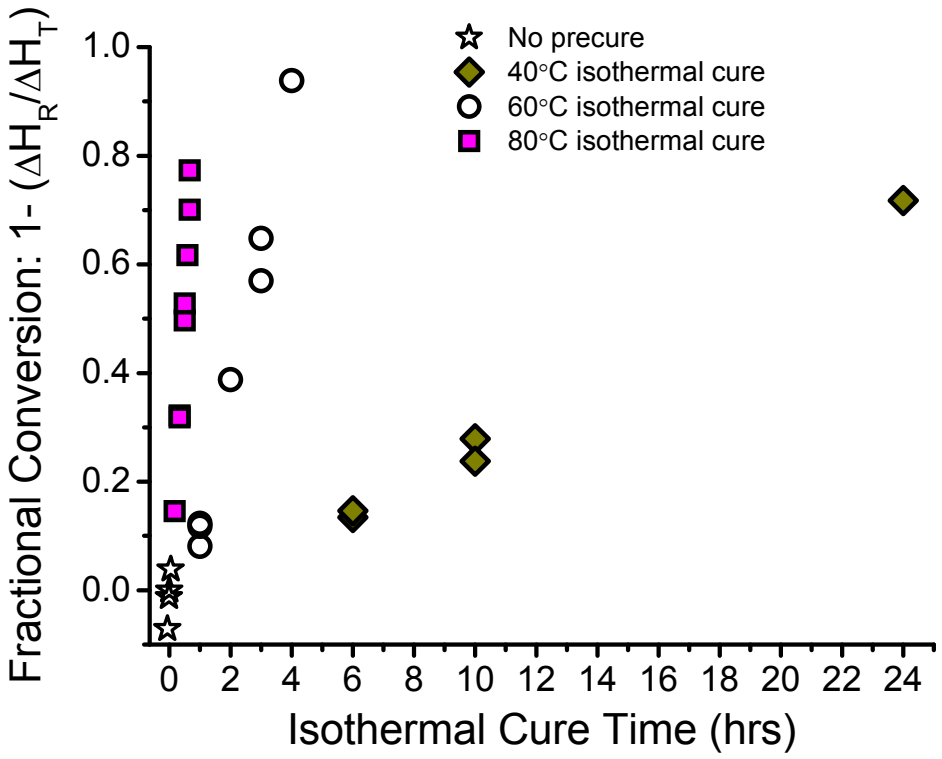

Figure A.2.5. Comparison of fractional conversion versus isothermal cure time at different temperatures for samples analyzed using conventional DSC.

The corresponding plot of T_g versus fractional conversion is presented in Figure A.2.6. The overall trend was similar to that observed in Figure A.2.3 using the MDSC method. Again, the T_g serves as an accurate indicator of fractional conversion despite the noted variation between fractional conversion and isothermal cure time. However, the techniques employed in the conventional DSC method result in less scatter with discernable Tg's even at very high fractional conversions. This greater sensitivity and lower variability of the conventional DSC method is especially significant, considering that the conventional specimen contained approximately 60% less pMDI than the MDSC specimen.

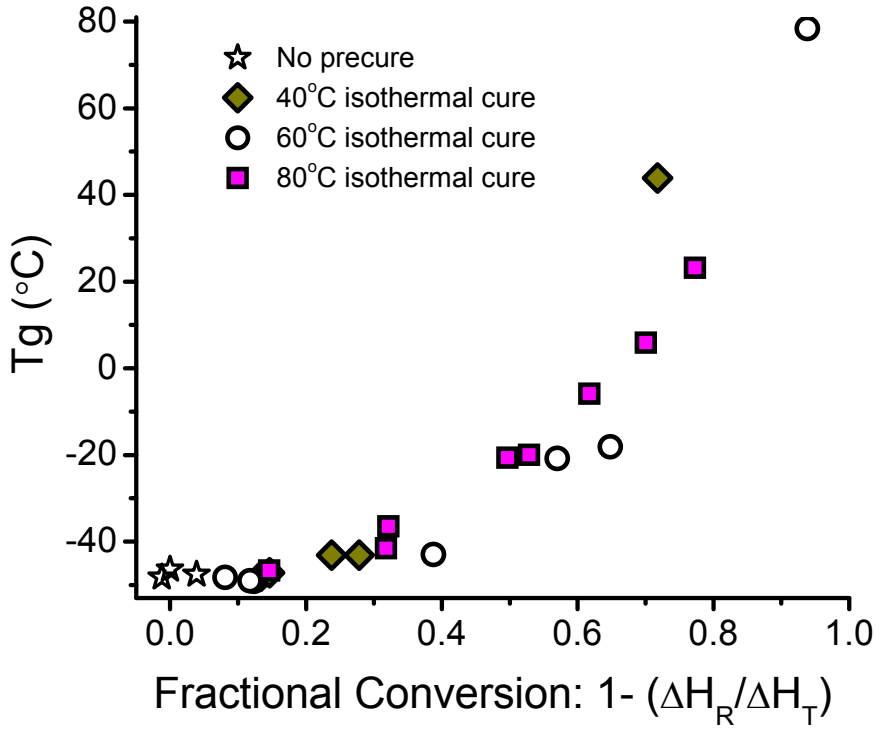

Figure A.2.6. Comparison of T_g versus fractional conversion for conventional DSC specimens.

Finally, T_g versus fractional conversion data for the two different DSC techniques (Figs. 3 and 6) is overlaid in Figure A.2.7. Despite the differences in sample preparation, DSC operation and data analysis techniques, the two methods compared favorably. As such, using DSC to measure the T_g of pMDI impregnated wood appears to be a robust and reproducible method for determining the degree of conversion.

Curing of pMDI impregnated wood significantly differs from that of most neat thermosets; wood provides a complex and catalytic surface. Perhaps arising from this complexity, both the conventional and MDSC methods exhibited significant variability between T_g and isothermal cure time. Despite these complexities the fundamental relationship indeed still exists between the T_g and the fractional conversion of the wood-pMDI system. However, it remains questionable whether this method can actually be extended to the study of commercial OSB. Certainly the resin loadings used in this study were significantly greater than those of commercial OSB. Furthermore, actually adopting

this method to a pilot-scale press system seems rather challenging. Perhaps this method's greater utility will be in investigating the species dependence of pMDI performance or as a general method for analyzing various wood/adhesive systems.

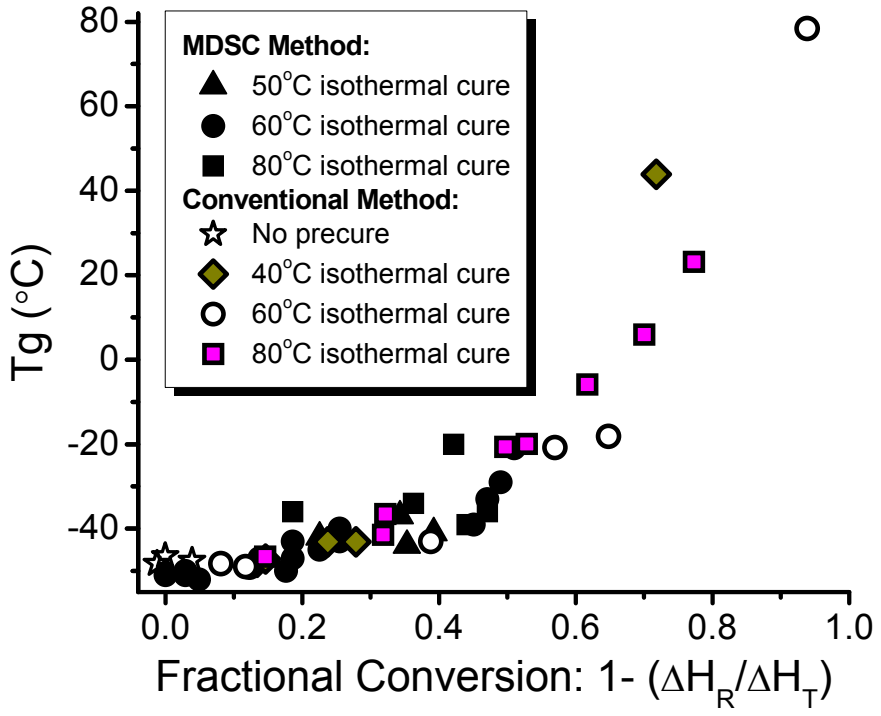

Figure A.2.7. Overlay of Tg versus fractional conversion for both the MDSC and conventional DSC specimens.

A.2.4. Conclusions

1. This study demonstrated a fundamental relationship between the T_g and the fractional conversion of pMDI impregnated wood. Whereas this relation has previously been demonstrated for neat thermosets, the pMDI impregnated wood introduces an added layer of cure complexity involving catalytic interactions between the water, wood and resin.
2. For both the MDSC and conventional DSC techniques significant variability was noted in the T_gs of specimens cured under identical conditions. However, despite the inability to accurately predict T_g from the isothermal curing conditions, both methods demonstrated that the T_g remains a good indicator of the system's fractional conversion.

3. The MDSC method was limited to fractional conversions below approximately 0.6, beyond which the T_g could not be accurately detected. The conventional DSC techniques provided greater sensitivity with accurate T_g detection possible at fractional conversion greater than 0.9. The conventional DSC results also exhibited less variability than those of the MDSC method.

A.2.5. Acknowledgments

Support from the USDA CSREES is gratefully acknowledged, project 2003-35103-12897.

A.2.6. References

Cook, W. D., Scott, T. F., Quay-Thevenon, S., and Forsythe, J. S. (2004). "Dynamic mechanical thermal analysis of thermally stable and thermally reactive network polymers," *Journal of Applied Polymer Science* 93(3), 1348-1359.

Cook, W. D., Simon, G. P., Burchill, P. J., Lau, M., and Fitch, T. J. (1997). "Curing kinetics and thermal properties of vinyl ester resins," *Journal of Applied Polymer Science* 64(4), 769-781.

Das, S., Malmberg, M. J., and Frazier, C. E. (2007). "Cure chemistry of wood/polymeric isocyanate (pMDI) bonds: Effect of wood species," *International Journal of Adhesion & Adhesives* 27(3), 250-257.

Harismendy, I., Gomez, C. M., Del Rio, M., and Mondragon, I. (2000). "Cure monitoring of catalysed cyanate ester resins," *Polymer International* 49(7), 735-742.

Harper, D. P., Wolcott, M. P., and Rials, T. G. (2001). "Evaluation of the cure kinetics of the wood/pMDI bondline," *International Journal of Adhesion & Adhesives* 21, 137-144.

He, G., and Yan, N. (2005). "Effect of moisture content on curing kinetics of pMDI resin and wood mixtures," *International Journal of Adhesion & Adhesives* 25, 450-455.

He, G., and Yan, N. (2007). "Curing kinetics of polymeric diphenylmethane diisocyanate with different wood species," *International Journal of Adhesion & Adhesives* 27, 244-249.

Li, S. Y., Vatanparast, R., Vuorimaa, E., and Lemmetyinen, H. (2000). "Curing kinetics and glass-transition temperature of hexamethylene diisocyanate-based polyurethane," *Journal of Polymer Science Part B-Polymer Physics* 38(17), 2213-2220.

Malkin, A. Y., Gorbunova, I. Y., and Kerber, M. L. (2005). "Comparison of four methods for monitoring the kinetics of curing of a phenolic resin," *Polymer Engineering and Science* 45(1), 95-102.

Owen, N. L., Banks, W. B., and West, H. J. (1988). *J. Molec. Struct.* 175, 389-394.

Park, I. K., Lee, D. S., and Nam, J. D. (2002). "Equivalent processing time analysis development in glass transition development in epoxy/carbon fiber composite systems," *Journal of Applied Polymer Science* 84(1), 144-154.

Scott, T. F., Cook, W. D., and Forsythe, J. S. (2002). "Photo-DSC cure kinetics of vinyl ester resins. I. Influence of temperature," *Polymer* 43(22), 5839-5845.

Teil, H., Page, S. A., Michaud, V., and Manson, J. A. E. (2004). "TTT-cure diagram of an anhydride-cured epoxy system including gelation, vitrification, curing kinetics model, and monitoring of the glass transition temperature," *Journal of Applied Polymer Science* 93(4), 1774-1787.

Toffey, A., and Glasser, W. G. (1997). "Cure characterization of polyurethanes with lignin and cellulose derivatives," *Holzforschung* 51(1), 71-78.

Weaver, F. W., and Owen, N. L. (1995). *Applied Spectroscopy* 49, 171-176.

Wendler, S. L., and Frazier, C. E. (1996). "The effects of cure temperature and time on the isocyanate-wood adhesive bondline by 15N CP/MAS NMR," *International Journal of Adhesion & Adhesives* 16, 179-186.

Wisanrakkit, G., and Gillham, J. K. (1990). "The glass transition temperature (T_g) as an index of chemical conversion for a high-Tg amine/epoxy system: Chemical and diffusion-controlled reaction kinetics," *Journal of Applied Polymer Science* 41, 2885-2929.